THE IMMUNOSUPPRESSIVE FUNCTION OF VEGF SIGNALING IN THE TUMOR MICROENVIRONMENT

APPROVED BY SUPERVISORY COMMITTEE

Rolf A. Brekken, Ph.D. (Mentor)

Todd Aguilera, M.D., Ph.D. (Chair)

Diego Castrillon, M.D., Ph.D.

Michael T. Dellinger, Ph.D.

THE IMMUNOSUPPRESSIVE FUNCTION OF VEGF SIGNALING IN THE TUMOR MICROENVIRONMENT

by

YUQING ZHANG

DISSERTATION

Presented to the Faculty of the Graduate School of Biomedical Sciences

The University of Texas Southwestern Medical Center at Dallas

In Partial Fulfillment of the Requirements

For the Degree of

DOCTOR OF PHILOSOPHY

The University of Texas Southwestern Medical Center at Dallas

Dallas, Texas

December, 2021

DEDICATION

I would like to express my sincere gratitude and appreciation to my mentor, Dr. Rolf A. Brekken, not only for his constant encouragement and guidance on my academic projects but also for continuous support for my career development throughout my graduate life, which changed me significantly in the past five years. He provides me with all resources and independence to explore in science and is always the person standing behind me when I run into difficulties. Without his support, I would never be able to grow up as a confident and independent scientist. I would like to acknowledge the Cancer Biology program for providing a flexible and diversified research environment that I could learn and get precious feedbacks from my colleagues. I would also like to extend my appreciation to my Thesis Committee, Dr. Todd Aguilera, Dr. Diego Castrillon and Dr. Yang-Xin Fu for their invaluable instructions, critical suggestions and encouragement and to Dr. Michael Dellinger for stepping in to the committee at the end. I am also sincerely grateful to all the Brekken lab members, for helping me with new experimental skills, brainstorming fantastic ideas and fulfilling me with happiness as friends and the Brekken Lab family; especially Dr. Huocong Huang for his guidance and critical thinking since my beginning in the lab. Additionally, I would like to thank my friends, specifically my 10-year friend Junqiu Zhang for her companionship throughout my graduate life, with whom I can always share my joys and hard time. Finally, I would like to thank my beloved family, especially my parents, my father Shaopu Zhang, my mother Hongge Chen and my boyfriend Yi Zheng for their understanding and backing up. They are my warmest harbor all the time. Without their love, care, companion, and spiritual support, I would never be able to enjoy the colorful life in Dallas and complete my Ph.D. degree abroad.

THE IMMUNOSUPPRESSIVE FUNCTION OF VEGF SIGNALING IN THE TUMOR MICROENVIRONMENT

Publication No. _____

Yuqing Zhang

The University of Texas Southwestern Medical Center at Dallas, 2021

Rolf A. Brekken, Ph.D.

Angiogenesis, a hallmark of cancer, is induced by vascular endothelial growth factor-A (VEGF). As a result, anti-VEGF therapy is commonly employed for cancer treatment. However, anti-VEGF therapy generally provides modest efficacy in cancer patients and therapy-induced hypoxia results in a less differentiated mesenchymal-like tumor cell phenotype, which reinforces the need for effective companion therapies. Cyclooxygenase-2 (COX-2) inhibition has been shown to promote tumor cell differentiation and improve standard therapy response in pancreatic cancer. Here, I evaluate the efficacy of COX-2 inhibition and

VEGF blockade in preclinical models of pancreatic cancer and identity it as a strategy to overcome therapy-induced resistance in pancreatic cancer. Combination therapy reverses anti-VEGF–induced epithelial-mesenchymal transition, collagen deposition and promotes an immune stimulatory microenvironment. Recent studies have also found that VEGF expression is also associated with immune suppression in cancer patients. This connection has been investigated in preclinical and clinical studies by evaluating the therapeutic effect of combining anti-angiogenic reagents with immune therapy. However, the mechanisms of how anti-VEGF strategies enhance immune therapy are not fully understood. We and others have shown selective elevation of VEGFR2 expression on tumor-associated myeloid cells in tumor-bearing animals. I further investigate the function of $VEGFR2^{+}$ myeloid cells in regulating tumor immunity and find VEGF induces an immunosuppressive phenotype in $VEGFR2^{+}$ myeloid cells including directly upregulating the expression of programmed cell death 1-ligand 1 (PD-L1). Moreover, I demonstrate that VEGF blockade inhibits the immunosuppressive phenotype of $VEGFR2^{+}$ myeloid cells, increases T cell activation and enhances the efficacy of immune checkpoint blockade. These studies highlight the function of VEGFR2 on myeloid cells and provide mechanistic insight on how VEGF inhibition potentiates immune checkpoint blockade.

TABLE OF CONTENTS

PRIOR PUBLICATIONS

1. Zhang Y, Huang H, Coleman M, Ziemys A, Gopal P, Kazmi SM, Brekken RA. VEGFR2 activity on myeloid cells mediates immune suppression in the tumor microenvironment. *JCI Insight*, 2021 Oct.

2. Zhang Y, Arner EN, Toombs JE, Huang H, Warner SL, Foulks JM, Brekken RA. Axl Inhibitor TP-0903 Reduces Metastasis and Therapy Resistance in Pancreatic Cancer. *Mol Cancer Ther*, 2021 Oct.

3. Zhang Y, Coleman M, Brekken RA. Perspectives on Hypoxia Signaling in Tumor Stroma. *Cancers (Basel)* 2021 Jun;13(12):3070.

4. Du W, Phinney NZ, Huang H, Wang Z, Toombs JE, **Zhang Y**, Brekken RA. AXL is Critical for Pancreatic Cancer Cellular Plasticity and Metastasis. *Mol Cancer Res*. 2021 Aug;19(8):1412-1421.

5. Huang H, **Zhang Y**, Gallegos V, Sorrelle N, Zaid MM, Toombs J, Du W, Wright S, Hagopian M, Wang Z, Hosein AN, Sathe AA, Xing C, Koay EJ, Driscoll KE, Brekken RA. Targeting TGFβR2-mutant Tumors Exposes Vulnerabilities to Stromal TGFβ Blockade in Pancreatic Cancer. *EMBO Mol Med*. 2019 Nov 7;11(11):e10515.

6. Zhang Y, Kirane A, Huang H, Sorrelle NB, Burrows FJ, Dellinger MT, Brekken RA. Cyclooxygenase-2 Inhibition Potentiates the Efficacy of Vascular Endothelial Growth Factor Blockade and Promotes an Immune Stimulatory Microenvironment in Preclinical Models of Pancreatic Cancer. *Mol Cancer Res*. 2019 Feb;17(2):348-355.

7. Sorrelle N, Ganguly D, Dominguez ATA, **Zhang Y**, Huang H, Dahal LN, Burton N, Ziemys A, Brekken RA. Improved Multiplex Immunohistochemistry for Immune

Microenvironment Evaluation of Mouse Formalin-Fixed, Paraffin-Embedded Tissues. *J Immunol*. 2019 Jan 1;202(1):292-299.

IN REVISION

1. Huang H, Wang Z, **Zhang Y**, Brekken RA. Mesothelial cell-derived antigen-presenting cancer-associated fibroblasts induce expansion of regulatory T cells in pancreatic cancer. (in revision at *Cancer Cell*)

LIST OF FIGURES

LIST OF DEFINITIONS

ATRA – All-trans retinoic acid

Arg-1 – Arginase 1

BM – Bone marrow

BM-MQ – Bone marrow-derived macrophage

BM-MDSC – Bone marrow-derived MDSC

CAR – Chimeric antigen receptor

CC3 – Cleaved caspase-3

cDC – conventional Dendritic cell

CM – Conditioned media

CTLA-4 – Cytotoxic T lymphocyte antigen 4

CTL – Cytotoxic T lymphocyte

COX-2 – Cyclooxygenase-2

DC – Dendritic cell

ELISA – Enzyme-linked immunosorbent assay

EMT – Epithelial-mesenchymal transition

EMT-TF – EMT-inducing transcription factor

FasL – Fas ligand

FDA – Federal Drug Administration

GBM – Glioblastoma multiforme

HPC – Hemopoietic progenitor cells

ICAM-1 – Intercellular adhesion molecule 1

ICI – Immune checkpoint inhibitor

IFN – Interferon

LAG-3 – Lymphocyte activation gene–3

LLC – Lewis lung carcinoma

mAb – monoclonal antibody

MDC – Myeloid dendritic cells

MDSC – Myeloid-derived suppressor cell

M-MDSC – Monocytic MDSC

MMP-9 – Matrix metallopeptidase 9

MIF – Macrophage migration inhibitory factor

NSCLC – Non-small cell lung cancer

NTB – Non-tumor-bearing

PBMC – Peripheral blood mononuclear cell

PDA – Pancreatic ductal adenocarcinoma

PD-1 – Programmed cell death protein 1

PD-L1/L2 – Programmed cell death 1-ligand 1/2

PFS – Progression-free survival

PGE_2 – Prostaglandin E2

PIGF – Placenta growth factor

PMN-MDSC – Polymorphonuclear MDSC

RCC – Renal cell carcinoma

RTK – Receptor tyrosine kinase

TAM – Tumor-associated macrophage

TB – Tumor-bearing

TEC – Tumor-associated endothelial cell

TEM – Tie2-expressing monocyte/macrophage

TGFβ – Transforming growth factor-β

TIL – Tumor-infiltrating lymphocyte

TIM-3 – T-cell immunoglobulin mucin-3

Treg – Regulatory T cell

VCAM-1 – Vascular cell adhesion protein 1

VEGF – Vascular endothelial growth factor-A

VEGFR1/R2 – Vascular endothelial growth factor-A receptor 1/2

CHAPTER ONE

DIRECT AND INDIRECT REGULATION OF IMMUNE SYSTEM BY VEGF

1.1 Introduction

Tumors exploit conserved immune regulatory pathways to evade immune response-mediated elimination. Tumor and stromal cells in the tumor microenvironment engage immune checkpoints, including cytotoxic T lymphocyte antigen 4 (CTLA-4) and programmed cell death protein 1 (PD-1) expressed on T cells to suppress the function of cytotoxic T lymphocytes (CTLs) and prevent anti-tumor immune activity. The advent of immune checkpoint blockade therapy has revolutionized therapy for many tumors and has become a central therapeutic strategy for subsets of patients with advanced malignancies. This strategy was first demonstrated using antibodies that block CTLA-4 function and resulted in inhibition of tumor growth and durable antitumor memory in mice (1). CTLA-4 expressed on T cells binds to the B7 molecules such as CD80 and CD86 on antigen-presenting cells and subsequently blocks T cell priming and activation (2). Blockade of PD-1 on T cells or its ligands programmed cell death 1-ligand 1 (PD-L1) and 2 (PD-L2), expressed by cancer cells and host myeloid cells, also enhances the anti-tumor activity of tumor antigen primed CTLs (3). Under physiological conditions, activation of CTLA-4 or PD-1 pathways on T cells contributes to the maintenance of tolerance to self-antigens and prevents autoimmunity. However, tumors upregulate the expression CLTA-4 and PD-1 ligands to abrogate the downstream effects of T cell activation (4). In essence, immune checkpoint blockade removes

the brake on T cell activation and triggers adaptive immune responses in appropriately primed CTLs (3).

Immune checkpoint strategies are approved for first-line therapy in multiple indications, such as melanoma, lung cancer, metastatic colorectal cancer and combination with other treatments has elicited remarkable antitumor responses in patients with a variety of solid tumors (5–7). Although immune checkpoint blockade leads to durable responses as long as over ten years in melanoma patients, only a fraction of cancer patients benefit from the immune checkpoint blockade and the rate of complete response to anti-PD-1 or anti-CTLA-4 antibodies remains low (5,8). Therefore, multiple strategies are currently under development to improve therapeutic efficacy of immunotherapies. Importantly, tumors with preexisting tumor-infiltrating lymphocytes (TILs) and a less immunosuppressive microenvironment, which are considered as immunologically “hot” tend to have better response with immune checkpoint inhibitors (ICIs) (9). Abnormal tumor angiogenesis has been described as major component among various factors in the immunosuppressive tumor microenvironment that limit the therapeutic benefit of immune checkpoint blockade in patients (10). The abnormal vascular network that results from tumor angiogenesis restricts efficient lymphocytes infiltration into the tumor site, which compromises the efficacy of immunotherapies (11). Angiogenesis, the process of generating a new vascular network through sprouting of an existing vessel in response to proangiogenic factors, is crucial for the progression and metastasis of solid tumors (12). However, besides the effect on blood vessel formation, angiogenesis has been suggested to be associated with immunosuppression, thus angiogenesis and immunosuppression might

happen in parallel during tumor formation and progression (13). Indeed, a variety of proangiogenic factors, especially vascular endothelial growth factor-A (hereafter referred as VEGF), a primary stimulus for angiogenesis, have immunosuppressive functions. Thus, targeting angiogenic pathways has been exploited to restore antitumor immune response (11,14). In this chapter, I discuss the effects of VEGF on regulating the immune system, including the modulatory effects of VEGF on tumor endothelium and different immune cell types. As VEGF receptors and their functions on myeloid cells have been under investigation recently, I focus on the direct effects of VEGF on regulating different myeloid cells and review the latest preclinical and clinical observations on the immunostimulatory outcomes of antiangiogenic agents.

1.2 VEGF family and VEGFRs

The vascular endothelial growth factor family comprises VEGFA-D and placenta growth factor (PIGF). These growth factors bind to receptor tyrosine kinases (RTKs) VEGF receptors VEGFR1-3 with different affinities and many of them also interact with neuropilins and heparan sulfate proteoglycans as coreceptors (15). Among these receptors, VEGFR2 is the dominant receptor mediating VEGF proangiogenic activity in endothelial cells (16). VEGF binding leads to receptor homodimerization resulting in phosphorylation of tyrosine and activation of the kinases domain, which recruits adaptor molecules and mediates intracellular signaling pathways that regulate endothelial cell survival, migration and proliferation (17,18).

VEGF is a potent angiogenic factor that exists as four different isoforms, $VEGF_{121}$, $VEGF_{165}$, $VEGF_{189}$ and $VEGF_{206}$ due to alternative splicing (19). These isoforms differ in their interaction with the coreceptors and extracellular matrix while maintaining the similar affinities for VEGFR2 (20). VEGF has two main receptors: VEGFR1 and VEGFR2, which are expressed widely in vascular endothelial cells. Although VEGF has at least 10-fold higher affinity for VEGFR1 compared to VEGFR2, VEGFR1 phosphorylation induced by VEGF is weak and VEGFR1 signaling remains poorly understood (15,21). Furthermore, convincing genetic data utilizing mice homozygous for VEGFR1 targeted mutation support that VEGFR1 functions during development as a negative regulator of VEGF-induced VEGFR2 (22). Furthermore, a soluble VEGFR1 variant has been reported to form heterodimer with VEGFR2 and reduce VEGFR2 signaling (21). Therefore, VEGFR1 is typically considered as the decoy of VEGF that controls the amount of available VEGF, thus negatively regulating VEGFR2 signaling. VEGFR2 is essential for vasculature formation during embryonic development. Mice deficient in VEGFR2 die in utero as a result of failure in developing organized blood vessels and disrupted hematopoietic precursors (23). Although VEGFRs were considered to be expressed exclusively on endothelial cells, it is now well established that VEGFRs are also expressed on other cell types, including some tumor cells, T cells, dendritic cells, tumor-associated macrophages and myeloid-derived suppressor cells (MDSCs) (19,24–26).

1.3 VEGF on tumor endothelium

The success of immunotherapy requires infiltration of effector immune cells, extravasation into the tumor stroma and their direct interaction with tumor cells. However, the tumor

vasculature is characterized as leaky, irregular, lacking pericyte support and inefficient in perfusion (12). Tumor-associated endothelial cells have suppressed expression of adhesion molecules, such as vascular cell adhesion protein 1 (VCAM-1) and intercellular adhesion molecule 1 (ICAM-1), in part due to the activity of angiogenic factors, including VEGF. Reduced endothelial expression of adhesion molecules limits T cells attachment to the vessel and decreases efficient T cells infiltration (27,28). In vitro stimulation of normal endothelial cells with VEGF results in the activation of NF-κB through PLCγ-sphingosine kinase-PKC pathway, which stimulates the transcription of adhesion molecules, including ICAM-1 and VCAM-1. However, VEGF-A mediated activation of the PI3K pathway suppresses the expression of ICAM-1 and VCAM-1 (29). On tumor-associated endothelial cells (TECs), VEGF inhibits TNF-α induced VCAM-1 and ICAM-1 expression (30). These effects could be reversed by VEGF blockade (30). CD34 expression is also suppressed on TECs in response to VEGF and fibroblast growth factors (31).

Besides the regulation of adhesion molecules expression, VEGF is also reported to interfere with proinflammatory TNF-α signaling in endothelial cells (32). VEGF treatment inhibits TNF-α-mediated regulation of CXCL10 and CXCL11, which contributes to decreased T cells adhesion to endothelial cells. VEGFR2 signaling inhibition by small molecule inhibitors upregulated CXCL10 and CXCL11 expression on tumor vasculature in a B16 melanoma model, thus improving T cells recruitment (32). Dual inhibition of angiopoietin-2 and VEGF also results in activation of proinflammatory signaling pathways, including TNF-α, type I and II IFN, NF-κB pathways, in endothelial cells sorted from murine breast tumors. Consistently,

blockade of angiogenic factors results in upregulation of CXCL10, VCAM-1 and PD-L1 expression on $CD31^+$ blood vessels (33). VEGF and TNF-α produced by tumor cells also enables human proangiogenic monocyte extravasation to tumors through GATA3-induced suppression of CX3CL1 on vessels (34).

Furthermore, tumor endothelial cells create a selective immune barrier by upregulating the death mediator Fas ligand (FasL) (35). A prior study found no correlation between FasL expression and VEGF level in acute myeloid leukemia patient samples (36); however, recent studies showed that VEGF-A, IL-10 and prostaglandin E2 (PGE_2) induce FasL expression on tumor endothelium cooperatively (35). FasL expression limits cytotoxic $CD8^+$ T cells infiltration but does not affect regulatory T cell (Treg) accumulation (35). Blockade of VEGF together with pharmacological inhibition of PGE_2 or COX-2 (the enzyme that is responsible for formation of PGE_2) results in decreased FasL expression by TECs and a significant increase of cytotoxic $CD8^+$ T cell infiltration into the tumor niche in multiple models (35,37). Thus, optimized doses of anti-angiogenic therapies can normalize the tumor vasculature in multiple aspects and support immune cell trafficking (38,39).

1.4 Direct effects of VEGF on T cells

VEGF has direct effects on T cells. VEGF at concentrations found in advanced stage cancer patients disrupts the development of T cells from hematopoietic progenitor cells and leads to thymic atrophy (40). Additionally, VEGF infusion into tumor-free mice decreases T cell fraction and the T cell/B cell ratios in lymph nodes and spleen (41).

1.4.1 VEGF on effector T cells

Among VEGFRs, VEGFR2 is expressed on T cells. Studies evaluating expression of different types of VEGFRs on T lymphocytes from heathy donors show that VEGFR1 and VEGFR3 are difficult to detect, while VEGFR2 is detected on the surface of $CD3^+$ T cells. Moreover, after anti-CD3 activation, VEGFR2 is upregulated (42). Similarly, purified $CD8^+$ T cells from tumor-free mice have a low level of VEGFR1 and VEGFR2 expression, but stimulation with an anti-CD3 antibody increases VEGFR expression (43). Furthermore, the same study found that tumor infiltrating $CD8^+$ T cells have higher expression of VEGFR1 and VEGFR2 compared to splenic T cells (43). Hypoxia also induces VEGF and VEGFR2 expression in murine T cell lines in a time-dependent manner and VEGF secreted by activated T cells leads to Th1 polarization (44). For T lymphocytes from human PBMCs and T cells isolated from the ascites of ovarian cancer patients, VEGF has been shown to directly suppress T cell proliferation and reduce the cytotoxic activity of T cells through VEGFR2 (42,45). These effects can be attenuated by administration of anti-VEGFR2 antibodies.

In addition, VEGF contributes to the regulation of expression of inhibitory checkpoint molecules on $CD8^+$ T cells in tumors through activation of the VEGFR2-PLCγ-calcineurin-NFAT pathway (43). By upregulating immune checkpoint molecules PD-1, CTLA-4, T-cell immunoglobulin mucin-3 (TIM-3) and lymphocyte activation gene–3 (LAG-3), VEGF directly enhances T cells exhaustion, which contributes to immune escape. A recent study has revealed that T cell exhaustion-specific transcriptional program including the upregulation of immune

inhibitory molecules induced by VEGF is dependent on the transcription factor TOX in microsatellite stable colorectal cancers (24). VEGFR2 specific knockout in T cells by crossing $VEGFR2^{flx/flx}$ mice with LCK-Cre mice resulted in improved overall survival in a syngeneic MC38 model. Tumor infiltrating lymphocytes from VEGFR2 conditional knockout mice displayed higher proliferation and cytokine production capacity with downregulated TOX and immune inhibitory molecules expression (24).

Given the importance of $CD8^+$ T cells in the antitumor immune response and the direct modulation of $CD8^+$ T cells by VEGF, multiple strategies of VEGF blockade decrease immune checkpoint molecules expression on T cells and restore antigen-specific $CD8^+$ T cells effector function in preclinical models (24,43,46,47). A recent study has demonstrated that anti-VEGFR2 antibody, but not VEGFR1 inhibition enhances cytokine production and antigen-specific response of $CD8^+$ effector T cells (46). In response to anti-VEGF therapy which leads to a hypoxic environment, $CD8^+$ T cells in CT26 tumors possess stabilized HIF-1α and upregulated HIF-1α target genes that support $CD8^+$ effector T cell function (46). In addition, in PBMCs from patients with recurrent glioblastoma, treatment with the VEGFR inhibitor axitinib suppressed TIM-3 expression on $CD4^+$ and $CD8^+$ T cells (48). Further, therapy with the VEGF blocking antibody bevacizumab results in elevated expression of genes related to Th1 chemokines and further enhances the infiltration of proliferating $CD8^+$ T cells in metastatic renal cell carcinoma (49). Recently, immune profile analysis of PBMCs and TILs from pre- and post-ramucirumab (anti-VEGFR2) therapy in advanced gastric cancer patients

confirmed enhanced $CD8^+$ T cells infiltration and reduced PD-1 expression by $CD8^+$ T cells (50).

1.4.2 VEGF on regulatory T cells

Regulatory T cells (Tregs) characterized as $CD4^+CD25^+FoxP3^+$, which are critical for maintaining peripheral tolerance under normal condition, are considered to inhibit effective immune response in the tumor microenvironment (51). Tregs inhibit the anti-tumor activity of $CD8^+$ T cells and NK cells, thus, high intratumoral Tregs correlate with poor disease outcomes in multiple tumor types including pancreatic, ovarian and liver cancer (52). The expression pattern of VEGFRs on Tregs is similar to effector T cells: VEGFR1 and VEGFR2 are expressed on a small population of Tregs in naïve mice, but the percentages of $VEGFR1^+$ and $VEGFR2^+$ Tregs are elevated in tumor-bearing mice (53). Inhibition of VEGF in CT26 tumor-bearing mice reduced Treg accumulation by directly inhibiting Treg proliferation through VEGFR2 but did not affect the suppressive capacity of Tregs (53). Consistently, selective blocking of VEGF from binding to VEGFR2 decreases the number of Tregs in genetically engineered mouse model of pancreatic cancer (54). Similarly, silencing tumor-derived VEGF limits Treg infiltration and proliferation in tumor-draining lymph nodes in B16 melanoma (55).

Consistent with preclinical studies, VEGF blockade by bevacizumab reduces Treg recruitment and decreases the proportion of $Ki67^+$ Tregs in peripheral blood of patients with metastatic colorectal cancer and glioblastoma (53,56,57). Primary tumor-infiltrating lymphocytes from advanced gastric cancer patients treated with the VEGFR2 blocking antibody ramucirumab

also exhibit reduced Tregs and in vitro assays confirmed VEGF promotes $VEGFR2^+$ Treg proliferation which could be reversed by ramucirumab (50). In addition, studies also indicate that upregulation of Treg signature genes or increased number of Tregs contributes to immunologic resistance to anti-VEGF therapy in glioblastoma (48,58).

1.5 Effects of VEGF on myeloid cells

1.5.1 Dendritic cells

Dendritic cells (DCs) are professional antigen-presenting cells that are critical for initiation of an antigen-specific anti-tumor immune response. Immature DCs derive from bone-marrow hematopoietic progenitor cells and have low expression level of costimulatory molecules and MHC class molecules, thus have limited capacity for antigen processing and presenting (59,60). DCs can be activated to undergo maturation by a variety of environmental inflammatory stimuli including soluble factors secreted from tumor cells (61). The maturation of DCs results in efficient antigen presenting and reduced antigen uptake (60,62). Activated DCs are characterized by upregulated MHC and costimulatory molecule (CD80 & CD86) expression. Activation of DCs also alters the expression of chemokine receptors and cytokines (59).

Multiple factors in the tumor microenvironment can lead to the dysfunction of DCs. Immature DCs in PBMCs from cancer patients of different cancer types are closely correlate with an increased level of VEGF in plasma (63). VEGF was initially reported to directly inhibit DCs maturation from $CD34^+$ precursors (41,61). The mechanism was illustrated later by evaluating

the binding of VEGF to hemopoietic progenitor cells (HPC). VEGF binding to VEGFR1 on HPC inhibits the activation of NF-κB signaling in HPC resulting in defective maturation of DCs (64). Exposure of embryonic stem cells from VEGFR1 or VEGFR2 deficient mice to VEGF or PIGF revealed that VEGFR1 is the dominant mediator for the inhibitory effect of VEGF on DCs maturation, whereas tyrosine kinase activity of VEGFR2 contributes to early hemopoietic differentiation (25). Recent studies confirmed in peripheral blood from chronic myeloid leukemia and prostate cancer patients that VEGF inhibits the maturation and function of DCs, and this inhibitory effect is associated with a high plasma VEGF level (65,66). Neuropilin-1, a co-receptor for VEGF is necessary for the suppression of LPS-induced murine bone marrow-derived DC maturation (67). Although VEGF has no significant effect on mature DCs with regard to phenotype, cytokine production and induction of apoptosis, VEGF disrupts mature DC stimulation of allogeneic T cells, an effect mediated by VEGFR2, indicating different functions of VEGF receptors in the maturation process of DCs (68). Furthermore, VEGFR2 expression is abundant on plasmacytoid DCs from human and mouse tissues, but not on those isolated from blood and contributes to homeostasis of plasmacytoid DCs and their response to IFN-α (69). In addition, investigation of blood monocyte-derived myeloid dendritic cells (MDCs) from ovarian cancer patients demonstrated VEGF can suppress MDC maturation from progenitor cells and upregulate PD-L1 expression on MDCs, which can be reversed by blocking VEGF activity (70). Elevated PD-L1 expression on MDCs impairs MDC-mediated T cell activation. However, VEGF does not alter PD-L1, CD80 or CD86 expression level on LPS-stimulated mature MDCs.

The modification of DC function by targeting VEGF axis has been explored widely. Small molecule tyrosine kinase inhibitors such as sunitinib, sorafenib and axitinib have been approved for therapy of multiple malignant diseases. However, the effects of these inhibitors on DC function remain controversial. Sorafenib, but not sunitinib was reported to inhibit DC function including reduced cytokine secretion and suppressed costimulatory molecule expression as well as an induction of antigen-specific T cells (71). In contrast, another study demonstrated that sorafenib, but not sunitinib reversed the inhibitory effect of VEGF on DC differentiation with enhanced expression of HLA-DR and CD86 (72). Sunitinib was shown to increase the level of blood myeloid DCs in patients with advanced renal cell cancer experiencing regression (73). Treatment with axitinib, on the other hand, leads to dysfunction of DCs with inhibited expression of activation markers, costimulatory receptors and impaired induction of T cell proliferation (74). However, treatment with bevacizumab restored differentiation of human monocytes to DCs (72). Besides, elevated DCs and reduced immature progenitor cells in peripheral blood have been detected in cancer patients after bevacizumab administration (75). In vitro studies also suggest that supernatant from breast cancer cell lines with VEGF expression ablated by shRNA induces PBMC-derived DCs to upregulate CD80, CD86 and HLA-DR expression and enhances DC-mediated T cell cytotoxicity (76).

1.5.2 Tumor-associated macrophages

Macrophages are professional phagocytes of the innate immune system that contribute to maintaining tissue homeostasis (77). They respond to danger signals and endogenous molecules and are capable of inducing an inflammatory response and triggering adaptive T cell

responses together with other immune cells (77,78). Macrophages respond differently to various microenvironment stimuli and traditionally, macrophages can be divided into two general phenotypes based on their functions: pro-inflammatory macrophages (M1) in response to Th1-associated cytokines or LPS and anti-inflammatory macrophages (M2) activated by IL-4 or IL-13 from Th2 cells. While M1 and M2 categorization of macrophages is convenient, reality has demonstrated that macrophages in tissues or tumors exist within a spectrum of phenotypes and protein expression (79,80). Generally, M1 macrophages are considered to have anti-tumorigenic activity while M2 macrophages are considered to have pro-tumorigenic activities (78,81). Tumor-associated macrophages (TAMs) are recruited early to tumor sites, mostly resemble M2 type macrophages and can generally promote metastasis, stimulate tumor angiogenesis and lead to immunosuppression (82–84). Clinical studies have shown that infiltration of M2 macrophages into tumors confers a poor clinical prognosis in many types of cancers, such as pancreatic, prostate, breast cancers and Hodgkin's lymphoma (83,85–87).

The infiltration of macrophages into tumors is mediated by a variety of cytokines, chemokines and growth factors, including VEGF (88). VEGFR1 is known to be expressed on macrophages and functions as a chemotactic receptor (89,90). VEGFR1 was initially found to mediate VEGF-induced human monocytes migration (91). Qian et al. identified a subset of TAMs expressing VEGFR1 in breast cancer, which are remarkably enriched in metastatic sites, named metastasis-associated macrophages (92). By utilizing macrophage-specific VEGFR1 deleted genetic model, they further suggested VEGFR1 signaling on metastasis-associated macrophages is essential for breast cancer metastasis (92). Relatedly, a recent study has shown

that VEGFR1^{+} metastasis-associated macrophages are highly angiogenic in murine cancer models and colorectal cancer patients with liver metastasis. Additionally, high VEGFR1^{+} monocytes in liver metastasis or in circulating blood correlate with worse prognosis in colorectal cancer patients (93). VEGFR1 signaling on bone-marrow derived macrophages is also able to inhibit IL-4 induced arginase-1 expression (94). In contrast to VEGFR1, which has been widely acknowledged to be expressed on macrophages, macrophages express low to no VEGFR2 under normal conditions (26). However, studies have demonstrated that a subset of TAMs express VEGFR2, which is the dominant receptor mediating VEGF-induced TAM infiltration into tumors (26). Furthermore, selectively inhibiting VEGF binding to VEGFR2 decreases the recruitment of VEGFR2^{+} TAMs (26,95). Consistent with preclinical studies, the population of VEGFR2^{+}/CD45^{bright}/CD14^{+} monocytes become prominent in circulating blood from cancer patients compared to healthy donors, which might be a potential marker for the efficacy of anti-angiogenic treatment (96). Huang et al. recently evaluated the function of VEGFR2 in myeloid cell lineage and confirmed an elevated expression level of VEGFR2 on myeloid cells is associated with murine glioma grade and progression-free survival in high-grade glioma patients (97). Mechanistically, VEGFR2 expression on bone marrow-derived cells contributes to the differentiation of myeloid lineages and proangiogenic function. These authors also found that inhibitor of DNA binding protein 2 is an upstream regulator of VEGFR2 activation (97). On the other hand, TAMs recruit endothelial cells by producing a variety of proangiogenic factors and chemokines, including VEGF, bFGF, CXCL8 and CXCL12, thus promoting tumor angiogenesis (78). TAMs also express MMP9 which mediates extracellular matrix degradation releasing matrix-associated VEGF (98). VEGF produced by

TAMs induces a high-density vessel network, infiltration of macrophages and acceleration of tumor progression in the PyMT tumor model (99). Additional studies validated that myeloid lineage (mainly macrophages and neutrophils) -derived VEGF is critical for the characteristics of tumor vasculature as myeloid-specific deletion of VEGF attenuated the formation of tumor vasculature. However, myeloid depletion of VEGF resulted in accelerated tumor progression but sensitization to chemotherapy in multiple breast cancer models (100).

Preclinical evidence suggests that VEGF blockade significantly reduces the recruitment of immunosuppressive macrophages in breast cancer models (95,101). Others demonstrated that low doses of anti-mouse VEGFR2 antibody DC101 can polarize TAMs from the immunosuppressive M2-type macrophages towards an immunostimulatory M1 phenotype that show elevated chemokines (such as CXCL9, CXCL11) secretion that facilitate T cell recruitment (38). Similarly, apatinib, a tyrosine kinase inhibitor selectively targeting VEGFR2, when used at low-dose also limits the recruitment of TAMs and modulates the immunosuppressive tumor microenvironment to benefit immune checkpoint blockade in lung cancer (102).

However, resistance to anti-angiogenic therapies is commonly associated with TAMs as hypoxia caused by anti-angiogenic agents promotes compensatory recruitment of angiogenic TAMs and other myeloid cells (103,104). Depletion of macrophages after adaptive resistance to VEGF blockade improved survival of ovarian cancer tumor-bearing animals (105). Microarray analysis identified macrophage migration inhibitory factor (MIF) as another

mediator for increased macrophages (106). Reduced MIF contributes to bevacizumab resistance in glioblastoma patients and xenograft models by promoting expansion of M2-type macrophages (106). Tie2-expressing monocytes/macrophages (TEMs) with high proangiogenic capacity are also observed to be involved in the escape of malignant gliomas from anti-angiogenic treatment (107,108). Angiopoietin-2, the ligand of Tie2, contributes to the homing of TEMs and promotes the proangiogenic activity of TEMs (109). Dual targeting Angiopoietin-2/VEGF in multiple preclinical models has been shown to suppress tumor growth efficiently and reprogram TAMs towards a pro-inflammatory M1-type phenotype (33,110,111).

1.5.3 Myeloid-derived suppressor cells (MDSCs)

Myeloid-derived suppressor cells (MDSCs) are a population of highly immunosuppressive immature myeloid cells that co-express CD11b and Gr1 initially identified under tumor settings, while in healthy individuals immature myeloid cells normally differentiate into mature myeloid cells such as macrophages, DCs and granulocytes (112). There are two main populations of MDSCs that increase significantly in tumors: monocytic MDSCs (M-MDSC) and polymorphonuclear MDSCs (PMN-MDSC) (113). PMN-MDSCs are the dominant population in tumor-bearing animals and are able to inhibit antigen-specific $CD8^+$ T cells, while they are less immunosuppressive than M-MDSCs in suppressing T cells activation in vitro (112,114). Multiple mechanisms exploited by MDSCs to modulate innate and adaptive immune response have been discovered, including: expression of Arginase-1 which depletes arginase, a lymphocyte nutrient; production of reactive oxygen species; reduction of effector

cell trafficking; and the expansion of Tregs (112,115,116). Tumor-derived soluble factors contribute to myeloid cell recruitment and function. For example, pro-inflammatory factors such as IL-1β, IL-6, IFN-γ and IL-4 trigger the rapid generation of MDSCs from precursors and induce MDSC-induced immunosuppression (117,118). Gabrilovich et al., demonstrated in vivo infusion of VEGF leads to dysfunction of DCs and increases the production of immature myeloid cells (41). Immature myeloid cells, especially MDSC accumulation in cancer patients correlates with serum VEGF and disease progression (63,119,120). Additionally, increased levels of all MDSC subpopulations in circulation are associated with disease progression (121). A pronounced accumulation of MDSCs have been detected in murine pancreatic tumors with their levels associated with elevated intratumoral VEGF level during tumor progression. Further, depletion of MDSCs improves the survival of tumor-bearing animals (122).

VEGFR1 and VEGFR2 are reported to have distinct contributions to cancer-associated hematopoiesis. Huang et al., dissected the functions of VEGFR1 and VEGFR2 by VEGF infusion and demonstrated that VEGFR2 is the main mediator for VEGF-induced accumulation of $CD11b^{+}Gr1^{+}$ cells while the effect of VEGFR1 is limited (123). The accumulation of immature myeloid cells and their deficiency in differentiating to mature DCs caused by VEGF are associated with constitutive activation of Jak2/STAT3 signaling (124). A recent study confirmed VEGFR1 and VEGFR2 expression on tumor infiltrating MDSCs in an ovarian tumor model (125). However, different from $VEGFR1^{+}$ MDSCs whose proportion remains unchanged across organs, the frequency of $VEGFR2^{+}$ MDSCs increases significantly in tumors, indicating MDSC recruitment to tumors is mainly dependent on VEGFR2 signaling

(125). Further evaluation shows that VEGFR2$^+$ MDSCs are mainly Arginase-1$^+$, suggesting VEGFR2$^+$ MDSCs possess high immunosuppressive capacity (125).

Therefore, it is reasonable to restrain MDSC accumulation by disrupting the VEGF-VEGFR2 axis. We and others have previously demonstrated multiple anti-VEGF strategies including antibodies and sunitinib decrease the number of MDSCs in the inflammatory 4T1 breast cancer model and MCA26 colon cancer model (101,126). Sunitinib could inhibit MDSC recruitment via VEGFR inhibition or inhibition of STAT3 in MDSCs (127). Sunitinib treatment also significantly decreases PD-L1 expression on MDSCs and plasmacytoid DCs (126). The depletion of MDSCs caused by sunitinib treatment further benefits vaccine efficacy and leads to enhanced antigen-specific T cell response in preclinical tumor models (128). Further studies suggested although anti-VEGFR2 antibody DC101 does not effect MDSC mobilization, the inhibitory ability of M-MDSCs on T cells proliferation is attenuated by DC101 (129). Consistently, M-MDSCs from axitinib-treated mice also exhibit reduced suppressive capacity on T cells in a melanoma model (130). Clinical studies also reveal sunitinib treatment in renal cell carcinoma patients results in remarkable reduction in peripheral MDSCs, which correlates with a reduction in Tregs and type 1 T-cell suppression (131). Similarly, bevacizumab significantly reduces the percentage of PMN-MDSCs in the peripheral blood of patients with unresectable non-small cell lung cancer (NSCLC).

Myeloid cells including MDSCs have been considered to be involved in the resistance of tumors to anti-VEGF treatments. Compared to anti-VEGF sensitive tumors, refractory tumors

are often associated with an increase in tumor infiltrating $CD11b^{+}Gr1^{+}$ MDSCs and bone marrow MDSCs, which produce high level of MMP9 and can acquire an endothelial phenotype, directly leading to tumor vascularization (132,133). Gene expression analysis of bone marrow MDSCs from refractory tumors reveals enrichment of inflammatory cytokines, markers of myeloid cell differentiation as well as proangiogenic factors (132). STAT3 signaling is also found to be essential for MDSC-mediated tumor angiogenesis (134). In ovarian cancer murine models and clinical samples that are resistant to anti-VEGF therapy, there is a significant increase in $Gr1^{+}$ MDSCs in hypoxic regions. This elevated infiltration is thought to be mediated by GM-CSF (135). Thus, strategies targeting MDSCs are being explored to overcome the resistance to anti-angiogenic therapy (136). The vitamin A metabolite all-trans retinoic acid (ATRA) induces the differentiation of MDSCs into mature myeloid cells and potentiates anti-VEGFR2 therapy in breast cancer models (137). Also, MDSC depletion with an anti-Ly6G antibody combined with small molecule kinase inhibitor sorafenib suppresses MDSC infiltration and improves therapeutic efficacy of sorafenib in syngeneic orthotopic liver tumors (138). Similarly, combination therapy of an anti-Gr1 antibody and anti-VEGF neutralizing antibody also shows significant activity in controlling the growth of refractory tumors (132).

1.6 Anti-angiogenic therapy in combination with immunotherapy

As discussed above, VEGF has direct and indirect effects on the immune system and contributes to tumor immune evasion. As a result, strategies targeting VEGF or the VEGF-VEGFR axis can promote an immunostimulatory microenvironment. However, for patients

with advanced disease, single agent anti-angiogenic therapy is likely not sufficient to generate a robust and durable immune response. Therefore, combination of anti-angiogenic therapy with immunotherapeutic strategies is being pursued vigorously.

1.6.1 Immune checkpoint blockade

The combination of ICIs with certain anti-angiogenic agents has been investigated in preclinical models and in cancer patients. In preclinical models including pancreatic neuroendocrine tumors and mammary carcinoma models that are poorly responsive to anti-VEGFR2, PD-L1 was found to be upregulated due to IFN-γ produced by T cells. Antibody-mediated blockade of PD-L1 and VEGFR2 prolonged the anti-tumor response, reduced tumor burden and increased animal survival. Efficacy were associated with the formation of high endothelial venules mediating lymphocytes infiltration (139). Similarly, combination of anti-PD-1 antibody with DC101 enhanced antigen-specific T cell response and improved animal survival in microsatellite stable colorectal cancer model (24). A recent study also demonstrated the efficacy of dual inhibition of VEGF and angiopoietin-2 together with PD-1 blockade in a murine model of glioblastoma. Response was associated with elevated tumor associated $CD8^+$ T cells and vessel normalization (140). Additionally, small molecule inhibitor axitinib in combination with anti-PD-1 or anti-TIM-3 antibodies resulted in enhanced therapeutic efficacy in syngeneic murine models (141). Furthermore, blocking CD47, which is the ligand of another immune checkpoint regulator SIRPα, in NSCLC resistant to anti-angiogenic therapy potentiated the benefits of VEGFR blockade (142).

The level of serum VEGF before treatment was reported to negatively correlate with clinical response in patients with metastatic melanoma treated with anti-CTLA-4 antibody and patients with advanced NSCLC receiving anti-PD-1 antibody, indicating VEGF as a potential biomarker for therapy and highlighting the rationale of targeting VEGF in these patients (143,144). Indeed, clinical trials have shown tolerable toxicity with the combination of a selective VEGF inhibitor, axitinib and pembrolizumab (anti-PD-1 antibody) in treatment-naïve advanced renal cell cancer patients (145). A randomized phase 2 clinical trial of atezolizumab (anti-PD-L1) alone or atezolizumab combined with bevacizumab versus sunitinib was completed in previously untreated patients with metastatic renal cell carcinoma. Median progression-free survival (PFS) with combination therapy was 11.7 months (95% CI, 8.4–17.3) compared to 8.4 months (95% CI, 7.0–14.0) in sunitinib treatment group and 6.1 months (95% CI, 5.4–13.6) with atezolizumab monotherapy (146). The efficacy of combination therapy was superior in PD-L1^{+} patients with median PFS 14.7 months (95% CI, 8.2–25.1) (146). Biomarkers analysis of patient tissue from this trial further demonstrated that high expression of effector T cell gene signature is associated with improved overall objective response rates and PFS in the combination arm (146). A phase 3 clinical trial is currently ongoing to confirm these results (2). In patients with metastatic renal carcinoma who had already received first line immune checkpoint inhibitors, second-line VEGFR tyrosine kinase inhibitors led to 39.7% partial response and 52.9% stable disease (147). Besides renal cell carcinoma, axitinib together with pembrolizumab (anti-PD-1 antibody) has been applied to patients with advanced sarcomas in a phase 2 trial, indicating manageable toxicity and preliminary efficacy. Particularly in patients with alveolar soft-part sarcoma, the 3-month progression-free survival

reached 72.7% (95% CI 37.1-90.3) (148). Combination of bevacizumab and nivolumab (anti-PD-1 antibody) was also assessed to have activity in patients with relapsed ovarian cancer in a phase 2 clinical trial, while interestingly, the majority of responses occurred in patients with lower tumor PD-L1 expression (149).

In conclusion, multiple preclinical studies have demonstrated promising results after combination of anti-angiogenic agents with immune checkpoint inhibitors. Clinical trials have demonstrated manageable toxicity with some indications of improved efficacy. A large number of clinical trials are currently underway to assess application of combination regimens in various cancer types.

1.6.2 Tumor vaccines

Tumor vaccines are designed to induce proper immune response towards one or multiple self-antigens or tumor-specific antigens, such as DC vaccines and vaccines targeting tumor associated antigens. However, challenges in the development of cancer vaccines still remain due to immune self-tolerance (150). Besides, compromised immune system in most patients in clinical trials leads to disappointing results in the field of tumor vaccines (151,152). As discussed before, anti-angiogenic agents promote effector cells infiltration and reverse the immunosuppressive microenvironment. Therefore, it might be beneficial to utilize anti-angiogenic treatment to boost immune response towards tumor vaccines. In other preclinical studies, vaccines targeting pro-angiogenic factors or tumor vasculature have the potential of

anti-vascular effects and control of tumor growth by simultaneous targeting angiogenesis and stimulating immune response (153).

Previously, sunitinib treatment combined with OVA peptide-pulsed DC (VAC) has been shown to exhibit superior anti-tumor effect in B16-OVA melanomas by facilitating antigen-specific T cells response while reducing MDSCs and regulatory T cells in tumors and tumor-draining lymph nodes (154). The anti-tumor effect was more potent when sunitinib was administrated at the time of initial vaccine boost (154). A HER-2 peptide vaccine in combination with DC101 was investigated in a genetic murine model of $Her2^{+}$ breast cancer, which resulted in inhibited tumor growth (155). Similarly, low dose DC101 treatment combined with a whole cancer cell vaccine enhanced vaccine therapy in an orthotopic breast cancer model and improved animal survival in the MMTV-PyVT model (38).

A preliminary clinical study reported that a vaccine (ERC-1671) generated from cellular and tumor lysate components of glioblastoma multiforme (GBM) showed signs of efficacy in patients with progressive gliomas after bevacizumab failure (156). A larger cohort of GBM patients who failed bevacizumab therapy were treated with ERC-1671, resulting in minimal toxicity and a 100% six-month overall survival and 77% 40-week survival compared to 33% and 10% in patients in the control group (157). A phase 2 clinical trial is ongoing to verify the efficacy of ERC-1671 in combination with bevacizumab in recurrent GBM (158). Recently, a personalized cancer vaccine developed by autologous DCs pulsed with whole-tumor cell lysates was tested in recurrent ovarian cancer patients to address the safety and feasibility of

combination with bevacizumab and cyclophosphamide (159). Besides bevacizumab, sunitinib has also been exploited to combine with a multi-peptide cancer vaccine containing 10 tumor-associated peptides for advanced renal cell carcinoma. However, a phase 3 trial of the strategy was disappointing as the combination did not improve the overall survival compared to first-line therapy (160), highlighting the complexity of combining small molecule inhibitors with tumor vaccines.

1.6.3 Adoptive cell transfer

An adoptive immune cell transfer based antiangiogenic strategy was first developed based on engineered cytotoxic T lymphocytes that were introduced with a chimeric T cell receptor comprising VEGF sequences (161). After adoptive transfer into tumor-bearing mice, these engineered T cells are designed to efficiently target cells expressing VEGF receptors and lead to inhibition of tumor growth in multiple syngeneic murine models and human xenografts. Combination with the angiogenesis inhibitor, TNP-470, further enhanced this effect (161). Consistently, investigators later demonstrated adoptive transfer of mouse and human T cells expressing chimeric antigen receptor (CAR) targeting VEGFR2 generates antigen-specific immune responses and significantly suppresses tumor growth and improves survival in 5 different vascularized syngeneic tumors (162). The CAR-T cells targeting VEGFR2 also reduce $VEGFR2^{+}$ MDSCs and reverse the immunosuppressive microenvironment (163). Simultaneous transfer of engineered syngeneic CAR-T cells targeting VEGFR2 and T cells specific for tumor antigens induces tumor regression in B16 melanomas compared to treatment with either CAR-T alone (164). In this study, researchers also observed remarkable expansion

and durable persistence of transferred tumor antigen-specific T cells (164). Similarly, anti-VEGF antibody treatment enhanced the efficacy of adoptive cell transfer therapy with infused T cells targeting B16 melanoma cell-specific markers even in established tumors (~200 mm^2) that don't respond well to anti-VEGF therapy. The enhancement was likely due to increases in tumor infiltrating T cells caused by VEGF blockade (165). In addition, bevacizumab in combination with adoptive transfer of cytokine-induced killer cells, derived from peripheral blood mononuclear cells, had synergistic effects on controlling tumor growth in NSCLC murine models (166).

Clinically, bevacizumab together with a tumor cell lysate-pulsed DC vaccine followed by adoptive transfer of autologous vaccine-primed T cells was performed to treat a small cohort of recurrent ovarian cancer patients (167). This combination strategy turned out to be well tolerated and elicit durable immune responses including reduced circulating Tregs and elevated $CD8^+$ T cells (167). Further investigation including modification of this combination are warranted in clinical studies in larger cohorts.

1.6.4 Type I IFN and STING agonist

The interferons (IFNs) are a family of cytokines that modulate immune response or have a direct effect on target cells therefore protect against diseases. In tumor microenvironment, IFNs can be produced by multiple cell types, where they directly target tumor cells or stimulate T cells and activate immune responses (168). They can also cause cancer cells to release chemicals that attract immune cells to attack cancer cells (169). There are three major types of

IFNs, among which type I IFN, IFN-α has been widely explored in clinic for treatment of different types of cancer, such as haematological cancers, melanoma and other advanced metastatic disease (168,170,171).

A decade ago, a phase 3 clinical trial was performed by combining bevacizumab with IFN-α, the historic standard treatment for renal cell carcinoma (RCC) in patients with previously untreated metastatic RCC. Although there were benefits in overall survival, they did not reach the criteria for significance, likely due to toxicity (172). Similar results were observed with bevacizumab combined with IFNα -2α (173).

The STING signaling pathway triggered by cytosolic DNA is essential in host defense and inducing anti-tumor immune responses. Activation of the STING pathway in antigen-presenting cells drives production of type I IFN and enhances T cell priming (174). Based on accumulating evidence showing the importance of STING expression in endothelial cells, Yang et al., recently confirmed the correlation of endothelial STING expression and intratumoral $CD8^+$ T cell infiltration (175). They further reported that a STING agonist delivered by intratumoral injection normalizes the tumor vasculature in Lewis lung carcinoma (LLC) models and demonstrated the combination of a STING agonist with VEGFR2 blockade results in complete tumor regression. Triple combination of STING agonist, immune checkpoint blockade (anti-PD-1 or anti-CTLA-4) and anti-VEGFR2 antibody also leads to dramatic tumor control and mice receiving the triple therapy exhibit long-lasting tumor-specific immune memory (175).

Compelling evidence indicates that the effect of blocking VEGF activity in solid tumors extends beyond inhibition of angiogenesis and can modulate the immune system. In preclinical and clinical settings, dozens of studies have demonstrated the benefit of combining VEGF blockade with anti-cancer immunotherapy. However, increased therapy-induced toxicity is a concern especially in the context of small molecule tyrosine kinase inhibitors that have a significant toxicity profile as single agents. Thus, anti-angiogenic agents with higher specificity might be more manageable regarding toxicity and be the preferred combinatorial agent with immunotherapy. For example, selective blockade of VEGF-VEGFR2 signaling results in potent tumor control with limited toxicity as well as an improved immune microenvironment compared to broader spectrum inhibitors (101,176).

CHAPTER TWO

COX-2 INHIBITION POTENTIATES THE EFFICACY OF VEGF BLOCKADE AND PROMOTES AN IMMUNE STIMULATORY MICROENVIRONMENT IN PRECLINICAL MODELS OF PANCREATIC CANCER

This chapter is based on a research article written by the author (Zhang & Kirane et al, 2019)

2.1 Introduction

Primary tumors and metastases require nutrients and oxygen delivered by blood vessels (12). Although angiogenesis is complex, it is widely recognized that vascular endothelial growth factor-A (VEGF-A) is the predominant angiogenic factor that promotes tumor neovascularization (177,178). Inhibitors of angiogenesis have become a central part of systemic therapy for a variety of malignancies (179,180). However, angiogenesis inhibition has in general resulted in only modest gains in clinical outcomes in cancer patients as many patients treated with anti-angiogenic/anti-VEGF therapy either fail to respond or relapse on therapy (181,182). Additionally, anti-angiogenic therapy has been implicated in promoting tumor progression and accelerating metastasis in preclinical models (183,184).

Pancreatic cancer, the third-leading cause of cancer-related death (185), is highly metastatic and poorly responsive to standard therapy (186,187). It is also an immunologically "cold" tumor that has remained largely refractory to immune checkpoint blockade (187,188). Anti-VEGF therapy has been studied in pancreatic cancer patients (179); however, it has not

provided significant clinical benefit in combination with gemcitabine, the standard chemotherapy for pancreatic ductal adenocarcinoma (PDA) (189–191). Previously, we investigated the efficacy and biology of anti-VEGF therapy in preclinical models of PDA using the antibody mcr84 (184,192). We found that mcr84 alone or in combination with gemcitabine slowed the growth of PDA but induced hypoxia-induced epithelial plasticity that resulted in a less differentiated tumor cell phenotype and continued metastatic burden (184). These observations reinforce the need to develop companion therapies that combat therapy-induced epithelial plasticity.

Inflammation is a pathological phenotype that facilitates the "hallmarks" of cancer (193). Further, the incidence of several cancers is associated with inflammation, which contributes to tumor initiation and cancer cell survival by producing reactive oxygen species, cytokines, and proinflammatory mediators (194). Among mediators of inflammation that are associated with tumor progression is cyclooxygenase-2 (COX-2), an inducible enzyme that catalyzes the rate-limiting step in the synthesis of the prostaglandin E_2 (PGE_2). COX-2 is induced at sites of inflammation and during the process of tumor progression (195). Multiple studies have demonstrated that elevated COX-2 expression is prevalent in human malignancies, including PDA (196,197). In addition, elevated expression of COX-2 in tumors correlates with advanced stage and worse outcome by promoting chemoresistance, metastasis, and angiogenesis (198,199). COX-2 has also been identified as a potential mediator of VEGF-independent tumor angiogenesis (200). Thus, targeting COX-2 inhibition has been explored as a potential anticancer therapy (201). Additionally, COX-2 blockade can enhance the efficacy of anti-

angiogenic treatments in breast cancer, which supports the investigation of COX-2 inhibitors with VEGF blockade in other tumors (202).

Apricoxib is a selective COX-2 inhibitor that has shown significant anti-tumor activity in various xenograft models (203) and has been under clinical investigation. Previously, we demonstrated that apricoxib improved the efficacy of standard therapy in preclinical models of PDA (204). Further, we found that inhibition of COX-2 reversed epithelial-mesenchymal transition (EMT), leading to a shift toward a more epithelial phenotype in xenograft models of PDA (204). In the present study, we investigated the combination of anti-VEGF therapy and COX-2 inhibition as a therapeutic strategy in robust preclinical models of PDA with the hypothesis that apricoxib would prevent or reduce therapy-induced epithelial plasticity. We also investigated the effect of anti-VEGF and COX-2 inhibition on the immune landscape of PDA given that prior reports have demonstrated VEGF and PGE_2 can limit T cell infiltration into tumor cell nests (35) and reports that EMT can be a significant driver of immune suppression in tumors (205–208).

2.2 Results

2.2.1 Pharmacologic blockade of COX-2 and VEGF inhibits tumor growth and limits metastatic burden in pancreatic cancer models

To investigate the efficacy of COX-2 inhibition with apricoxib and VEGF blockade with mcr84 (192) in preclinical models of PDA, we used a genetically engineered mouse model of PDA and SCID mice bearing established orthotopic pancreatic xenografts. Therapy was

initiated in 3-week-old KIC mice. Mice were randomized to receive saline, mcr84, apricoxib, or mcr84 + apricoxib and were sacrificed after 4 weeks (7 weeks old). Therapy with mcr84 or apricoxib reduced primary tumor weight by ~30% whereas mcr84 + apricoxib reduced primary tumor weight by 62% compared to the control group ($P < 0.0001$; Figure 1A). At the time of sacrifice, the extent of liver metastasis was determined based on gross metastasis. Seven out of 10 evaluable mice in the control group had at least 1 macroscopic metastasis; this number was reduced to 1/5, 2/7, 1/6 for the mcr84, apricoxib, and combination therapy groups, respectively (Figure 1A). To further define the effect of COX-2 inhibition and anti-VEGF therapy on tumor burden and liver metastases, we established human PDA xenografts in mice by orthotopically injecting Colo357, a human pancreatic cancer cell line, into the pancreas of SCID mice. Similar to in vitro data published previously (204), Colo357 cells showed high COX-2 expression and were responsive to apricoxib (data not shown). Mice with established tumors, which was confirmed by ultrasound, were randomized to receive treatment as described above. After 4 weeks of therapy, we found that single-agent therapy had a minimal effect on primary tumor growth (Figure 1B) and metastatic incidence, although the mean metastatic events per treatment group was reduced by mcr84 or apricoxib (Figure 1B). In contrast, combination therapy significantly reduced primary tumor weight ($P < 0.05$ vs. control) and substantially limited metastases ($P < 0.01$ vs. control; $P < 0.05$ vs. single-agent therapy; Figure 1B). H&E analysis of livers confirmed metastatic lesions in Colo357 tumor bearing mice (Figure 2A). The effect of mcr84 + apricoxib on primary tumor growth compared favorably to the effect of gemcitabine + erlotinib in the same model reported in our prior study (209) (Figure 2B).

COX-2 activity has been implicated in promoting angiogenesis (200,210,211). Previously, prostaglandins, products of COX-2 activity were shown to elevate VEGF expression and inhibition of COX-2 was shown to contribute to anti-angiogenic effects (212,213). Furthermore, fibroblasts from *Cox-2*-deficient mice were reported to produce significantly less VEGF than fibroblasts from wild-type or *Cox-1*-deficient animals (214). Additionally, treatment of wild-type fibroblasts with a selective COX-2 inhibitor resulted in a 90% reduction in VEGF production (214). However, recently Xu et al (200) determined that PGE_2 can contribute to angiogenesis in a VEGF-independent manner in colon cancer models. Given these data, we sought to investigate the relationship between COX-2 activity and VEGF production in PDA cell lines, we selected a COX-2 negative cell line, AsPC-1, and 2 COX-2 positive cell lines, one with a high expression of COX-2, Colo357, the other with moderate COX-2 expression, HPAF-II (204). Cells were treated with 500 nM apricoxib and the level of VEGF produced was determined by ELISA. Only in high COX-2 cell line, Colo357, COX-2 inhibition reduces VEGF production transiently. In HPAF-II and AsPC-1 cells, VEGF production was unaffected by apricoxib, with VEGF production in HPAF-II cells elevated over time (Figure 1C). To determine if EMT induction altered VEGF production and/or the effect of apricoxib, we plated Colo357 and AsPC-1 cells under conditions that stimulate EMT. Under normal culture conditions we observed similar trends as shown before. However, under EMT-inducing conditions VEGF production was elevated significantly and was largely independent of COX-2 inhibition in Colo357 cells. In AsPC-1 cells, VEGF production increased faster over time under induced EMT conditions compared to normal conditions (Figure 1C). We also

investigated the effect of apricoxib on PGE_2 production by Colo357 and Aspc-1 cells under normal and EMT-inducing culture conditions (Figure 3, A and B). The induction of EMT was confirmed by evaluating the expression level of E-Cadherin, N-Cadherin and Vimentin (Figure 3C). The induction of EMT reduced the effect of apricoxib on PGE_2 production in Colo357 cells. In contrast, AsPC-1 cells produced minimal PGE_2 under either culture condition (Figure 3, A and B). We corroborated these findings by examining the level of VEGF expression in Colo357 pancreatic xenografts by immunofluorescence staining and found that VEGF expression was not affected by apricoxib (Figure 1D). Importantly, apricoxib did reduce COX-2 expression in Colo357 tumors supporting the pharmacodynamic activity of the drug. The induction of hypoxia by mcr84 and the reduction of microvessel density by mcr84 in Colo357 tumors (Figure 4, A and B) are consistent with prior studies (184). We found that apricoxib alone did not reduce microvessel density in Colo357 tumors (Figure 4, A and B), which further supports that apricoxib anti-tumor activity is not mediated by inhibition of angiogenesis. However, we did observe that apricoxib alone or in combination with mcr84 increased the percentage of pericyte-associated blood vessels in Colo357 tumors (Figure 4C). These data suggest that COX-2 functions in a VEGF-independent manner in PDA to promote tumor progression.

2.2.2 Apricoxib in combination with mcr84 reverses anti-VEGF–induced EMT and collagen deposition

Although anti-VEGF therapy with mcr84 restricts tumor growth and improves the survival of *KIC* mice (184), therapy-induced hypoxia results in a less differentiated tumor cell phenotype

(184). We previously found that COX-2 inhibition with apricoxib reverses EMT in HT29 xenografts (203) and Colo357 tumor-bearing mice (204). To determine whether apricoxib can prevent or reduce hypoxia-induced epithelial plasticity as a result of mcr84 treatment, we analyzed tumor tissue from *KIC* mice in each treatment group. Treatment with mcr84 alone increased the expression of N-cadherin, a common marker of mesenchymal cells and Slug, an EMT-inducing transcription factor (EMT-TF). Apricoxib alone or in combination with mcr84 significantly reduced N-cadherin expression and downregulated Slug expression to the same level of control group. Although the expression of Snail, another EMT-TF (215) was not affected by mcr84, treatment with apricoxib or apricoxib combined with mcr84 decreased Snail expression significantly (Figure 5A**)**. We also observed that collagen deposition was increased in *KIC* and Colo357 tumors after treatment with mcr84, a feature we identified previously that is associated with epithelial plasticity (184). This effect was attenuated by apricoxib alone or in combination with mcr84 (Figure 5B).

2.2.3 Blockade of VEGF and COX-2 pathways promotes an immune stimulatory microenvironment

Eicosanoids, including PGE_2, contribute to the immune microenvironment of solid tumors (195). For example, PGE_2 can induce a shift in cytokine expression in myeloid-derived suppressor cells (MDSCs) and macrophages towards an immune suppressive profile (e.g., IL-4, IL-10, IL-6) and PGE_2 can directly reduce T effector cell activity (216). Furthermore, EMT is also associated with an immunosuppressive tumor microenvironment (205,206,208). Thus, given our observations that COX-2 inhibition with apricoxib reduces PGE_2 production and

decreases therapy-induced EMT, we investigated the immune landscape in *KIC* tumors from the different treatment groups shown in Figure 1. Tumors harvested from mice that received mcr84 or apricoxib alone had an increase in the number of tumor-associated $CD3^+$ and $CD8^+$ T cells. Combination therapy further elevated $CD3^+$ and $CD8^+$ T cell levels (Figure 6A). Additionally, apricoxib alone and in combination with mcr84 significantly decreased $FoxP3^+$ regulatory T (Treg) cells (Figure 6A). Motz et al (35) previously reported that selective expression of the death mediator Fas ligand (FasL) on endothelial cells in human and mouse solid tumors was associated with scarce T-cell infiltration. They also identified that FasL was induced on endothelium by VEGF, IL-10, and PGE_2. Thus, we evaluated FasL expression on the vasculature of *KIC* tumors by dual staining of the endothelium for CD31 and FasL. We found that FasL was indeed present on $CD31^+$ endothelial cells in control treated *KIC* tumors and that treatment with mcr84, apricoxib, or the combination significantly reduced endothelial FasL expression (Figure 6B). To determine the effect of VEGF blockade and COX-2 inhibition on macrophages in the tumor microenvironment, we stained for CD11b, iNOS, and Arginase 1. We found that mcr84 alone and mcr84 in combination with apricoxib reduced $CD11b^+iNOS^+$ macrophages but apricoxib alone did not. In contrast, mcr84 or apricoxib alone decreased $CD11b^+Arg1^+$ macrophages, while the effect was more significant with combination therapy (Figure 6C). Although the number of total myeloid cells that were marked by CD11b was elevated in the combination treatment group, the total macrophage number (F4/80) was reduced with anti-VEGF and COX-2 inhibition (Figure 7, A and B).

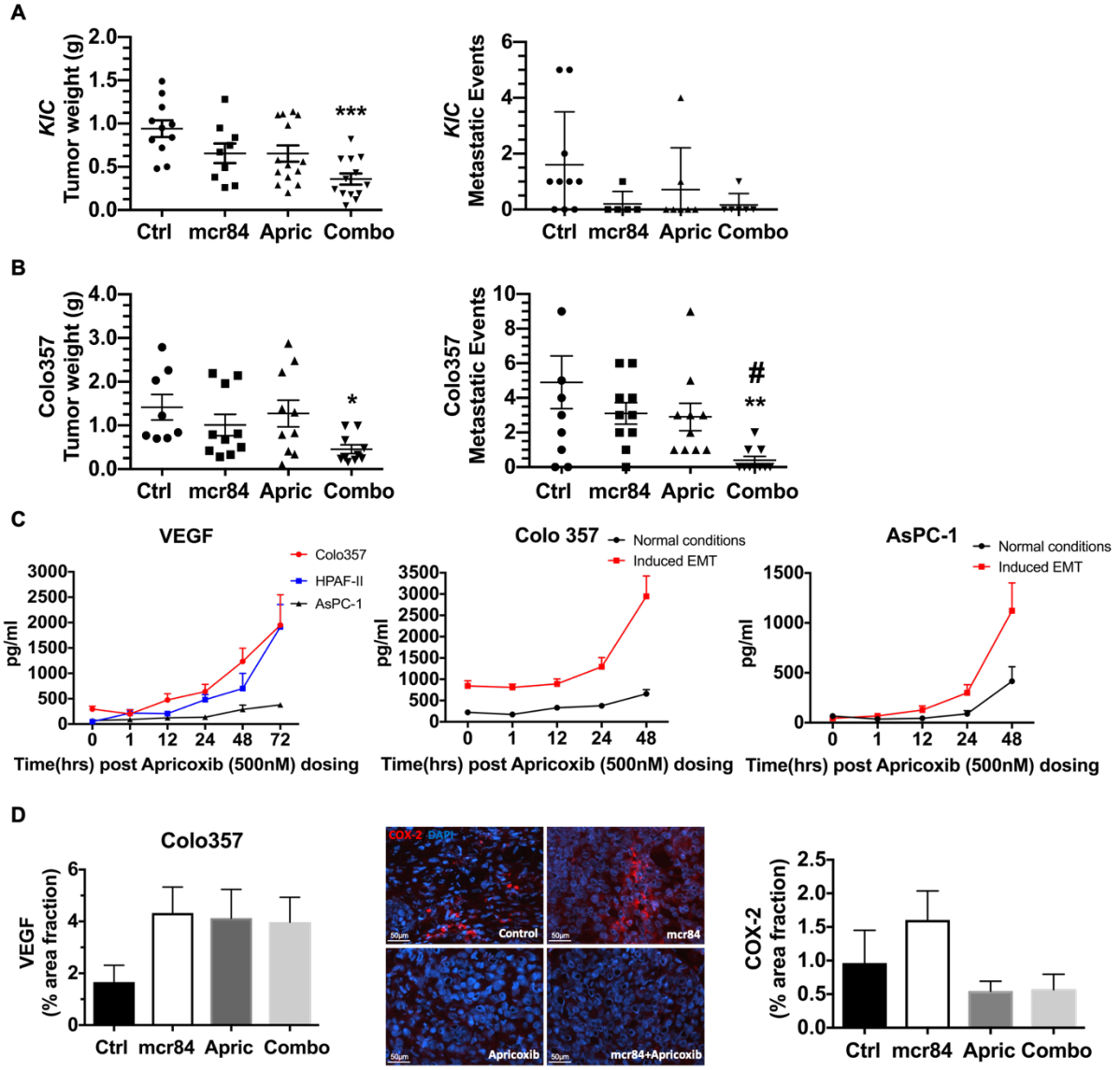

Figure 1. Combination therapy with apricoxib and mcr84 reduced tumor growth and metastasis in murine models of pancreatic cancer. (A) At 3 weeks of age, *Kras*$^{LSL\text{-}G12D}$*; Cdkn2a*$^{fl/fl}$*; Ptf1a*$^{Cre/+}$ (*KIC*) mice were randomized to receive saline (n = 11), mcr84 (n = 10), apricoxib (n = 13), or mcr84 plus apricoxib (n = 13). All mice were sacrificed when they were 7 weeks old. Mean tumor weight and metastasis burden were compared. **(B)** A total of 1×10^6 Colo357 cells were injected orthotopically into NOD/SCID mice. Treatment began when established tumors were visible by ultrasound and consisted of control (n = 8), mcr84 (n = 10), apricoxib (n = 10) or mcr84 plus apricoxib (n = 10) and continued for 4 weeks, after which mean tumor weight and metastasis burden were shown. Data are displayed in a scatter plot with mean ± SEM. *$P < 0.05$, **$P < 0.01$, ***$P < 0.005$ vs. control; $^{\#}P < 0.05$ vs. single-agent mcr84 or apricoxib by ANOVA with Dunn's MCT. **(C)** Human pancreatic cancer cell lines,

HPAF-II, Colo357, and AsPC-1 were treated with 500 nM apricoxib and evaluated by ELISA for the production of VEGF. Colo357 and AsPC-1 were plated under normal conditions or conditions of forced EMT (50 ng/ml TGFβ on collagen I -coated plates for 24 hours). VEGF levels were evaluated by ELISA after 500 nM apricoxib treatment. Biological repeats have been performed (n=3) and data are displayed as mean ± SEM. Paraffin-embedded tumor sections from Colo357 tumor-bearing mice were analyzed for **(D)** VEGF and COX-2 expression by immunofluorescence. Quantification of percentage area fraction is shown. Data are displayed as mean ± SEM and represent 5 images per tumor with 3 animals per group. Representative images (COX-2, red; DAPI, blue) are shown for Colo357 tumors. Total magnification is 400X. Scale bars are presented as indicated.

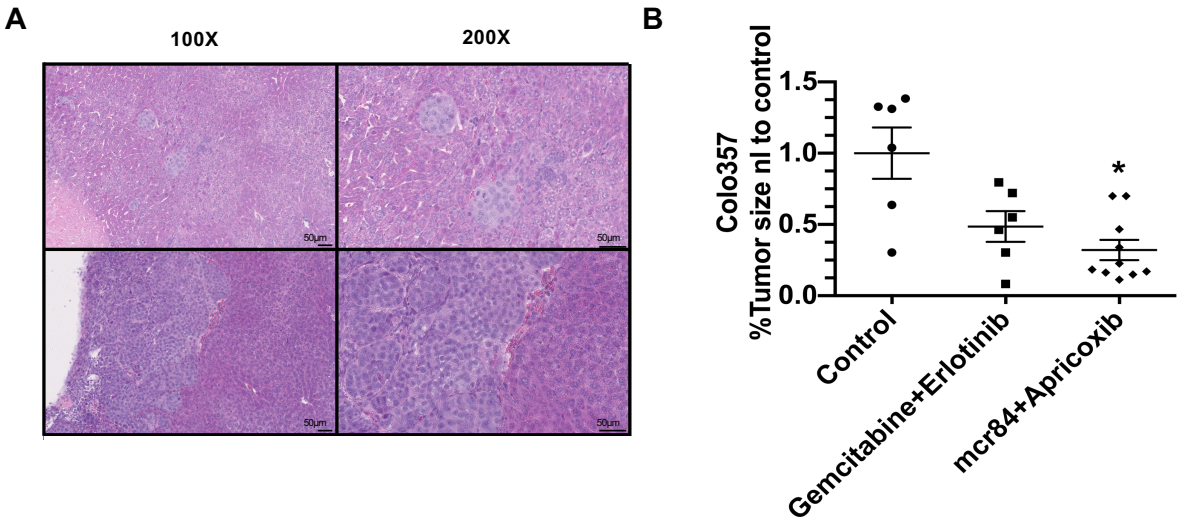

Figure 2. (A) Representative images of metastasis to the liver of control mice in Colo357 model was shown by H&E staining. Total magnifications are 100X and 200X. Scale bar, 50μm. **(B)** Colo357 human pancreatic cancer cells (1×10^6) were injected orthotopically into the pancreas of SCID mice. Treatment began when the established tumor was visible by ultrasound, and consisted of control (saline, n = 6), gemcitabine 25 mg/kg twice weekly plus erlotinib 100 μg daily (standard of care, n = 6) as described in Kirane et al. (29), or mcr84 plus apricoxib (n = 10) and continued for 3 weeks. Tumor weight was normalized to the control and data from the treatment groups were compared. Data are displayed as mean ± SEM. *$P < 0.05$ vs. control, by ANOVA with Dunn's MCT.

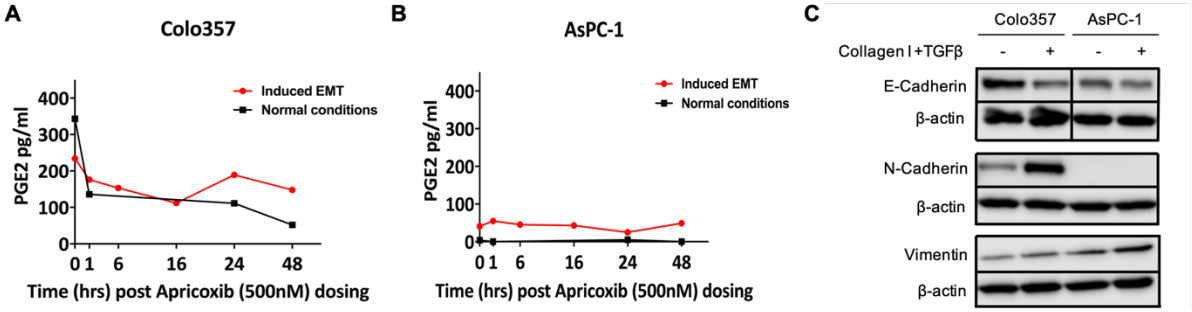

Figure 3. Human pancreatic cancer cell lines, Colo357 **(A)** and AsPc-1 **(B)** were plated either under normal conditions or under conditions of forced EMT (treated with 20 ng/mL TGFβ on collagen I -coated plates for 72 hours). PGE_2 levels were measured by ELISA after 500 nM apricoxib treatment. **(C)** Colo357 and AsPC-1 cells were plated under normal conditions or conditions of forced EMT (50 ng/ml TGFβ on collagen I -coated plates for 24 hours). Lysates were probed for the indicated targets by Western blotting. The induced EMT conditions promoted loss of E-Cadherin, gain of Vimentin expression. In Colo357, the expression of N-Cadherin was also upregulated by collagen I and TGFβ stimulation. β-actin was used as a loading control.

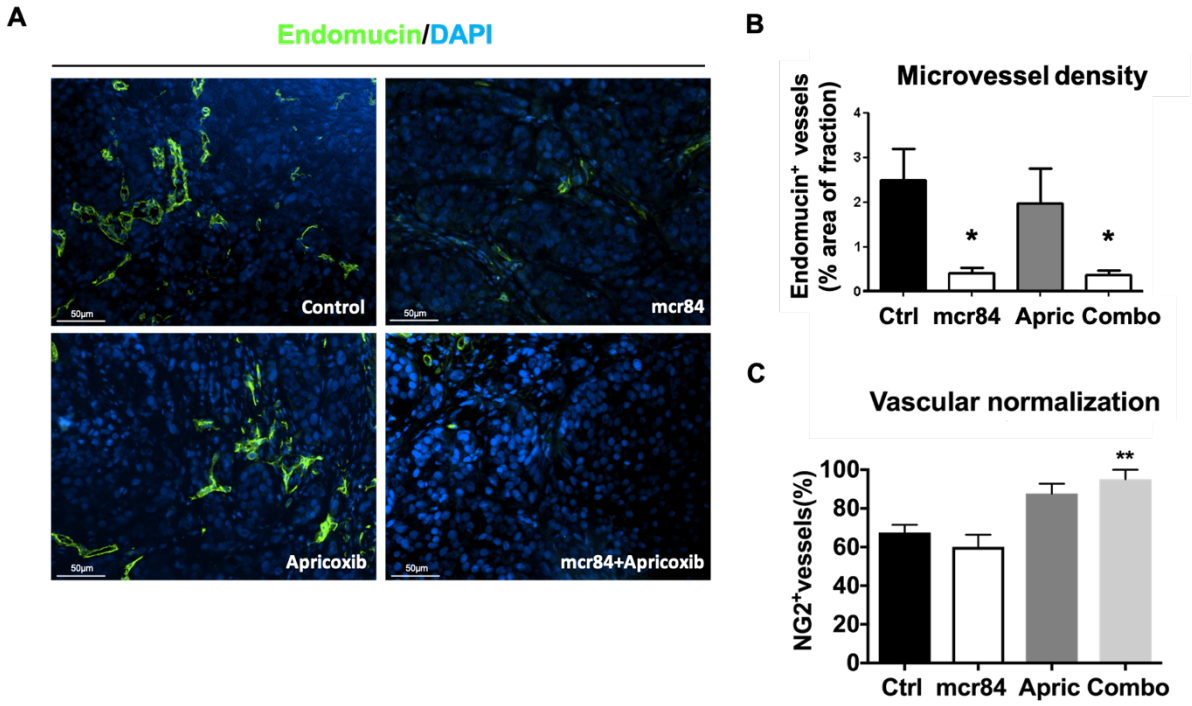

Figure 4. Microvessel density is not decreased by COX-2 inhibition. Paraffin-embedded tumor sections from Colo357 tumor-bearing mice were analyzed for endomucin **(A, B)** and

NG2 **(C)** expression by immunofluorescence. Quantification of percentage area fraction for endomucin is shown **(B)**. Data are displayed as mean ± SEM and represent 5 images per tumor with 3 animals per group. Representative images (endomucin, green; DAPI, blue) are shown for Colo357 tumors. Total magnification is 400X. **P* < 0.05, ***P* < 0.01 vs. control, by ANOVA with Dunn's MCT.

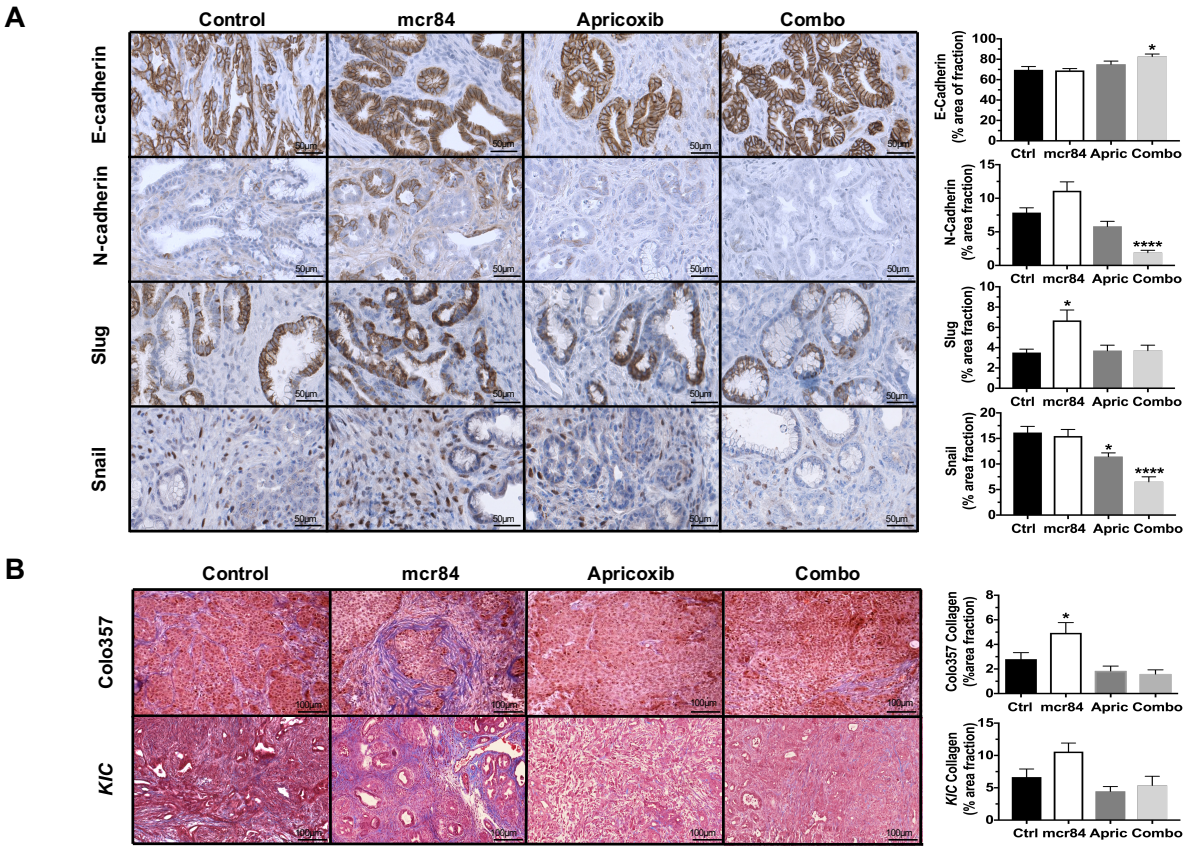

Figure 5. Apricoxib in combination with mcr84 reverses anti-VEGF–induced EMT and collagen deposition. (A) *KIC* pancreatic tissues from the treated mice underwent immunohistochemistry for E-cadherin, N-cadherin, Slug or Snail. Images are shown at 400X. Scale bars are presented as indicated. **(B)** Pancreatic tissues from Colo357 tumor-bearing mice and *KIC* mice were stained with Masson's trichrome. Total magnification is 200X. Scale bars are presented as indicated. The whole tumor areas were scanned with Hamamatsu Nanozoomer 2.0HT. Images of whole tumor areas were analyzed using ImageJ software. Quantification of percentage area fraction is shown. Data are displayed as mean ± SEM with 3 animals per group analyzed. **P* < 0.05, ***P* < 0.01, ****P* < 0.005 vs. control; by ANOVA with Dunn's MCT.

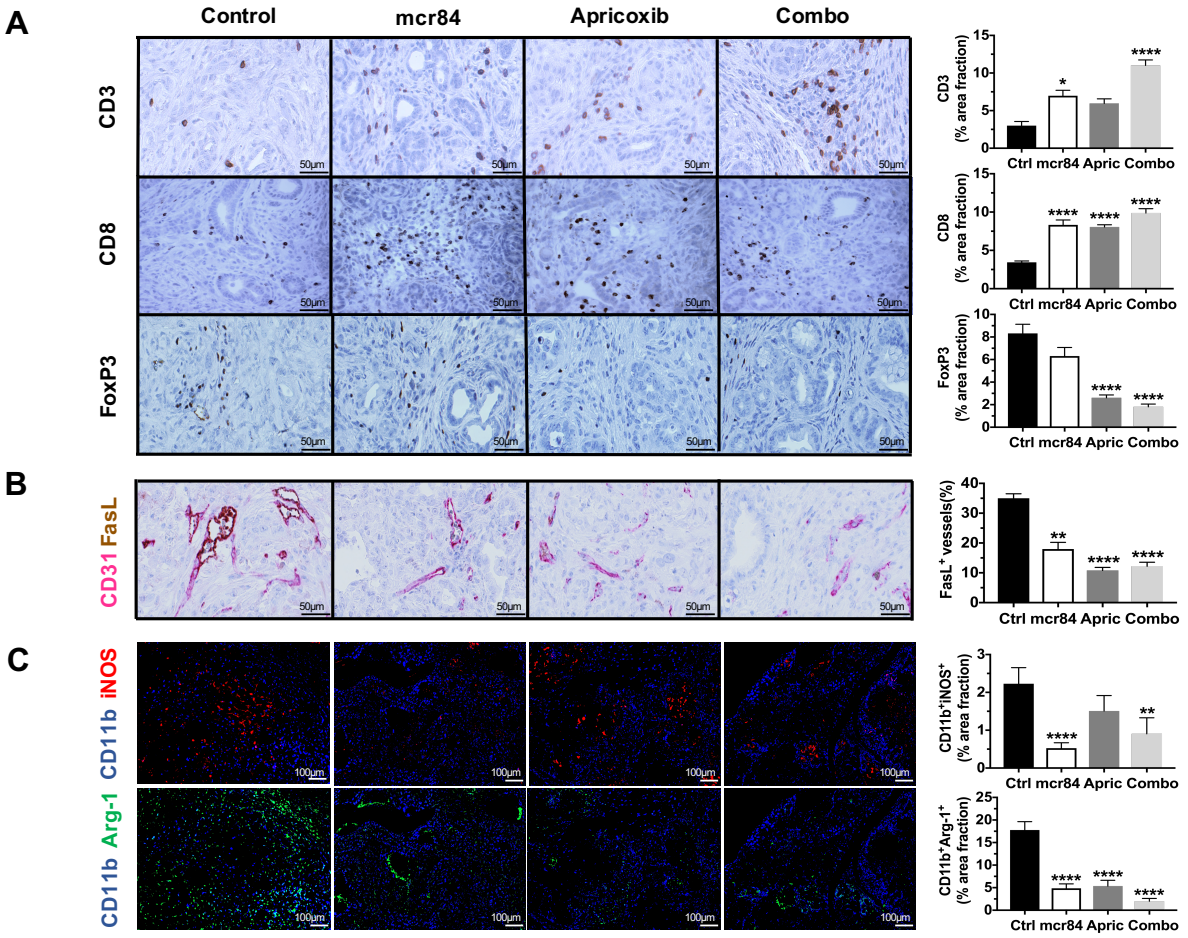

Figure 6. Combination blockade of VEGF and COX-2 pathway restores antitumor immunity. KIC pancreatic tissue was subjected to immunohistochemistry for **(A)** CD3, CD8, FoxP3, **(B)** CD31 and FasL, **(C)** CD11b and iNOS, CD11b and Arginase 1. The whole tumor areas were scanned with Hamamatsu Nanozoomer 2.0HT and Zeiss Aixoscan Z1. Images of whole tumor areas were analyzed using NIS Elements (Nikon) and Fiji software. Representative images are shown at 400X in **(A)** and **(B)**. Scale bars are presented as indicated. Schematic Quantification of percentage area fraction for each target in each treatment group is shown. Data are displayed as mean ± SEM with 3 animals per group analyzed. *P < 0.05, **P < 0.01, ***P < 0.005, ****P < 0.0001 vs. control, by ANOVA with Dunn's MCT.

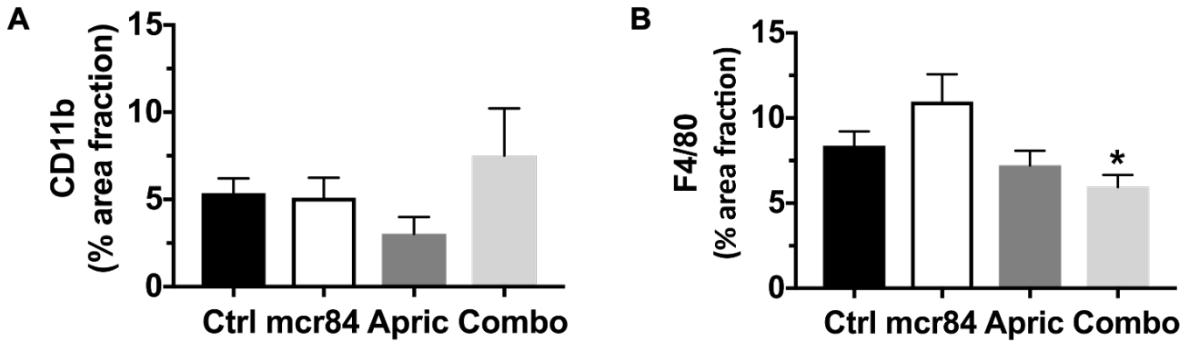

Figure 7. KIC pancreatic tissues from the treated mice were subjected to immunohistochemistry for **(A)** CD11b and **(B)** F4/80. Images were analyzed using NIS Elements (Nikon) and Fiji software. Quantification of percentage area fraction for each target in each treatment group is shown. Data are displayed as mean ± SEM and represent 5 images per tumor with 3 animals per group analyzed. *P < 0.05 vs. control, by ANOVA with Dunn's MCT.

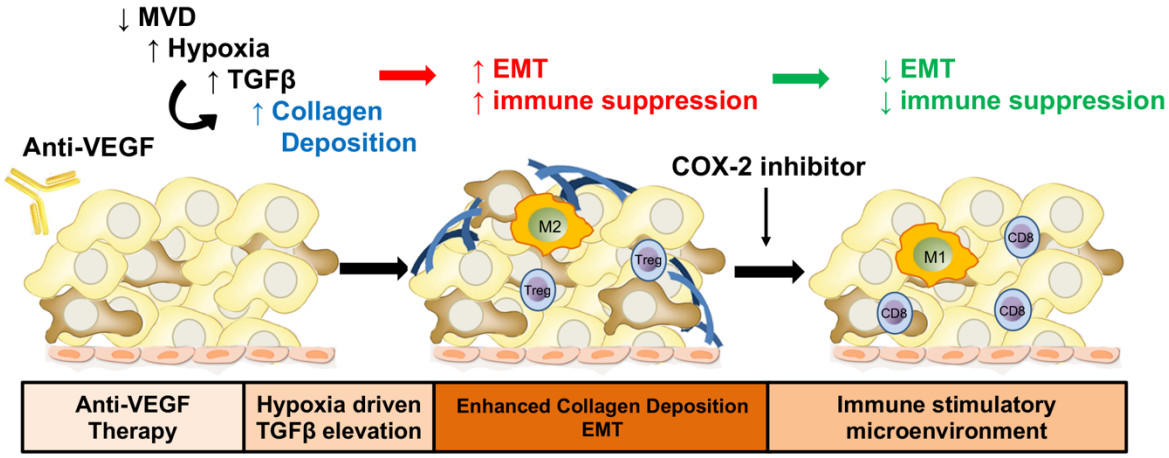

Figure 8. Anti-VEGF therapy results in reduced microvessel density, hypoxia induced TGFβ expression, epithelial plasticity and enhanced collagen deposition. These changes drive a mesenchymal-like tumor cell phenotype (brown tumor cells). TGFβ and EMT contribute to an immune suppressive microenvironment. Inhibition of COX-2 in combination with anti-VEGF therapy reduces EMT and promotes an immune stimulatory microenvironment that includes increased infiltrating $CD8^+$ T cells and decreased M2-like macrophages.

CHAPTER THREE

VEGFR2 ACTIVITY ON MYELOID CELLS MEDIATES IMMUNE SUPPRESSION IN THE TUMOR MICROENVIRONMENT

This chapter is based on a research article written by the author (Zhang et al, 2021)

3.1 Introduction

A malignant tumor that consists of rapidly dividing and growing cancer cells demands a dedicated blood supply to provide nutrients that support the growth and progression of the tumor. Angiogenesis can be induced by various growth factors secreted by cells in the tumor microenvironment, one such factor is vascular endothelial growth factor (VEGF)-A (hereafter referred as VEGF). VEGF induces endothelial cell survival, proliferation and migration, thus VEGF is a major driver of tumor neovascularization (177,217). The function of VEGF is mediated by binding to its receptor tyrosine kinases (RTKs) VEGFR1 and VEGFR2, with VEGFR2 (gene: *KDR, Flk-1*) being the dominant RTK that triggers VEGF-induced angiogenesis (217). Expression of VEGF, VEGFR1 and VEGFR2 are elevated in most solid tumors (14,217) and due to the importance of tumor angiogenesis, VEGF is an attractive therapeutic target. Multiple strategies have been developed to inhibit the VEGF pathway. Anti-angiogenic agents including small molecule inhibitors and monoclonal antibodies (mAbs) targeting VEGF (e.g, bevacizumab) or VEGFR2 (e.g., ramucirumab) are Federal Drug Administration (FDA)-approved for the treatment of renal cell carcinoma, colorectal cancer, gastric cancer and non-small cell lung cancer (NSCLC) and a number of other indications (6).

However, anti-angiogenic strategies used as a single agent generally provide modest efficacy in cancer patients due to insufficient response, therapy resistance and tumor adaptation (181,184,218).

Cancer immunotherapy is a breakthrough in the field of cancer therapy, with strategies disrupting immune checkpoint pathways being particularly effective in a subset of patients (3). Blocking immune checkpoint molecules can reverse tumor immune suppression, activate tumor cell specific cytotoxic $CD8^+$ T cells and trigger adaptive anti-tumor immune responses (3). Antagonistic mAbs specific for programmed cell death protein 1 (PD-1) and its ligand programmed cell death 1-ligand 1 (PD-L1) have shown efficacy and have been approved by the FDA for use in a variety of cancer types (6). However, immunotherapies, mainly immune checkpoint inhibitors (ICIs), are more effective in tumors with preexisting tumor-infiltrating lymphocytes (TILs) and an inflammatory microenvironment, thus clinical benefit with ICIs is often limited to a fraction of cancer patients (9). Multiple strategies are being investigated to reduce the immunosuppressive microenvironment of tumors in an effort to enhance the efficacy of ICIs (3,219). Angiogenesis and immunosuppression can occur in parallel, facilitating tumor development and progression (220). Indeed, multiple angiogenic factors, especially VEGF have been shown to have immunosuppressive functions and high VEGF expression is reported to be associated with the suppression of anti-tumor immune activity in cancer patients (6,14). Given the potential immune stimulatory effects of anti-angiogenic therapies, preclinical and clinical studies have investigated the therapeutic effects of combining anti-angiogenic reagents with ICIs (6). Therefore, understanding the mechanism of how anti-

angiogenic and in particular anti-VEGF therapies affect tumor immunity and ICI activity is urgent.

Although VEGFRs were initially considered to be expressed exclusively on endothelial cells, it is now appreciated that VEGFRs are also expressed on other cell types, including some tumor cells, dendritic cells (DCs), tumor-associated macrophages (TAMs) and T cells (25,26,44). Thus, VEGF can directly influence immune cell phenotype and function. For example, VEGF stimulation of VEGFR2 can inhibit dendritic cell maturation, thus reducing tumor neoantigen presentation (61,221). In addition, VEGF has been reported to directly suppress effector T cell proliferation and activation through VEGFR2 (45). It has also been demonstrated that VEGF contributes to $CD8^+$ T cell exhaustion by upregulating immune checkpoint molecules expression including PD-1, cytotoxic T-lymphocyte-associated antigen 4 (CTLA-4) and T-cell immunoglobulin mucin receptor 3 (Tim-3) (43). In contrast, VEGF stimulation of VEGFR2 on regulatory T cells (Tregs) results in proliferation (53). Furthermore, VEGF can affect immune cells and the immune system indirectly through modulation of the tumor endothelium (2).

In earlier studies, we and others have shown selective elevation of VEGFR2 expression on myeloid-derived suppressor cells (MDSCs) and macrophages in tumor-bearing animals (14,26,222). However, the function of $VEGFR2^+$ myeloid cells and their contribution to tumor immunosuppression is not understood. Previously, our lab developed a fully human mAb (r84) specific for VEGF that disrupts VEGF binding to VEGFR2 but does not disrupt VEGF-

VEGFR1 interaction (217,223). Prior work from our group and others have demonstrated that r84 alone or in combination with standard therapy controls the growth of primary tumors in multiple indications with limited toxicity (184,217,224). Here, by using mouse chimeric r84 (mcr84) that specifically inhibits the mouse VEGF-VEGFR2 axis and a genetic mouse model with VEGFR2 specific ablation on myeloid cells, I investigate the function of $VEGFR2^{+}$ myeloid cells in modulating tumor immunity and provide a comprehensive investigation of how VEGFR2 blockade facilitates an anti-tumor immune response. I show that VEGFR2 activity on myeloid cells mediates immunosuppression and that inhibition of VEGFR2 signaling results in reduction of PD-L1 expression on myeloid cells and contributes to reinvigorated T cell activation in the tumor microenvironment, which improves response to ICI.

3.2 Results

3.2.1 Inhibition of VEGF activation of VEGFR2 by mcr84 delays tumor progression and reduces the vascular immune barrier

We have previously demonstrated the effect of different anti-VEGF strategies on the growth of breast cancer xenografts and mouse syngeneic models (101). To evaluate the effect of mcr84 on the tumor immune landscape, I studied 4T1 and E0771 breast tumors implanted orthotopically in female C57BL/6 and BALB/c mice respectively and MC38 mouse colon tumors implanted subcutaneously in C57BL/6 mice. Mice-bearing established tumors were treated with mcr84 or an isotype-matched control IgG (C44) until the tumor volume in the control group reached 2000 mm^3. In all three models, VEGF blockade by mcr84 modestly

suppressed tumor growth as a single agent (Figure 9, A-C). mcr84 as a single agent also reduced metastasis to lungs in mice bearing 4T1 tumors (Figure 9D). In addition, I harvested tumors of similar size from these two groups, mcr84 treatment delayed 4T1 and MC38 tumor progression (Figure 10, A and B).

To determine the effect of mcr84 on angiogenesis, I analyzed tumor microvessel density and vessel maturation by immunohistochemistry. In 4T1 tumors, overall vascular area, marked by CD31, was decreased significantly by mcr84 compared to control-treated tumors (Figure 9E), consistent with previous studies (101). Since immature blood vessels without pericytes support tend to be more vulnerable to anti-VEGF therapies (225), I performed double staining of CD31 and the pericyte marker NG2 and observed that mcr84 increased pericyte coverage of the remaining tumor vessels (Figure 9E), which is typically associated with improved vascular function (12). In addition to nutrient and oxygen delivery, functional blood vessels also facilitate immune cell infiltration, which involves homing of immune cells, adhesion to the endothelium and diapedesis mediated by chemokines (2). Angiogenic factors can regulate the expression of adhesion molecules or secretion of chemokines by tumor endothelium which limit T cell attachment to the vessel and efficient T cell infiltration (28). I found that inhibition of VEGF with mcr84 elevated the expression of vascular cell adhesion protein 1 (VCAM-1) and intercellular adhesion molecule 1 (ICAM-1) on tumor endothelium in 4T1 tumors (Figure 9E). I also found that mc84 reduced microvessel density, and consistently upregulated adhesion molecule expression on tumor endothelium in MC38 tumors (Figure 10, C and D). These changes in tumor vasculature were confirmed by flow cytometry of 4T1 tumors after

short term treatment (one week) (Figure 10E). Furthermore, we and others have reported that VEGF can increase the expression of the death mediator Fas ligand (FasL) on tumor associated endothelial cells and this can reduce T cell infiltration (54,226). Here I confirmed that mcr84 suppressed FasL expression on tumor endothelium in 4T1 tumors (Figure 9E).

Together, these results demonstrate the single agent effect of mcr84 on control of tumor progression in multiple syngeneic models. Importantly, VEGF blockade effectively inhibited angiogenesis while increasing pericyte coverage and modulating tumor endothelium, resulting in a vasculature that supports immune cell trafficking.

3.2.2 Expression of VEGFR2 on myeloid cells is elevated specifically in tumor-bearing animals and is associated with an immunosuppressive myeloid phenotype

Different from VEGFR1, which has been widely acknowledged to be expressed by macrophages and other myeloid cells, myeloid cells express low to no VEGFR2 under normal conditions (26). Previously, we identified a subset of macrophages expressing VEGFR2 only in tumor-bearing animals (26). We found that VEGF was a potent chemoattractant for $VEGFR2^+$ macrophages and that selectively inhibiting VEGF binding to VEGFR2 decreased the recruitment of $VEGFR2^+$ macrophages (26). Consistent with preclinical studies, $CD45^{bright}/CD14^+$ monocytes expressing VEGFR2 become dominant in circulating blood from cancer patients compared to healthy donors (96). Recent studies have extended our findings to multiple indications. In an ovarian tumor model, in contrast to $VEGFR1^+$ MDSCs whose proportion remains unchanged across organs, the frequency of $VEGFR2^+$ MDSCs increases

significantly in tumors, indicating the importance of VEGFR2 for recruitment of MDSCs (14). However, the functional significance of VEGFR2 expression and activity of myeloid cells remains unclear.

I examined the expression level of VEGFR1 and VEGFR2 on bone marrow (BM)-derived macrophages (BM-MQs) and MDSCs (BM-MDSCs) in syngeneic murine cancer models, MC38, E0771 and 4T1 (Figure 11A). VEGFR1 expression was similar in myeloid cells from non-tumor-bearing (NTB) and tumor-bearing (TB) animals; however, VEGFR2 was elevated on BM-MQs and BM-MDSCs from TB mice (Figure 11B). Increased VEGFR2 expression on myeloid cells in TB mice was verified at protein level by flow cytometric analysis of BM-myeloid cells including total $CD11b^+$ myeloid cells, macrophages, M-MDSCs and PMN-MDSCs (Figure 12A). BM-myeloid cells from *Csf1r-Cre*$^+$ *Flk-1*$^{fl/fl}$ animals were used as a negative control. In addition, I sorted $Gr\text{-}1^+Ly\text{-}6G^+$ MDSCs from splenocytes of NTB and TB mice and found VEGFR2 was upregulated on splenic MDSCs from TB animals (Figure 12B). These results are consistent with our prior findings that VEGFR2 is expressed by macrophages in mice bearing pancreatic or breast tumors (26). I further compared the phenotype of BM-myeloid cells from NTB and TB mice. In 4T1 and MC38 models, higher baseline level of PD-L1 was observed in BM-$Ly6C^+Ly6G^-$, $Ly6C^+Ly6G^+$ and $F4/80^+$ myeloid cells (Figure 11, C and D). Furthermore, BM-MQs from TB mice showed decreased iNOS expression but an elevated $Arg\text{-}1^+/iNOS^+$ ratio (Figure 11, E and F). Moreover, after injecting a MMTV-PyMT-derived breast cancer cell line, F246-6 into control *Flk-1*$^{fl/fl}$ and *Csf1r-Cre*$^+$ *Flk-1*$^{fl/fl}$ mice, in which *Vegfr2* (*Flk-1*) was specifically ablated in $CSF1R^+$ myeloid cells, I harvested the bone

marrow from *Cre*$^{-}$ and *Cre*$^{+}$ littermates and differentiated into macrophages or MDSCs in vitro. Interestingly, elevated PD-L1 and Arg-1 expression in BM-MQs and M-MDSCs from TB mice were lowered in those from *Cre*$^{+}$ TB mice (Figure 12, C and D), indicating the involvement of VEGFR2 in mediating PD-L1 and Arg-1 expression.

To demonstrate the immunosuppressive function of VEGFR2^{+} myeloid cells, I co-cultured BM-myeloid cells from NTB mice, MC38, *Flk-1*$^{fl/fl}$ and *Csf1r-Cre*$^{+}$ *Flk-1*$^{fl/fl}$ TB mice with CFSE labeled wild-type CD8^{+} T cells. The proliferation of CD8^{+} T cells was inhibited by BM-myeloid cells from NTB mice in a dose-dependent manner (Figure 11G), and the inhibition effect was further enhanced by myeloid cells from TB animals (Figure 12E). However, specific deletion of *Vegfr2* in myeloid cells, partially rescued the effect (Figure 12E). Consistent findings were observed by analyzing Ki67 level in proliferating CD8^{+} T cells (Figure 12F).

To further characterize the phenotype of myeloid cells with elevated expression of VEGFR2, I utilized a CD11b^{+}Gr1^{+} MDSC-like cell line J774M (227) and expressed human VEGFR2, *KDR*, by lentiviral infection. Two clones with high KDR expression were chosen: J774M-KDR (A6) and J774M-KDR (F6) (Figure 13A). J774M-Ctrl cells were infected with an empty vector. Interestingly, J774M-KDR (A6) and J774M-KDR (F6) cells demonstrated macrophage phenotype with decreased Ly-6C and Ly-6G expression but increased F4/80 expression (Figure 13B). Meanwhile, J774M-KDR cells have higher baseline levels of PD-L1 expression on Ly6C^{+}Ly6G^{-}, Ly6C^{+}Ly6G^{+} and F4/80^{+} subpopulations (Figure 12G). J774M-KDR cells also exhibited an enhanced immunosuppressive phenotype evidenced by elevated Arg-1

expression but decreased iNOS and MHCII expression (Figure 12H). To test the function of the secretome of J774M-KDR, I treated $CD8^+$ T cell with conditioned medium harvested from J774M and J774M-KDR cells and found the conditioned medium from J774M-KDR inhibited $CD8^+$ T cell proliferation (Figure 13, C and D). Overall, results using BM-myeloid cells from *Csf1r-Cre*$^+$ *Flk-1*$^{fl/fl}$ mice and VEGFR2 overexpressing J774M cells demonstrate that elevated VEGFR2 expression on myeloid cells in TB animals is associated with their immunosuppressive phenotype and T-cell suppressive function.

3.2.3 VEGFR2 specific blockade reduces the immunosuppressive function of tumor-infiltrating myeloid cells

Given that I have observed the expression of VEGFR2 on myeloid cells results in an immunosuppressive phenotype in vitro (Figure 12, C-H), I analyzed how VEGF-VEGFR2 specific blockade affects the phenotype of infiltrating myeloid cells in 4T1 tumors. By performing flow cytometry, I identified that consistent with the in vitro assay (Figure 12, C and G), the expression of PD-L1 on two populations of MDSCs ($Ly6G^+Ly6C^{dim}$ PMN-MDSCs and $Ly6G^-Ly6C^+$ M-MDSCs) in the tumors was significantly downregulated by treatment with mcr84 (Figure 14, A-C). Importantly, I observed the decrease of PD-L1 was myeloid cell specific since I did not find a decrease of PD-L1 expression in non-myeloid cell populations (Figure 14D). I investigated PD-L1 expression in other myeloid cell types and found that downregulation of PD-L1 was a general phenomenon in myeloid cells, including $CD11b^+$ cells (Figure 14E), Ly-$6C^+$ cells, Ly-$6G^{high}$ cells, total MDSCs and neutrophils (Figure 15A). However, PD-L1 expression on $CD31^+$ endothelial cells and $EpCAM^+$ tumor cells remained

unchanged, while there was a trend of decrease in $CD45^+$ cells (Figure 15B). Interestingly, I found that mcr84 treatment reduced PD-L1 expression on splenic myeloid cells (Figure 15C), indicating a systemic effect of VEGF blockade on PD-L1 expression. Results in the 4T1 model were generally recapitulated in MC38 (Figure 14, F-I) and E0771 tumors (Figure 15, D-G). Similarly, I did not detect PD-L1 downregulation on endothelial cells nor tumor cells in the MC38 model (Figure 15H). However, in MC38 model, mcr84 treatment induced a significant decrease of PD-L1 on $CD45^+$ cells, which was mainly due to the myeloid component (Figure 15H). In addition, I found mcr84 treatment suppressed MDSC accumulation in E0771 tumors (Figure 15, D and E). To evaluate if the downregulated PD-L1 expression contributes to reversed immunosuppressive phenotype of tumor-infiltrating MDSCs, I sorted $Gr\text{-}1^+Ly\text{-}6G^+$ MDSCs from C44/mcr84 treated tumors using an MDSC isolation kit and co-cultured with anti-CD3/CD28 stimulated wild-type $CD8^+$ T cells at different ratios. The purity of sorted MDSCs was confirmed by flow cytometry (Figure 15I). Using cells from 4T1 and MC38 models, MDSCs isolated from mcr84 treated tumors demonstrated less suppressive capacity with higher percentage of $Ki67^+$ proliferating $CD8^+$ T cells in co-culture (Figure 14, J and K), indicating VEGF blockade by mcr84 resulted in less suppressive tumor-infiltrating MDSCs.

I also analyzed the phenotype of tumor-infiltrating myeloid cells by immunohistochemistry. I found that mcr84 limited macrophage infiltration and altered macrophage phenotype towards $iNOS^+$ immunostimulatory macrophages with decreased Arg-1 expression in 4T1 tumors (Figure 16A). As expected, I found that tumor cell conditioned media induced high Arg-1 expression on BM-myeloid cells from NTB mice, a response that is not sensitive to VEGF

blockade (Figure 16B). However, BM-MQs differentiated from 4T1 TB animals that were treated with mcr84 demonstrated decreased Arg-1 expression and lower Arg-1^{+}/iNOS+ ratio compared to TB animals treated with an isotype control antibody (Figure 16C). These findings indicate that VEGF inhibition has an effect on bone marrow differentiation where it contributes to macrophage polarization. These results were recapitulated in TAMs from MC38 bearing mice (Figure 16D). Furthermore, in MC38 tumors, mcr84 increased MHCII expression on conventional DCs (cDCs), which are the professional antigen-presenting cells (228), suggesting VEGF blockade enhances the maturation and antigen-presenting capacity of DCs (Figure 16E). In summary, these in vivo data support the in vitro observations and suggest that VEGF drives an immunosuppressive phenotype in tumor specific $VEGFR2^{+}$ myeloid cells and that blockade of VEGF activation of VEGFR2 on myeloid cells can reduce myeloid immunosuppressive function.

3.2.4 VEGF directly upregulates PD-L1 expression on myeloid cells through VEGFR2

Since I had observed a consistent decrease of PD-L1 expression on myeloid cells across different syngeneic animal models after treatment with mcr84, I investigated whether this was a direct or indirect consequence. Firstly, I analyzed the level of IFN-γ, a major inducer of PD-L1, in lysates from control and mcr84-treated tumors. Surprisingly, I found that the level of intra-tumoral IFN-γ was elevated after mcr84 treatment (Figure 17A), highlighting that the decrease of PD-L1 on tumor associated myeloid cells was not due to a reduction of IFN-γ in the tumor microenvironment. Therefore, I directly stimulated BM-myeloid cells from NTB mice with IFN- γ and VEGF with/without mcr84. As expected, IFN-γ alone elevated PD-L1

expression; however, VEGF +/- mcr84 did not affect PD-L1 expression. These results indicate that the downregulation of PD-L1 by mcr84 is independent of IFN-γ (Figure 16, F and G). Given the fact that anti-VEGF therapy disrupted tumor blood vessels, I evaluated whether the modulation of VEGFR2 signaling in endothelial cells could alter the endothelial cell secretome, thus changing PD-L1 expression on myeloid cells. I added conditioned media from mouse bEnd.3 endothelial cells stimulated with VEGF +/- mcr84 to the differentiation media of BM-MDSCs (Figure 17B). PD-L1 level on BM-MDSCs was then analyzed by flow cytometry. Although conditioned media alone slightly induced PD-L1 expression on BM-MDSCs, the expression level remained similar regardless of activation or inhibition of VEGFR2 signaling on endothelial cells (Figure 17C).

To determine if VEGF-VEGFR2 signaling on myeloid cells directly enhances PD-L1 expression, Gr-1^{+}Ly-6G^{+} MDSCs were sorted from splenocytes of NTB and TB mice and treated with VEGF for 24 hours. I found that PD-L1 expression level was elevated by VEGF on splenic MDSCs from TB mice compared to MDSCs from NTB mice (Figure 17D). To confirm the effect of VEGF, similar experiments were performed using splenic Gr-1^{dim}Ly-6G^{-} M-MDSCs isolated from *Flk-1$^{fl/fl}$* and *Csf1r-Cre^{+} Flk-1$^{fl/fl}$* TB mice. Consistent with Gr-1^{+}Ly-6G^{+} MDSCs, I found PD-L1 expression was stimulated by VEGF in MDSCs from *Flk-1$^{fl/fl}$* mice, however, VEGF treatment did not change PD-L1 expression in splenic MDSCs from *Csf1r-Cre^{+} Flk-1$^{fl/fl}$* mice (Figure 17E). In addition, in CD11b^{+}Ly6G^{+} MDSCs sorted from tumors, stimulation with VEGF led to a substantial increase of PD-L1 expression in both 4T1 and E0771 models (Figure 17F).

To further confirm the direct effect of mcr84 on myeloid cell PD-L1 expression in vivo, I implanted F246-6 breast cancer cell line in *Flk-1*$^{fl/fl}$ or *Csf1r-Cre*$^{+}$ *Flk-1*$^{fl/fl}$ mice. Mice with established tumors were randomized to receive control IgG or mcr84. First, I found that consistent with earlier results (Figure 9, A-C), mcr84 alone slowed tumor growth in *Flk-1*$^{fl/fl}$ control animals; however, ablation of *Vegfr2* on myeloid cells abrogated the efficacy of mcr84 (Figure 18A). In addition, I found that the effect of mcr84 on reducing total vessel density was also lost in the absence of *Vegfr2* on myeloid cells (Figure 18B). These data demonstrate that VEGFR2^{+} myeloid cells are important in the efficacy of anti-VEGF therapy. I also analyzed macrophage infiltration and phenotype by IHC and flow cytometry. I found that loss of *Vegfr2* on myeloid cells resulted in reduced macrophage tumor infiltration similar with mcr84 treatment while in the absence of *Vegfr2*, mcr84 did not reduce macrophage infiltration (Figure 18, C and D). I also observed decreased Arg-1 expression on macrophages and PMN-MDSCs with ablation of *Vegfr2* on myeloid cells (Figure 18E). I then assessed PD-L1 expression on myeloid cells by flow cytometry. Consistently, in multiple myeloid cell types including total CD11b^{+} myeloid cells, PMN-MDSCs, M-MDSCs and macrophages, mcr84 treatment significantly downregulated PD-L1 expression regardless of the relative frequency of the myeloid cell population in control mice (Figure 17, G-J). In contrast, *Csf1r-Cre*$^{+}$ *Flk-1*$^{fl/fl}$ mice had reduced levels of PD-L1 on myeloid cells compared to control mice and VEGF blockade by mcr84 did not further reduce PD-L1 expression (Figure 17, G-J). These findings support the in vitro data (Figure 17, D-F) and demonstrate that the downregulation of PD-L1 on

myeloid cells by VEGF blockade is a direct effect of inhibiting the VEGF-VEGFR2 signaling on myeloid cells.

Moreover, I also analyzed the phenotype of tumor-infiltrating T cells in *Flk-1$^{fl/fl}$* and *Csf1r-Cre^{+} Flk-1$^{fl/fl}$* TB mice. Although I found that loss of *Vegfr2* resulted in downregulation of immune checkpoint inhibitory receptors PD-1 and CTLA-4 expression on CD8^{+} T cells (Figure 18F), the total abundance of T cells and PD-1^{-}Ki67^{+} effector T cells were unchanged between these two groups (Figure 18, G and H). Functionally, splenocytes from *Csf1r-Cre^{+} Flk-1$^{fl/fl}$* TB mice have similar cytotoxic activity as those from *Flk-1$^{fl/fl}$* mice when co-cultured with parental F246-6 cells (Figure 18I).

3.2.5 VEGF blockade by mcr84 promotes perivascular accumulation of T cells and stimulates T cell activation

Since VEGFR2 specific blockade by mcr84 results in a tumor vasculature that favors immune cell trafficking and reduces the immunosuppressive phenotype of myeloid cells, I analyzed T cell infiltration and activation in tumors after treatment with mcr84. Flow cytometry and IHC showed an increase of CD3^{+} and CD8^{+} T cells one-week after the initiation of mcr84 therapy in 4T1 tumors (Figure 19A). In addition, distribution analysis of CD8^{+} T cells by IHC indicated that VEGF blockade promoted the perivascular accumulation of T cells in 4T1 tumors (Fig. 19B). These data support that VEGF blockade reduces the vascular immune barrier (139) and results in elevated T cell tumor infiltration. Moreover, I performed IHC analysis of liver metastasis from colorectal cancer patients receiving chemotherapy alone or chemotherapy

combined with avastin (bevacizumab) and found that VEGF blockade led to increased $CD3^+$ and $CD8^+$ T cell infiltration into metastatic sites (Figure 20A). Consistent with preclinical data, avastin treatment in colorectal cancer patients resulted in decreased recruitment of macrophages to liver metastases and downregulated PD-L1 expression on macrophages (Figure 20, B and C).

To evaluate whether 4T1 tumor-infiltrating T cells were functionally active, I analyzed the expression of immune checkpoint inhibitory receptors PD-1, CTLA-4, T-box transcription factor EOMES and cytokine production of intratumoral $CD8^+$ T cells by flow cytometry. I found that mcr84 treatment markedly decreased expression of PD-1, CTLA-4 and EOMES on $CD8^+$ T cells, suggesting a reduced exhaustion status of cytotoxic T lymphocytes (CTLs) (Figure 19C). Meanwhile, mcr84 significantly increased the proportion of $CD8^+$ T cells expressing IFN-γ and granzyme B (Figure 19D). Similarly, $CD8^+$ T cells in mcr84-treated MC38 tumors also exhibited an activated phenotype with elevated expression level of IFN-γ and TNF-α (Figure 19, E and F). Additionally, the ratio of T-effector cells to exhausted T cells was increased after VEGF blockade in 4T1 and MC38 tumors (Figure 19G). Furthermore, mcr84 inhibited Treg infiltration in 4T1 and MC38 tumors (Figure 19H) while elevating CTLA-4 expression on Tregs (Figure 20, D and E). These data suggest that the function of cytotoxic $CD8^+$ T cells was enhanced by VEGF blockade.

I then performed an in vitro cell cytotoxicity assay to evaluate the activity of CTLs from 4T1 and MC38 tumor-bearing mice after treatment with mcr84 or control IgG. Splenocytes from

mAb-treated mice were stimulated with plate-bound anti-CD3 and soluble anti-CD28 antibodies and co-cultured with CFSE-labeled 4T1 or MC38 tumor cells at different ratios. After 72 hours of co-culture, dead cells were labeled by 7-AAD and cells were analyzed by flow cytometry. Splenocytes from mcr84-treated mice had a higher level of cytotoxic activity in both models (Figure 19, I and J), suggesting that mcr84 treatment facilitates priming of CTLs. This phenotype was replicated by co-culturing sorted $CD8^+$ T cells from splenocytes of MC38 TB mice with parental MC38 tumor cells (Figure 20F). To demonstrate if the cytotoxic activity of splenocytes is antigen dependent, I implanted MC38 tumor cells subcutaneously into OT-1 mice and treated the mice with C44 or mcr84 after tumor established. MC38 tumor growth was faster in OT-1 mice since T cells were designed to recognize certain ovalbumin peptide (Figure 20G). $CD8^+$ T cells were isolated from splenocytes of mAb-treated mice and co-cultured with CFSE-labeled MC38-OVA tumor cells or MC38 parental cells at different ratios. Dead cells were then analyzed after 48 hours of co-culture. I found the cytotoxic capacity of $CD8^+$ T cells sorted from mcr84-treated mice was higher than those from C44-treated in the co-culture of MC38-OVA cells (Figure 19K), indicating antigen-specific cytotoxic activity. However, no significance was observed between $CD8^+$ T cells of different treatments in the co-culture of MC38 parental cells and in general, $CD8^+$ T cells exhibited low cytotoxic activity against MC38 cells (Figure 20H). Consistent with the in vitro cell cytotoxicity assay, histological analysis of in vivo 4T1 and MC38 tumors demonstrated that mcr84 treated tumors showed elevated cleaved caspase-3 (CC3) in the 4T1 model indicating increased tumor cell death and decreased Ki67 expression in the 4T1 and MC38 models (Figure 20, I and J).

Taken together, my data suggest that inhibition of VEGF-VEGFR2 signaling stimulates the activation of tumor-infiltrating T cells and facilitates the functional activity of CTLs in tumor-bearing animals, which might be attributed to the inhibition of $VEGFR2^+$ immunosuppressive myeloid cells.

3.2.6 VEGF blockade enhances the efficacy of CTLA-4 blockade in tumors

Given the fact that treatment with mcr84 results in the downregulation of PD-L1 on myeloid cells but upregulation of CTLA-4 on Tregs in multiple models (Figure 20, D and E), I sought to evaluate the therapeutic efficacy of combining VEGF blockade with PD-1 or CTLA-4 inhibition in 4T1 tumors. I found that mcr84 significantly enhanced the efficacy of CTLA-4 but not PD-1 blockade (Figure 21, A-C). These results are consistent with the data that PD-L1 on myeloid cells were downregulated by VEGF inhibition.

Moreover, I performed IHC and found that combination of mcr84 and anti-CTLA-4 reduced microvessel density, increased pericyte coverage of blood vessels, increased the expression ICAM-1 and importantly, increased $CD3^+$ T cell and $CD8^+$ cytotoxic T cell infiltration into tumors (Figure 22, A-D). At the same time, $FoxP3^+$ regulatory T cell and macrophage infiltration were significantly decreased by mcr84 and the combination therapy (Figure 22, E and F). Consistent with the earlier results, mcr84 in combination with anti-CTLA-4 also decreased immunosuppressive $Arg\text{-}1^+$ and increased immunostimulatory $iNOS^+$ macrophages (Figure 22, G and H). These results suggest that VEGF blockade potentiates the efficacy of

anti-CTLA-4 therapy by increasing T cell infiltration and polarizing macrophages to an immunostimulatory phenotype. Collectively, my findings provide a rationale for combining anti-VEGF therapy with ICIs and indicate potential possibility of combining VEGFR2 inhibition with immune checkpoint blockade other than anti-PD-1/PD-L1.

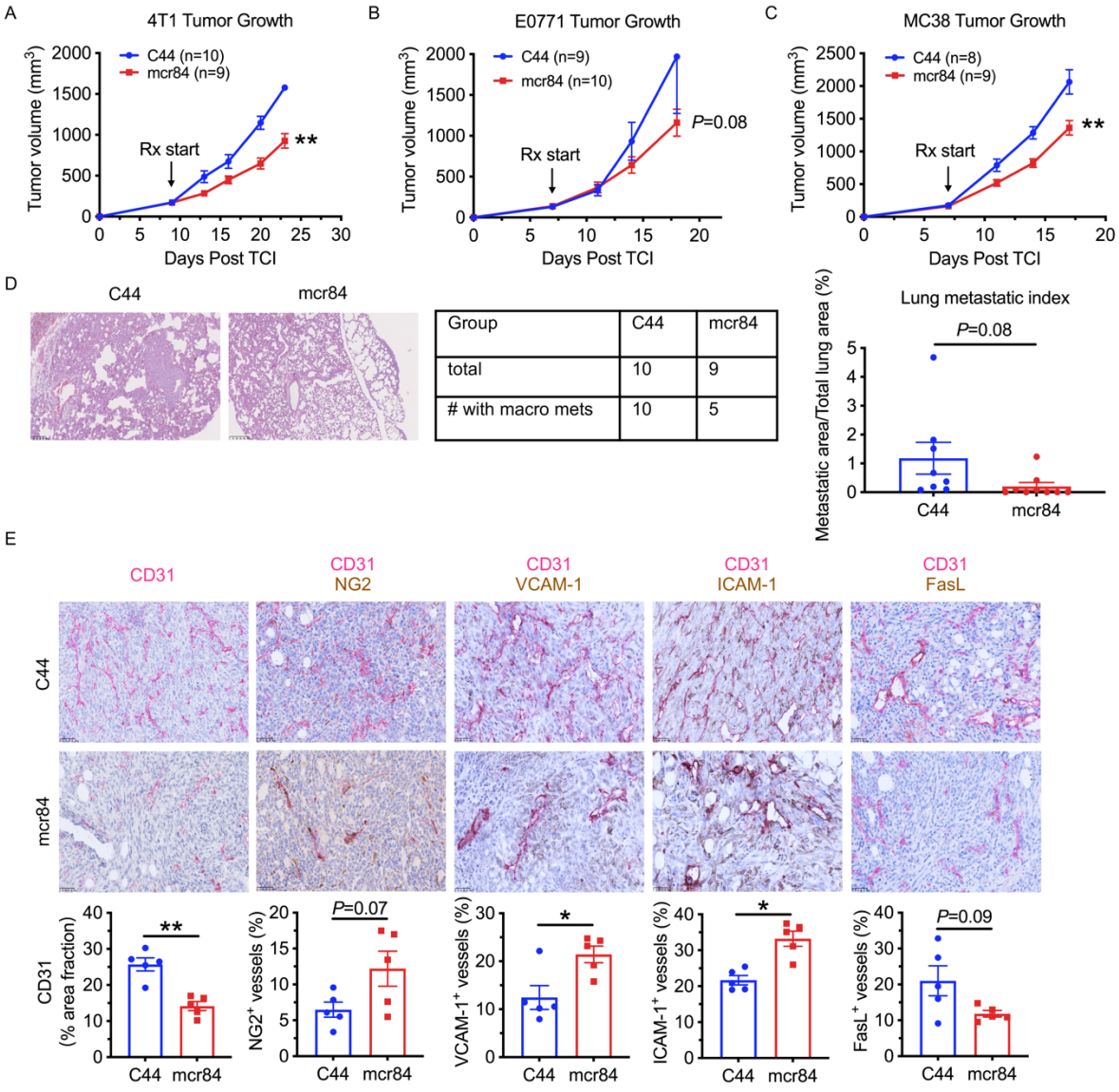

Figure 9. Selective inhibition of VEGF activation of VEGFR2 by mcr84 delays tumor progression and reduces the vascular immune barrier in syngeneic models. (A-C) In vivo assessment of tumor growth in response to mcr84 treatment in subcutaneously or orthotopically implanted tumors. **(A)** 1 × 10^5 4T1 cells (n=9-10/group) were injected orthotopically into 8-week-old BALB/c mice. **(B)** 1 × 10^5 E0771 cells (n=9-10/group) were injected orthotopically into 8-week-old C57BL/6 mice. **(C)** 1 × 10^5 MC38 cells were injected subcutaneously into 8-week-old C57BL/6 mice (n=8-9/group). Mice with established tumors (50–150 mm^3) were treated with control antibody (C44, 250 µg/dose, twice per week) or mcr84 (250 µg/dose, twice per week). Mice were monitored daily and tumor volume was measured twice per week. All mice were sacrificed when tumor volume in the control group reached

2000 mm^3. Data are displayed as mean ± SEM. **, $P < 0.01$ vs. control, by Welch's *t* test. **(D)** Lung metastasis burden was evaluated in the 4T1 model. Formalin-fixed paraffin-embedded **(FFPE)** lung tissues were sectioned serially at a 150 µm interval. H&E staining was performed to evaluate metastasis. Metastasis index was calculated with metastatic area/total lung area. Representative images of H&E staining are shown. Scale bar, 100 µm or 250 µm. **(E)** Immunohistochemistry of FFPE 4T1 tumors for CD31, CD31 and NG2, CD31 and VCAM-1, CD31 and ICAM-1, CD31 and FasL. Slides were scanned and images were analyzed using NIS Elements (Nikon) and Fiji software. Representative images are shown with CD31 in red and other markers in brown. Scale bar, 50 µm. Quantification is shown. Data are displayed as mean ± SEM (n=5/group). *, $P < 0.05$; **, $P < 0.005$ vs. control, by Welch's *t* test.

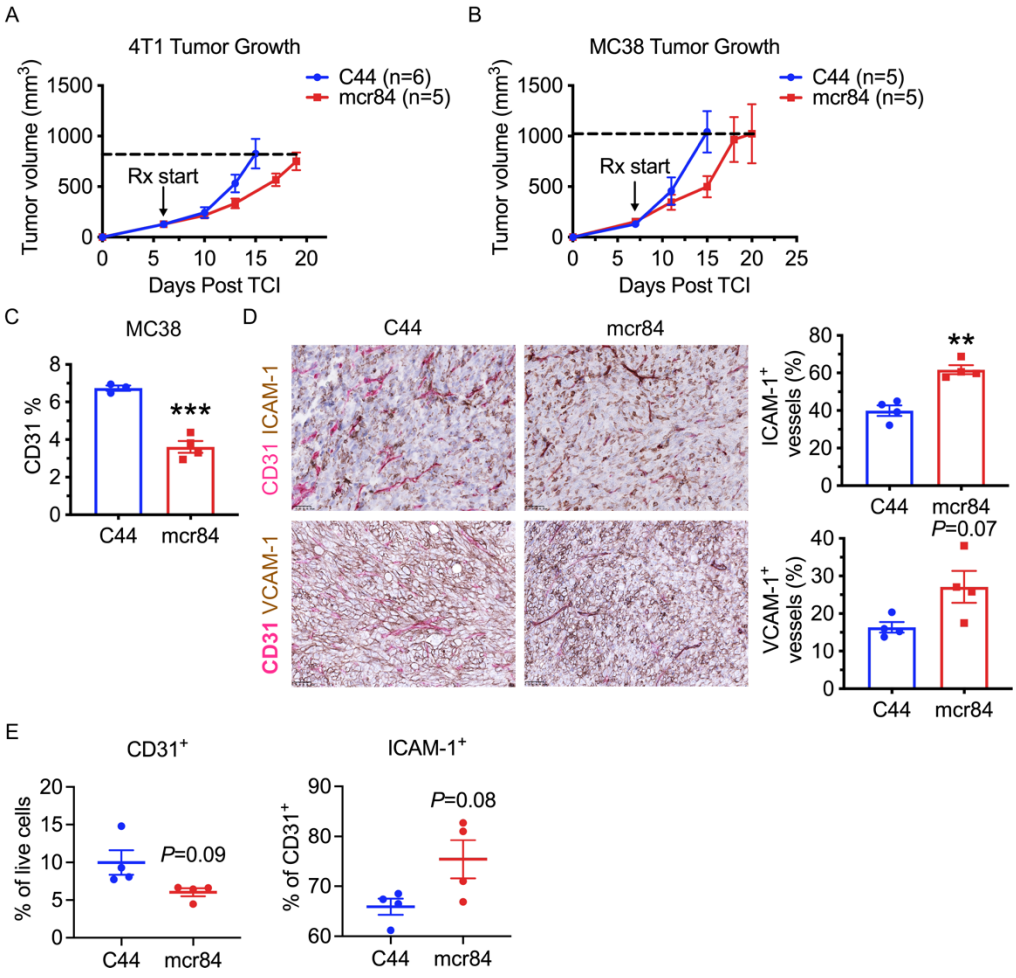

Figure 10. mcr84 reduces microvessel density but increases adhesion molecule expression on blood vessels. (A) 1 × 10^5 4T1 cells (n=5-6/group) were injected orthotopically into 8-week-old BALB/c mice. **(B)** 1 × 10^5 MC38 cells were injected subcutaneously into 8-week-old C57BL/6 mice (n=5/group). Mice with established tumors (50–150 mm^3) were treated with

control antibody (C44, 250 μg/dose, twice per week) or mcr84 (250 μg/dose, twice per week). Mice were monitored daily and tumor volume was measured twice per week. All mice were sacrificed at similar tumor sizes. Data are displayed as mean ± SEM. **(C-D)** Immunohistochemistry for CD31 and adhesion molecules (ICAM-1, VCAM-1) on FFPE MC38 tumors. Slides were scanned and images were analyzed using NIS Elements (Nikon) and Fiji software. Representative images are shown with CD31 in red and adhesion molecules in brown. Scale bar, 50 μm. Quantification is shown. Data are displayed as mean ± SEM (n=4/group). **, $P < 0.005$; ***, $P < 0.001$ vs. control by Welch's *t* test. **(E)** Flow cytometry analysis of endothelial cells (CD31) and endothelial expression of ICAM-1 in 4T1 tumors treated with mcr84 for one week. Each dot indicates one tumor. Data are displayed as mean ± SEM (n=4-5/group). *, $P < 0.05$, by Welch's *t* test.

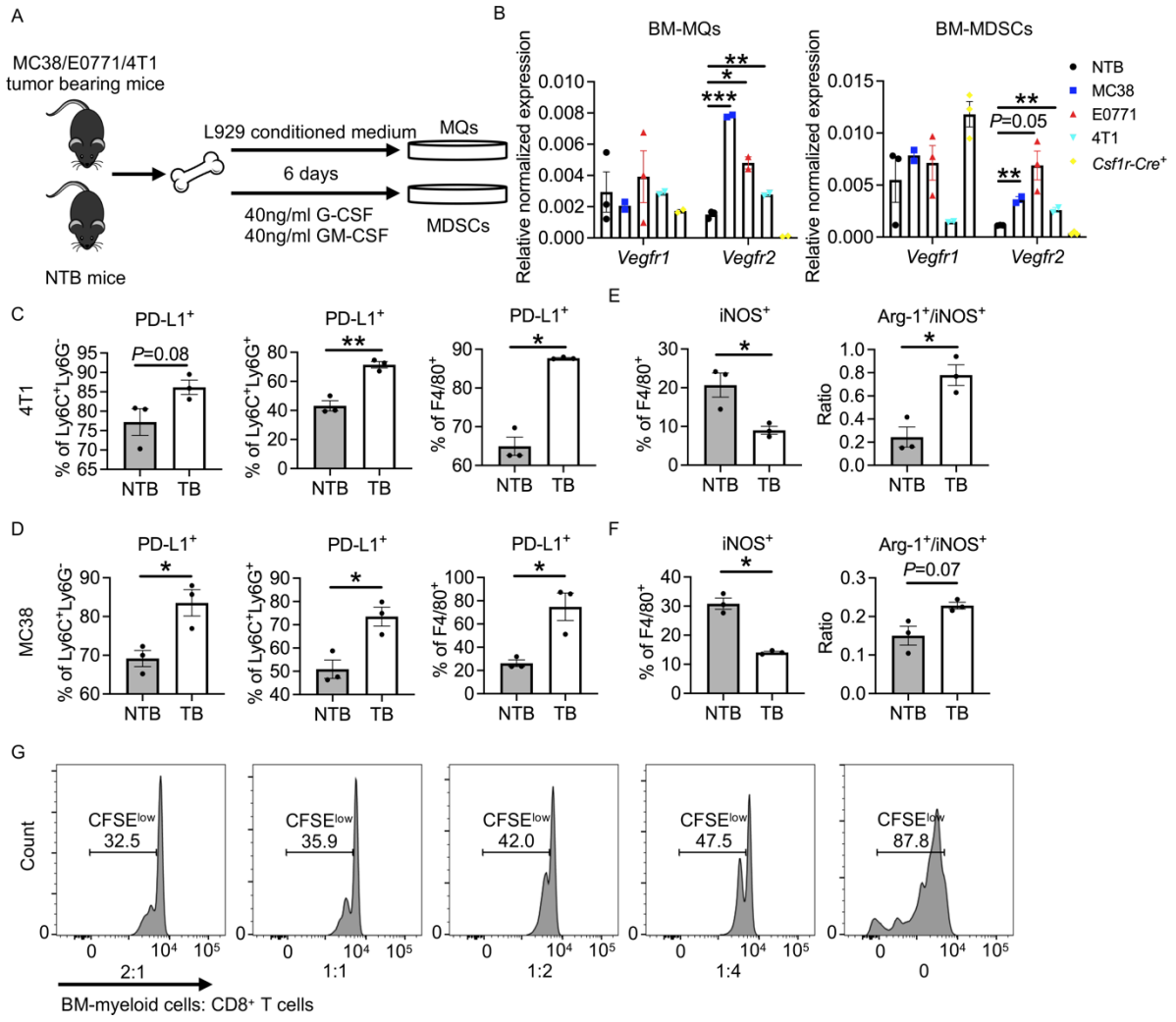

Figure 11. Expression of VEGFR2 on myeloid cells is elevated specifically in tumor-bearing animals and is associated with an immunosuppressive myeloid phenotype. (A-B) Bone marrow (BM)-derived macrophages (MQs) and MDSCs from non-tumor bearing (NTB) animals, MC38, E0771 and 4T1 tumor-bearing (TB) animals and *Csf1r-Cre*$^{+}$ *Flk-1*$^{fl/fl}$ animals were analyzed for *Vegfr1* and *Vegfr2* expression. Schematic experimental design is shown in **(A)**. *Vegfr1* and *Vegfr2* expression were evaluated by qPCR **(B)**. Data are displayed as mean ± SEM with three independent experiments using duplicate samples. *, $P < 0.05$; **, $P < 0.005$; ***, $P < 0.001$ vs. NTB control by Welch's *t* test. **(C-F)** BM-derived myeloid cells from NTB mice, 4T1 (C and E) and MC38 (D and F) TB mice were analyzed by flow cytometry for PD-L1 and other myeloid cells markers as indicated. Data are displayed as mean ± SEM with three independent experiments. *, $P<0.05$; **, $P<0.005$ by Welch's *t* test. **(G)** Representative images showing the CFSE gating of proliferating CD8^{+} T cells co-cultured with BM derived myeloid cells from NTB mice at different ratios.

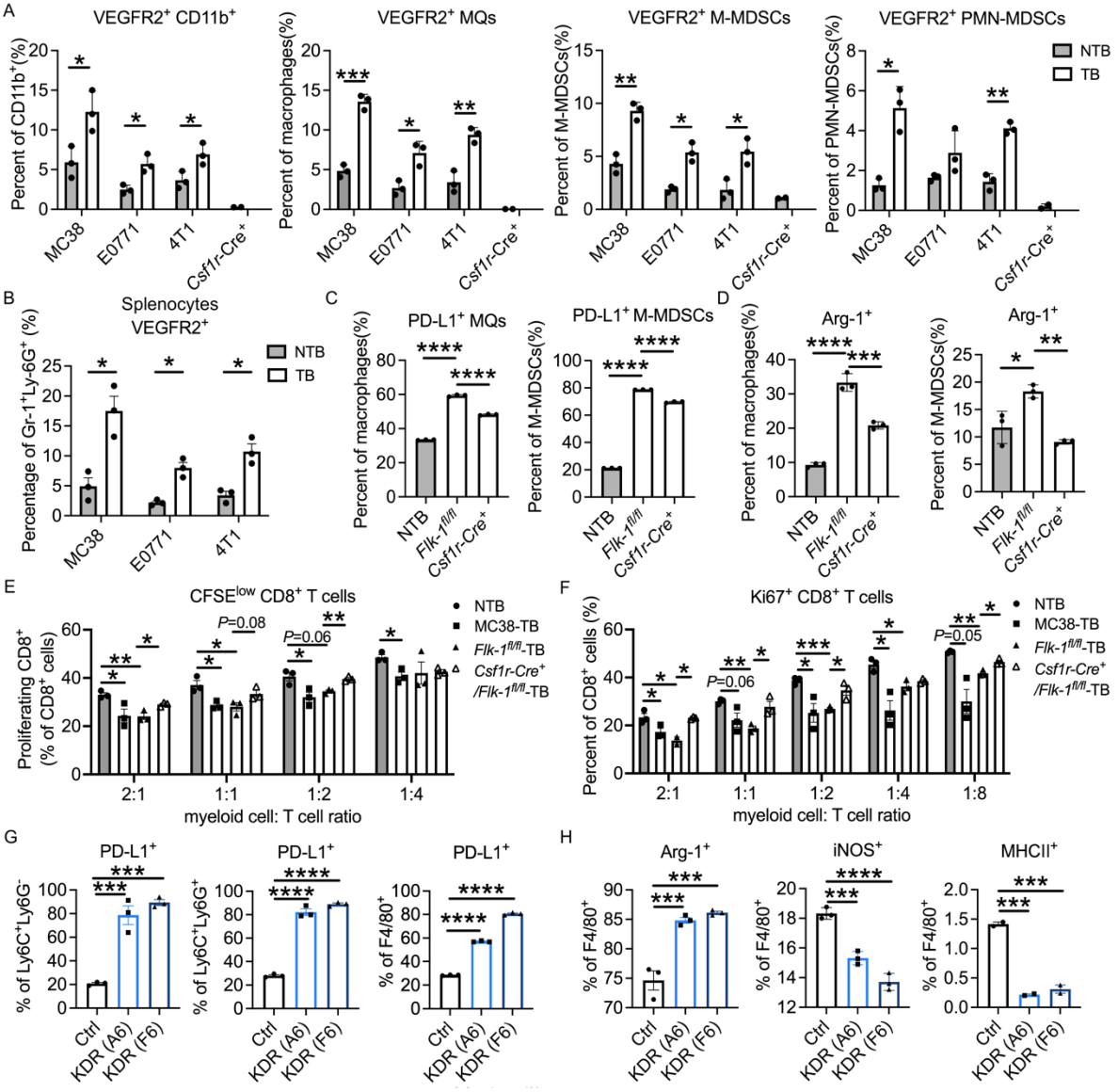

Figure 12. Expression of VEGFR2 on myeloid cells is elevated specifically in tumor-bearing animals and is associated with an immunosuppressive myeloid phenotype. (A) Bone marrow (**BM**)-derived total myeloid cells, macrophages (**MQs**) and MDSCs from non-tumor bearing (**NTB**) animals, MC38, E0771 and 4T1 tumor-bearing (**TB**) animals and *Csf1r-Cre*$^{+}$ *Flk-1*$^{fl/fl}$ animals were analyzed for VEGFR2 expression by flow cytometry. **(B)** Gr-1^{+}Ly-6G^{+} MDSCs were sorted from splenocytes of NTB mice, MC38, E0771 and 4T1 TB mice and VEGFR2 expression were evaluated by flow cytometry. Data are displayed as mean ± SEM with three independent experiments. *, $P < 0.05$; **, $P<0.005$; ***, $P<0.001$, by Welch's *t* test. **(C-D)** BM-derived myeloid cells from NTB mice, *Flk-1*$^{fl/fl}$ and *Csf1r-Cre*$^{+}$ *Flk-1*$^{fl/fl}$ mice bearing F246-6 breast tumors were analyzed by flow cytometry for PD-L1 and Arg-1

expression. Data are displayed as mean ± SEM with three independent experiments. *, $P<0.05$; **, $P<0.005$; ***, $P<0.001$; ****, $P<0.0001$ by ANOVA with Tukey's MCT. **(E-F)** BM-derived myeloid cells from NTB mice, MC38, *Flk-1*$^{fl/fl}$ and *Csf1r-Cre*$^{+}$ *Flk-1*$^{fl/fl}$ TB mice at Day 6 were harvested and added to CD8^{+} T cells at different ratios. Percentages of proliferating CD8^{+} T cells after 72 hours were analyzed by CFSE signal (E) or intracellular Ki67 staining (F) with flow cytometry. Data are displayed as mean ± SEM with three independent experiments. *, $P<0.05$; **, $P<0.005$; ***, $P<0.001$, by Welch's *t* test. **(G-H)** KDR was overexpressed by lentiviral transduction in J774M cells and clones (A6 and F6) were chosen. J774M-Ctrl and J774M-KDR (A6), J774M-KDR (F6) cells were analyzed for PD-L1 and other myeloid cells markers as indicated by flow cytometry. Data are displayed as mean ± SEM with three independent experiments. ***, $P<0.001$; ****, $P<0.0001$ by ANOVA with Tukey's MCT.

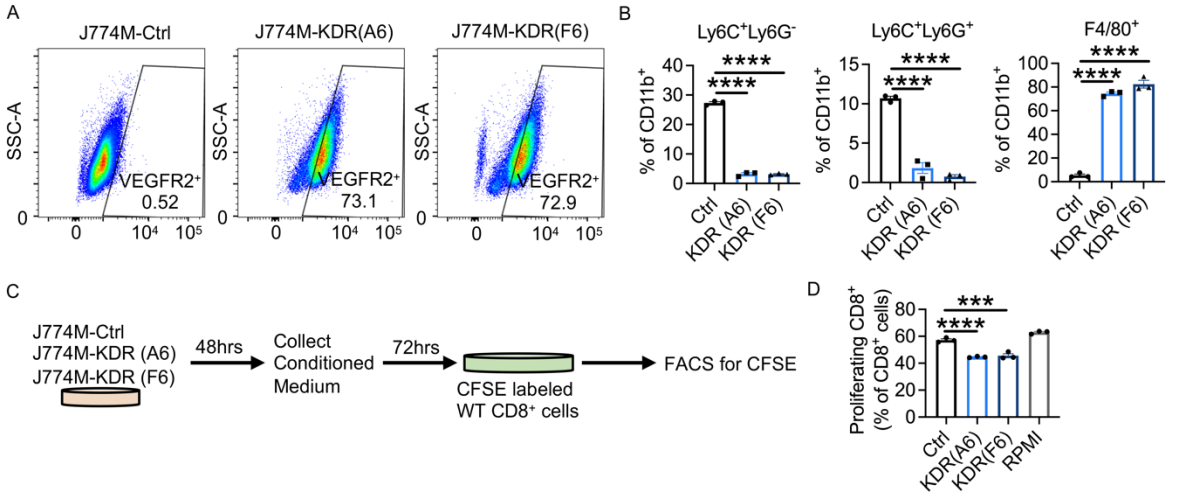

Figure 13. Development of a VEGFR2 over-expression myeloid cell line. (A) Representative flow cytometry analysis of VEGFR2 expression in J774M-Ctrl, J774M-KDR (A6), J774M-KDR (F6) cells. **(B)** Flow cytometry analysis of the indicated markers expression on J774M-Ctrl, J774M-KDR (A6), J774M-KDR (F6) cells. Data are displayed as mean ± SEM with three independent experiments. ****, $P<0.0001$ by ANOVA with Tukey's MCT. **(C-D)** Conditioned medium from 48hrs culture of J774M-Ctrl and J774M-KDR (A6), J774M-KDR (F6) cells were harvested and added to CFSE-labeled wild type CD8^{+} T cells (C). Percentage of proliferating CD8^{+} T cells after 72 hours was analyzed by flow cytometry (D). Data are displayed as mean ± SEM with three independent experiments. ***, $P<0.001$; ****, $P<0.0001$ by ANOVA with Tukey's MCT.

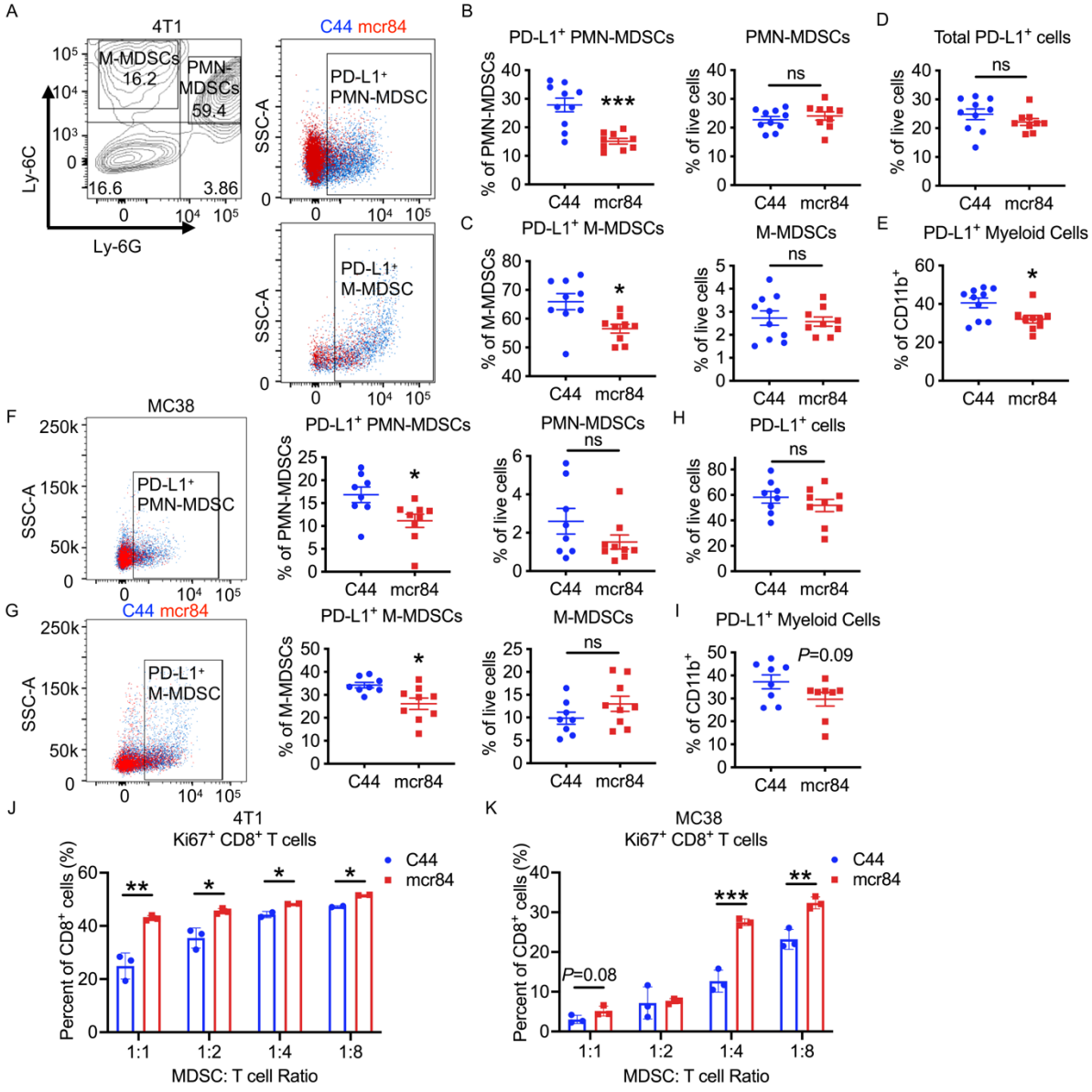

Figure 14. VEGF blockade by mcr84 decreases PD-L1 expression on myeloid cells. (A) Flow cytometry gating strategy for PMN-MDSCs, M-MDSCs and representative flow cytometry analysis of PD-L1 expression on gated PMN-MDSCs and M-MDSCs. **(B-E)** Flow cytometry analysis of the indicated cell types in 4T1 tumors treated as indicated. Each dot indicates one tumor. Expression of PD-L1 on PMN-MDSCs (B), M-MDSCs (C) and total CD11b$^+$ myeloid cells (E) as well as total numbers of MDSCs (B-C), PD-L1$^+$ cells (D) were evaluated. **(F-I)** Flow cytometry analysis of the indicated cell types in MC38 tumors. The left panels in (F) and (G) show representative flow cytometry analysis of PD-L1 expression on gated PMN-MDSCs and M-MDSCs. Data are displayed as mean ± SEM with n=9-10 per group analyzed. *, $P < 0.05$; ***, $P < 0.001$ vs. control, by Welch's t test. **(J-K)** Sorted tumor-

infiltrating MDSCs from C44 or mcr84 treated 4T1 (J) or MC38 (K) TB mice were co-cultured with CD8$^+$ T cells isolated from splenocytes of wild type C57BL/6 mice at ratios indicated. After 72 hours, Ki67 expression was evaluated by flow cytometry. Data are displayed as mean ± SEM with n=2-3 per group analyzed. *, P<0.05; **, P<0.005; ***, P<0.001, by Welch's t test.

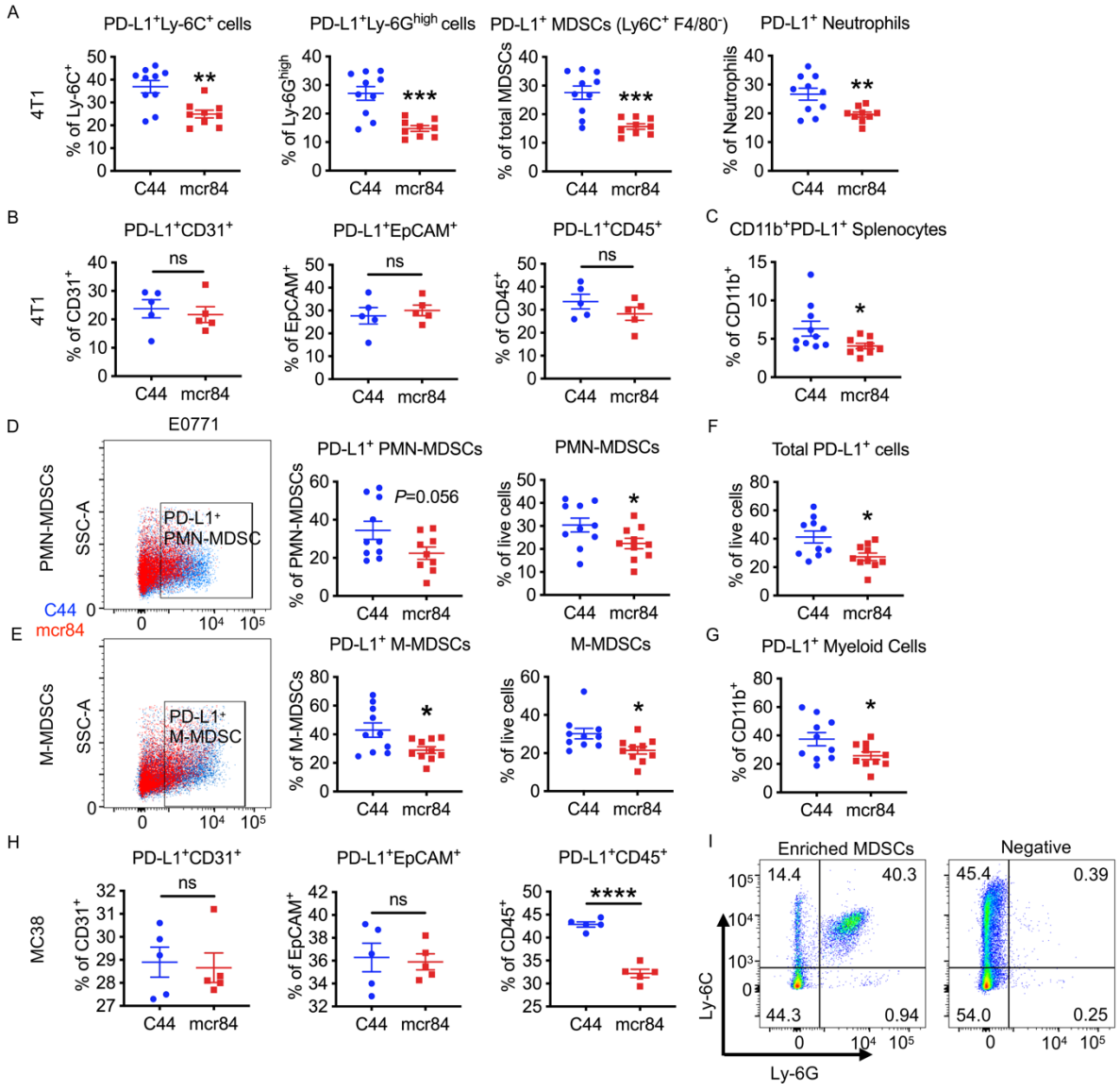

Figure 15. VEGF blockade by mcr84 decreases PD-L1 expression specifically on myeloid cells. (A) Flow cytometry analysis of the indicated cell types in 4T1 tumors. Neutrophils were characterized as Ly-6G$^+$Ly-6C$^-$. Each dot indicates one tumor. PD-L1 expression was evaluated on each cell type. Data are displayed as mean ± SEM (n=9-10/group). **, P<0.005;

***, $P<0.001$, by Welch's *t* test. **(B)** PD-L1 expression was evaluated on indicated cell types in 4T1 tumors. Data are displayed as mean ± SEM (n=5/group). **(C)** Flow cytometry analysis of PD-L1 expression on total $CD11b^+$ myeloid cells in splenocytes of 4T1 tumor-bearing animals treated as indicated. Data are displayed as mean ± SEM (n=9-10/group). *, $P<0.05$ by Welch's *t* test. **(D-G)** Representative flow cytometry analysis of PD-L1 expression on gated PMN-MDSCs and M-MDSCs in E0771 tumors and flow cytometry analysis of the indicated cell types in E0771 tumors. Expression of PD-L1 on PMN-MDSCs (D), M-MDSCs (E) and total $CD11b^+$ myeloid cells (G) as well as total numbers of MDSCs (D-E), $PD\text{-}L1^+$ cells (F) were evaluated. Data are displayed as mean ± SEM (n=8-9/group). *, $P<0.05$ by Welch's *t* test. **(H)** PD-L1 expression was evaluated on indicated cell types in MC38 tumors. Data are displayed as mean ± SEM (n=5/group). ****, $P<0.0001$ by Welch's *t* test. **(I)** Representative flow cytometry analysis of enriched MDSCs sorted from tumors and negative components after sorting.

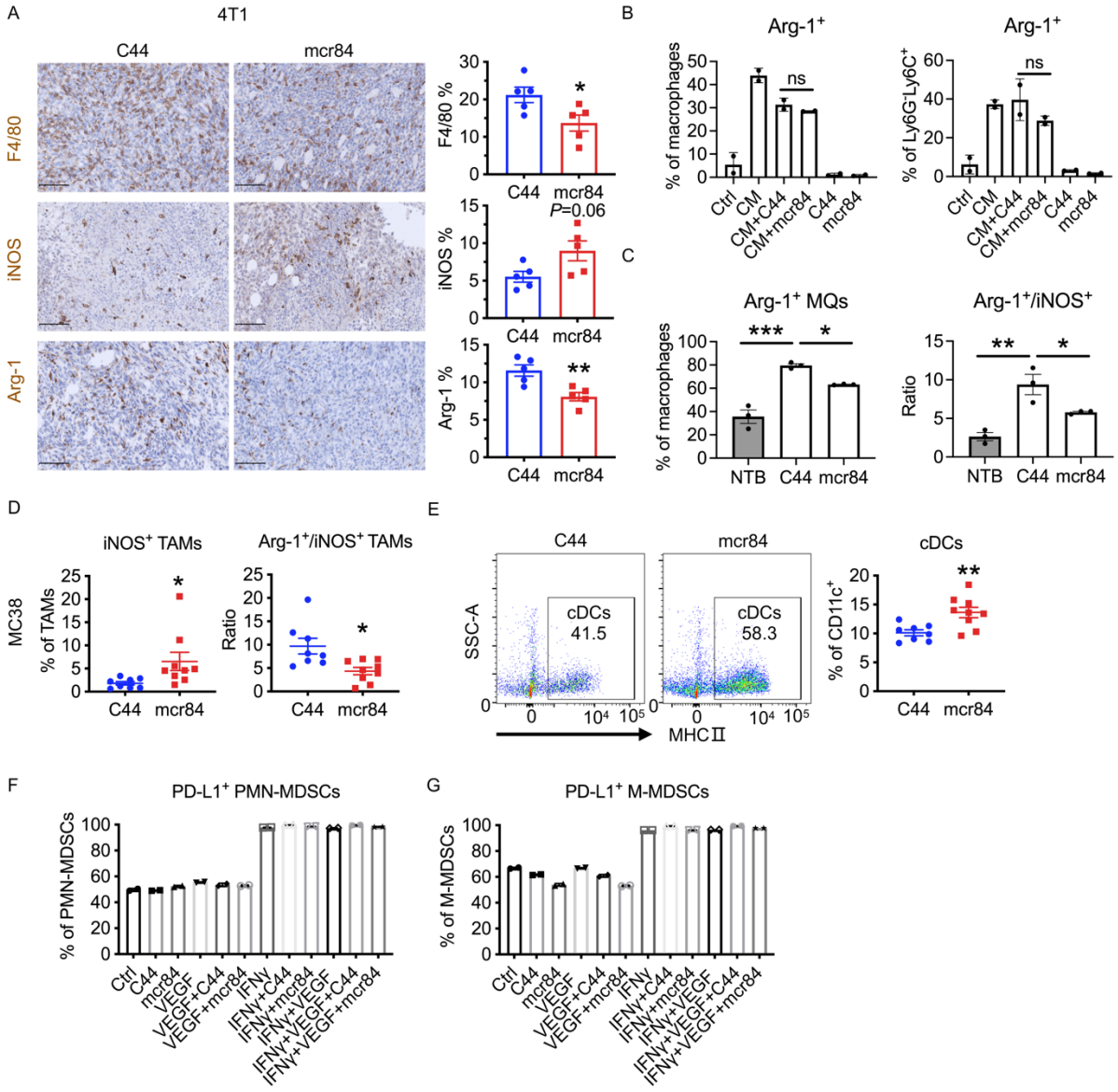

Figure 16. VEGF blockade by mcr84 polarizes macrophages to an immunostimulatory phenotype. (A) Immunohistochemistry of FFPE 4T1 tumors for F4/80, iNOS, Arg-1. Slides were scanned and images were analyzed using Fiji software. Representative images and quantification are shown. Scale bar, 100 μm. Data are displayed as mean ± SEM (n=5/group). *, $P < 0.05$; **, $P < 0.05$ by Welch's *t* test. **(B)** 4T1 tumor cell conditioned medium (CM) or with C44/mcr84 was added to BM-MQs from NTB at Day 6. After 48 hours, BM-MQs were harvested and Arg-1 expression on indicated cell types was analyzed by flow cytometry. Data are displayed as mean ± SD with two independent experiments. **(C)** BM-MQs differentiated from NTB mice, 4T1 TB mice treated with C44 or mcr84 were analyzed for Arg-1 and iNOS expression by flow cytometry. Data are displayed as mean ± SEM with three independent

experiments. *, $P<0.05$; **, $P<0.005$; ***, $P<0.001$ by ANOVA with Tukey's MCT. **(D-E)** Flow cytometry analysis of the indicated cell types in MC38 tumors. Tumor-associated macrophages (TAMs) (D) and cDCs (characterized as $CD11c^{+}F4/80^{-}CD45R^{-}MHCII^{+}$) (E) were evaluated. Data are displayed as mean ± SEM (n=8-9/group). *, $P < 0.05$; **, $P < 0.005$ by Welch's *t* test. **(F-G)** Bone marrow from C57BL/6 mice was harvested and differentiated into MDSCs in vitro. On Day 6, BM-myeloid cells were treated with VEGF +/- mcr84 or IFNγ+VEGF +/- mcr84 for 24 hours. MDSCs were analyzed by flow cytometry for PD-L1 expression. Flow cytometry analysis of PD-L1 expression on PMN-MDSCs and M-MDSCs are shown in (F-G). Data are displayed as mean ± SD with two independent experiments.

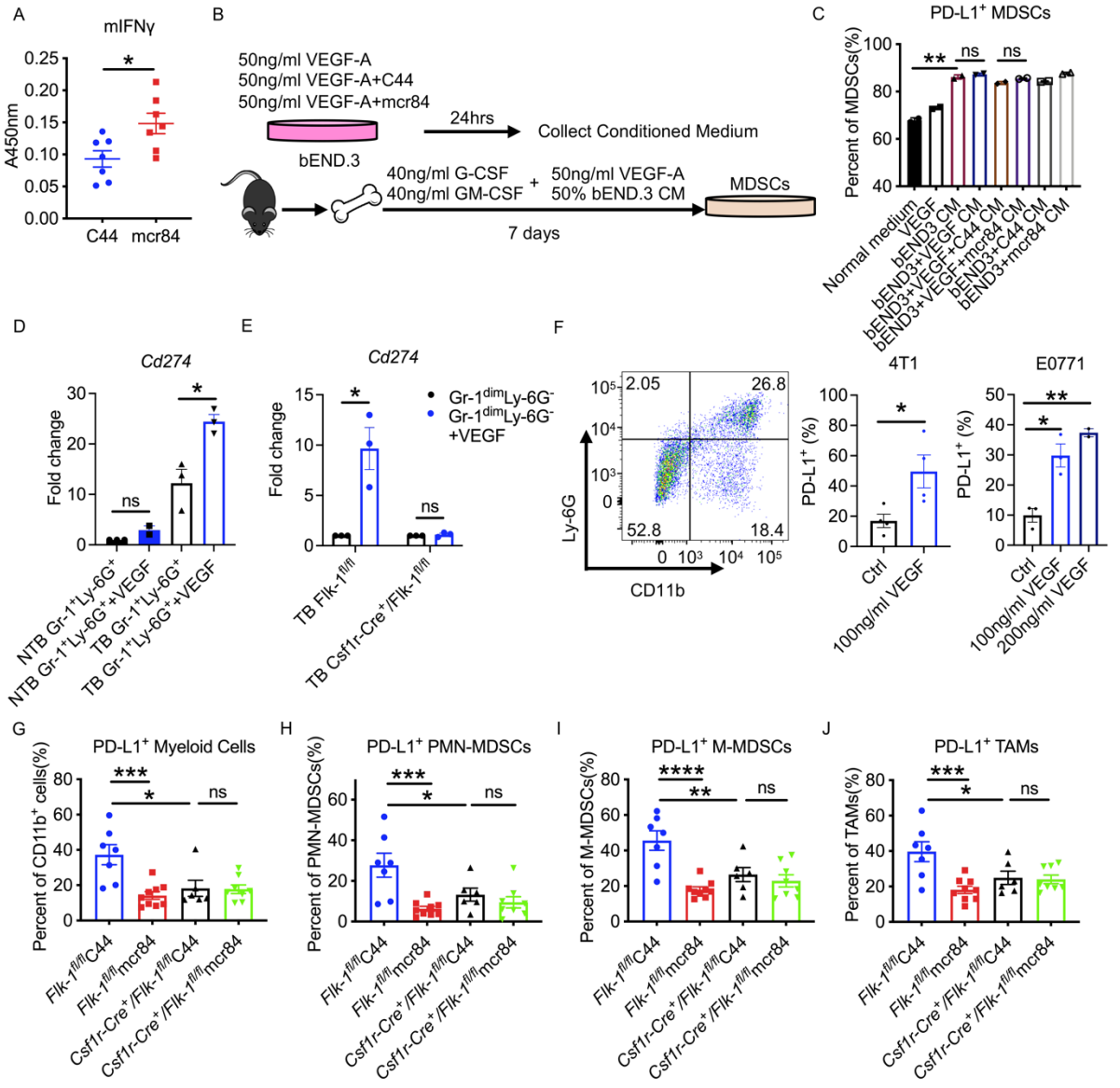

Figure 17. VEGF directly upregulates PD-L1 expression on myeloid cells through VEGFR2. (A) Intratumoral IFN-γ level was analyzed from whole tumor lysates with indicated treatments by ELISA. Data are displayed as mean ± SEM with n=7/group analyzed. *, $P < 0.05$ vs. control, by Welch's *t* test. **(B-C)** bEnd.3 endothelial cells were pre-treated with VEGF +/- C44 or mcr84 for 24 hours. Condition media (CM) were harvested, and BM from C57BL/6 mice was differentiated into MDSCs as shown in the schematics (B). On Day 7, PD-L1 expression on MDSCs was analyzed by flow cytometry as shown in (C). Data are displayed as mean ± SD with two independent experiments. **, $P < 0.01$, by Welch's *t* test. **(D)** Gr-1^{+}Ly-6G^{+} MDSCs were sorted from splenocytes of NTB mice and E0771 TB mice. **(E)** Gr-1^{dim}Ly-6G^{-} M-MDSCs were sorted from splenocytes of *Flk-1$^{fl/fl}$* and *Csf1r-Cre^{+} Flk-1$^{fl/fl}$* TB mice.

PD-L1 expression after VEGF (100 ng/ml) stimulation for 24 hours was evaluated by qPCR. Three independent experiments using duplicate samples were performed. Data are displayed as fold change normalized to NTB mice or control (mean ± SEM). *, $P < 0.05$, by Welch's *t* test. **(F)** $CD11b^{+}Ly\text{-}6G^{+}$ MDSCs were sorted from 4T1 and E0771 digested tumors (5-6 tumors pooled in each model) and were stimulated with VEGF (100 ng/ml or 200 ng/ml) for 48 hours. PD-L1 expression was analyzed by flow cytometry. Three to four independent experiments were performed (mean ± SEM). *, $P < 0.05$; **, $P < 0.005$, by Welch's *t* test. **(G-J)** F246-6 tumors grown in *Flk-1*$^{fl/fl}$ or *Csf1r-Cre*$^{+}$ *Flk-1*$^{fl/fl}$ mice were analyzed by flow cytometry for PD-L1 expression on indicated myeloid cells. Data are displayed as mean ± SEM with n=6-9/group analyzed. *, $P<0.05$; **, $P<0.005$; ***, $P<0.001$; ****, $P<0.0001$ by ANOVA with Tukey's MCT.

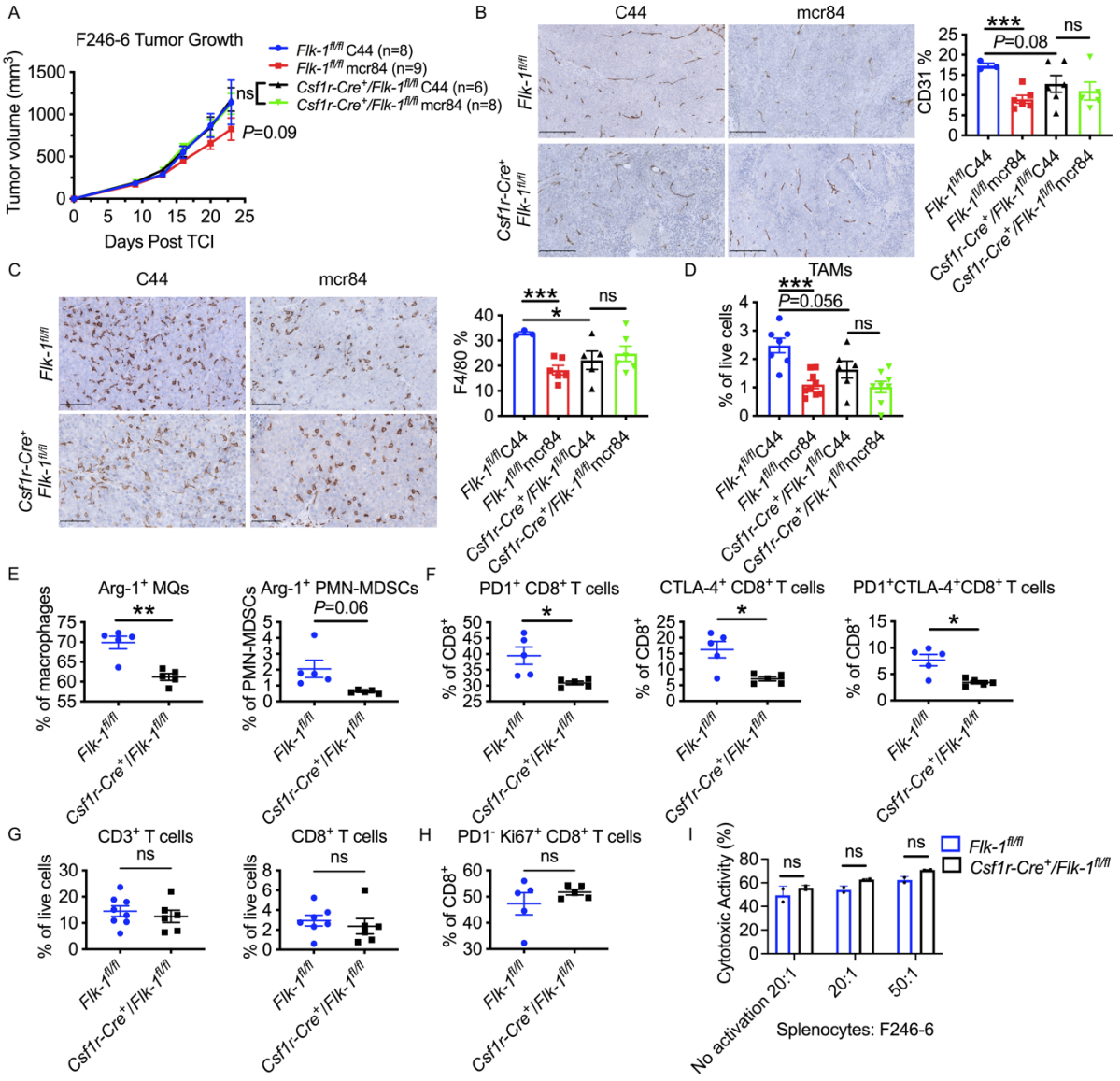

Figure 18. Genetic deletion of *Flk-1* on myeloid cells recapitulates the effect of mcr84. (A) 5×10^5 F246-6 cells, a murine breast cancer cell line derived from MMTV-PyMT mice, were injected orthotopically into mammary fat pad of *Flk-1*$^{fl/fl}$ and *Csf1r-Cre*$^{+}$ *Flk-1*$^{fl/fl}$ mice. Mice with established tumors (50–150 mm^3) were treated with control antibody (C44, 250 µg/dose, twice per week) or mcr84 (250 µg/dose, twice per week) for 5 doses in total. Mice were monitored daily and tumor volume was measured twice per week. Tumor growth was analyzed (n=6-9/group). All mice were sacrificed at the same time and tumors were harvested. **(B-C)** Tumors were analyzed for CD31 and F4/80 by immunohistochemistry. Representative images are shown in the left panel. Scale bar, 100 µm. Data are displayed as mean ± SEM (n=3-6/group). *, $P < 0.05$; ***, $P < 0.001$, by Welch's *t* test. **(D)** Flow cytometry analysis of TAMs.

Data are displayed as mean ± SEM with n=6-9 per group analyzed. ***, $P < 0.001$ by Welch's *t* test. **(E-H)** Flow cytometry analysis of indicated markers of myeloid cells and T cells in *Flk-1*$^{fl/fl}$ and *Csf1r-Cre*$^{+}$ *Flk-1*$^{fl/fl}$ F246-6 TB mice. Data are displayed as mean ± SEM with n=5-8 per group analyzed. *, $P < 0.05$; **, $P < 0.005$ by Welch's *t* test. **(I)** An in vitro cell cytotoxicity assay was performed following the instruction of the basic cytotoxicity assay kit. Splenocytes from *Flk-1*$^{fl/fl}$ and *Csf1r-Cre*$^{+}$ *Flk-1*$^{fl/fl}$ F246-6 TB animals were co-cultured with CFSE pre-labeled F246-6 tumor cells at different ratios for 72 hours and dead cells were labeled with 7-AAD. Samples were analyzed by flow cytometry. Data are displayed as mean ± SD with two independent experiments.

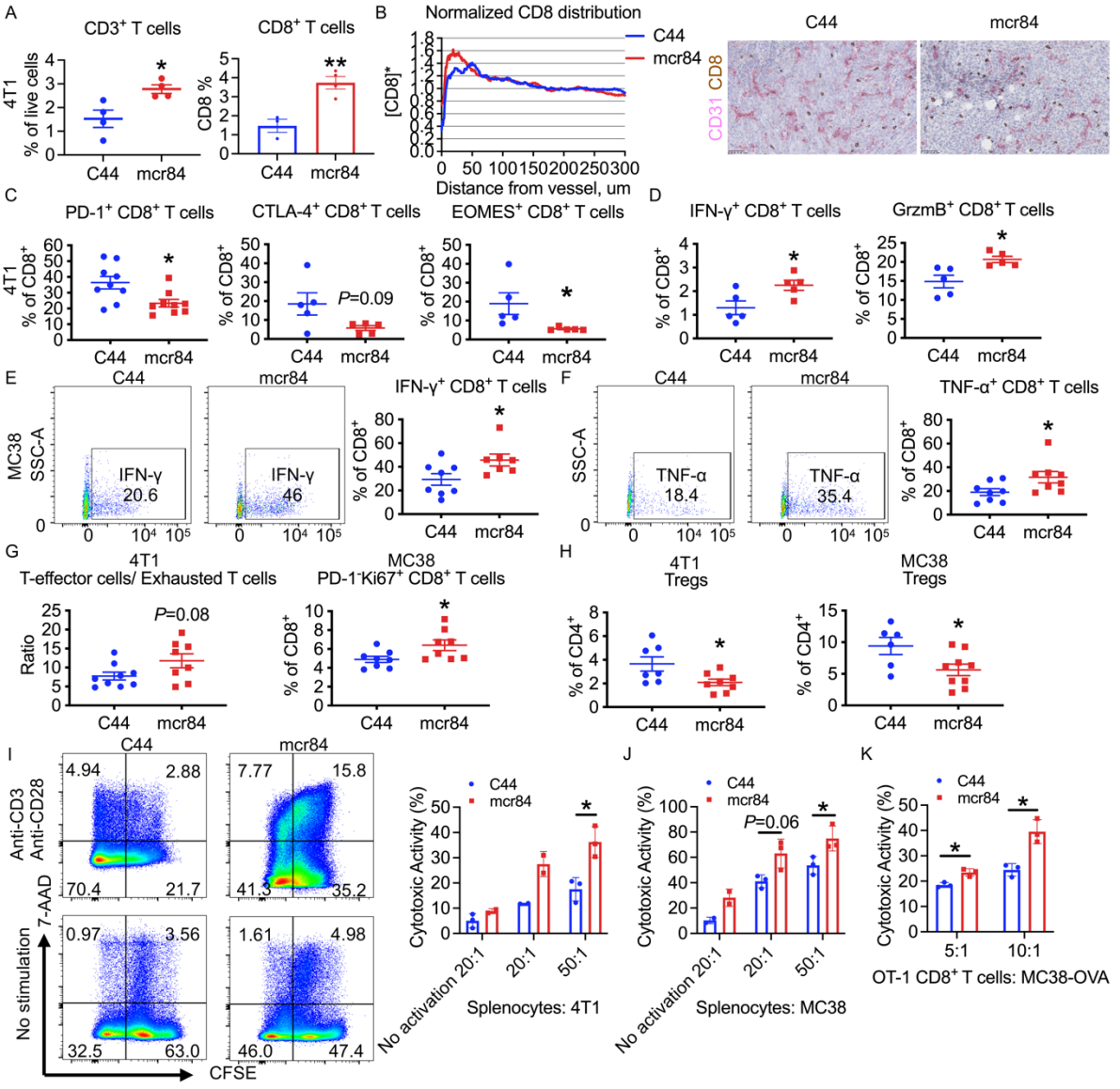

Figure 19. VEGF blockade by mcr84 promotes perivascular accumulation of T cells and stimulates T cell activation. (A) Flow cytometry analysis or IHC of the indicated cell types in 4T1 tumors. **(B)** Normalized distribution of CD8$^+$ T cells around CD31$^+$ blood vessels in 4T1 tumors (n=5/group). Representative images of CD8 (brown) and CD31 (red) staining in 4T1 tumors are shown. Scale bar, 50 μm. **(C-D)** Flow cytometry analysis of PD-1, CTLA-4, EOMES, intracellular IFN-γ and granzyme B on CD8$^+$ T cells in 4T1 tumors treated as indicated. **(E-F)** Flow cytometry analysis of intracellular IFN-γ (E) and TNF-α (F) expression on CD8$^+$ T cells in MC38 tumors treated as indicated. The left panels in (E) and (F) show representative flow cytometry analysis of indicated cytokines in gated CD8$^+$ T cells. **(G-H)** Flow cytometry analysis of T-effector cells/exhausted T cells (G) and regulatory T cells (H) in 4T1 and MC38 tumors treated as indicated. T-effector cells were characterized as PD-1$^-$

$Ki67^+CD8^+$ T cells. Exhausted T cells were characterized as $CTLA\text{-}4^+PD\text{-}1^+CD8^+$ T cells. Regulatory T cells (Tregs) were characterized as $CD25^+FoxP3^+CD4^+$ T cells. Each dot indicates one tumor. Data are displayed as mean ± SEM with 5-9 animals per group. **(I-K)** An in vitro cell cytotoxicity assay was performed following the instruction of the basic cytotoxicity assay kit. Splenocytes from animals treated as indicated or $CD8^+$ T cells from splenocytes of OT-1 mice were co-cultured with CFSE pre-labeled 4T1, MC38 or MC38-OVA cells at different ratios for 72 or 48 hours. Dead cells were labeled with 7-AAD. Samples were analyzed by flow cytometry. Representative images of gating strategy of 4T1 co-culture are shown in (I). Cytotoxicity percentages were calculated in (I) (4T1), (J) (MC38) and (K) (MC38-OVA). n =2-3/group. *, $P < 0.05$; **, $P<0.005$ vs. control, by Welch's *t* test.

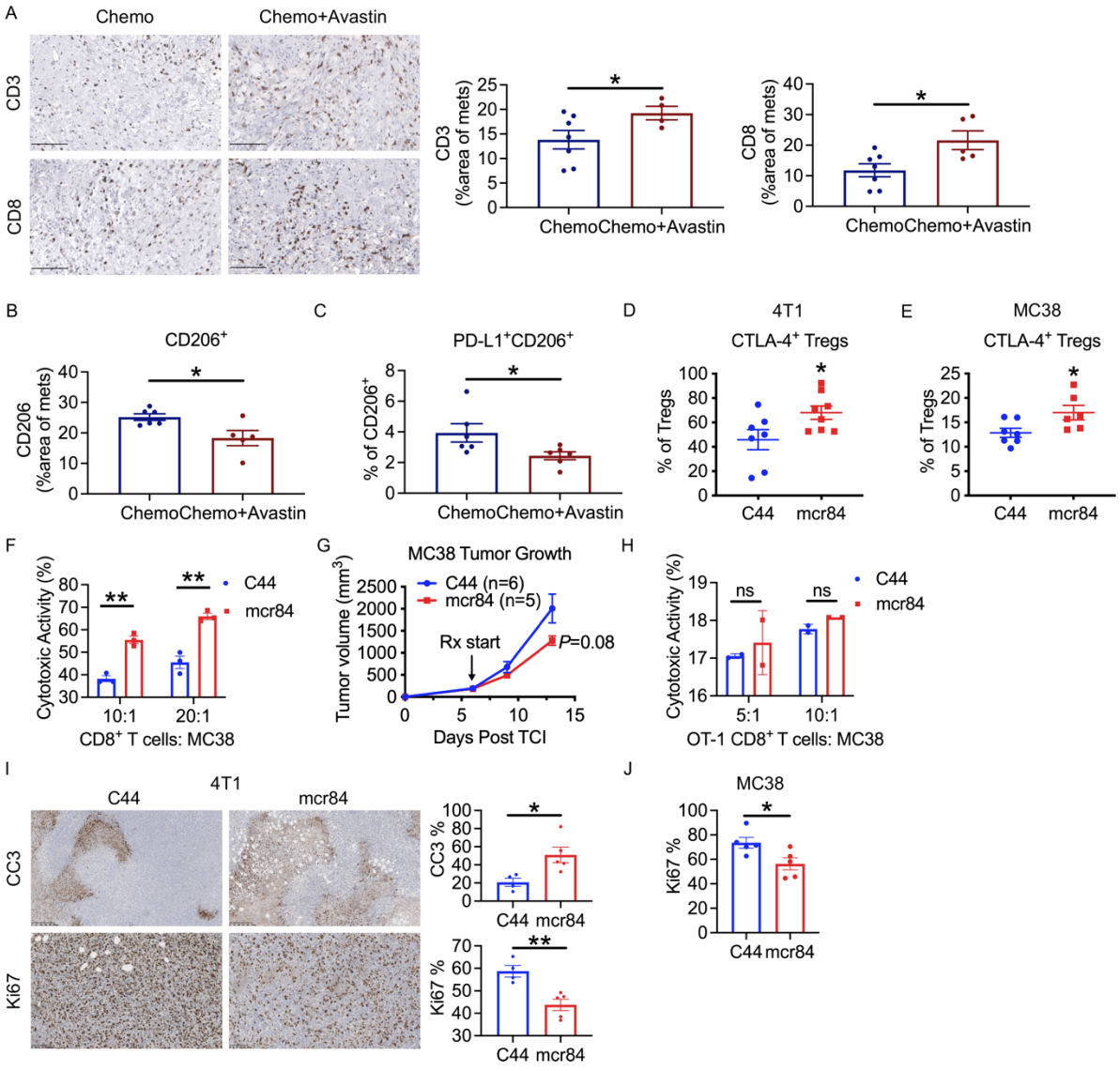

Figure 20. VEGF blockade by mcr84 increases T cell infiltration and stimulates T cell activation. (A-C) Immunohistochemistry for CD3, CD8, CD206 and PD-L1 on liver tissues of colorectal cancer patients underwent chemotherapy or chemotherapy and avastin treatment. Slides were scanned and images were analyzed using NIS Elements (Nikon) and Fiji software. Representative images of CD3 and CD8 staining are shown. Scale bar, 250 μm. Each dot indicates one patient. Data are displayed as mean ± SEM (n=4-7/group). *, $P < 0.05$, by Welch's *t* test. **(D-E)** CTLA-4 expression on Tregs was evaluated by flow cytometry in 4T1 and MC38 tumors treated as indicated. Data are displayed as mean ± SEM. *, $P < 0.05$, by Welch's *t* test. **(F)** $CD8^+$ T cells from splenocytes of MC38 TB mice treated as indicated were co-cultured with CFSE pre-labeled MC38 cells for 72 hours and dead cells were labeled with 7-AAD. Samples were analyzed by flow cytometry. n =3/group. **, $P < 0.005$, by Welch's *t*

test. **(G)** 1×10^5 MC38-OVA cells were injected subcutaneously into 6-week-old OT-1 mice (n=5-6/group). Mice with established tumors (50–150 mm^3) were treated with C44 or mcr84 (250 μg/dose, twice per week). Tumor volume was measured. Data are displayed as mean ± SEM. **(H)** $CD8^+$ T cells from splenocytes of OT-1 mice were co-cultured with CFSE pre-labeled MC38 cells for 48 hours and dead cells were labeled with 7-AAD. Samples were analyzed by flow cytometry. **(I-J)** FFPE 4T1 (I) and MC38 (J) tumors were assessed for cleaved caspase-3 (CC3) and Ki67. Slides were scanned and images were analyzed using Fiji software. Representative images of 4T1 model are shown. Scale bar, 250 μm or 100 μm. Data are displayed as mean ± SEM (n=5/group). *, $P < 0.05$; **, $P < 0.01$ by Welch's *t* test.

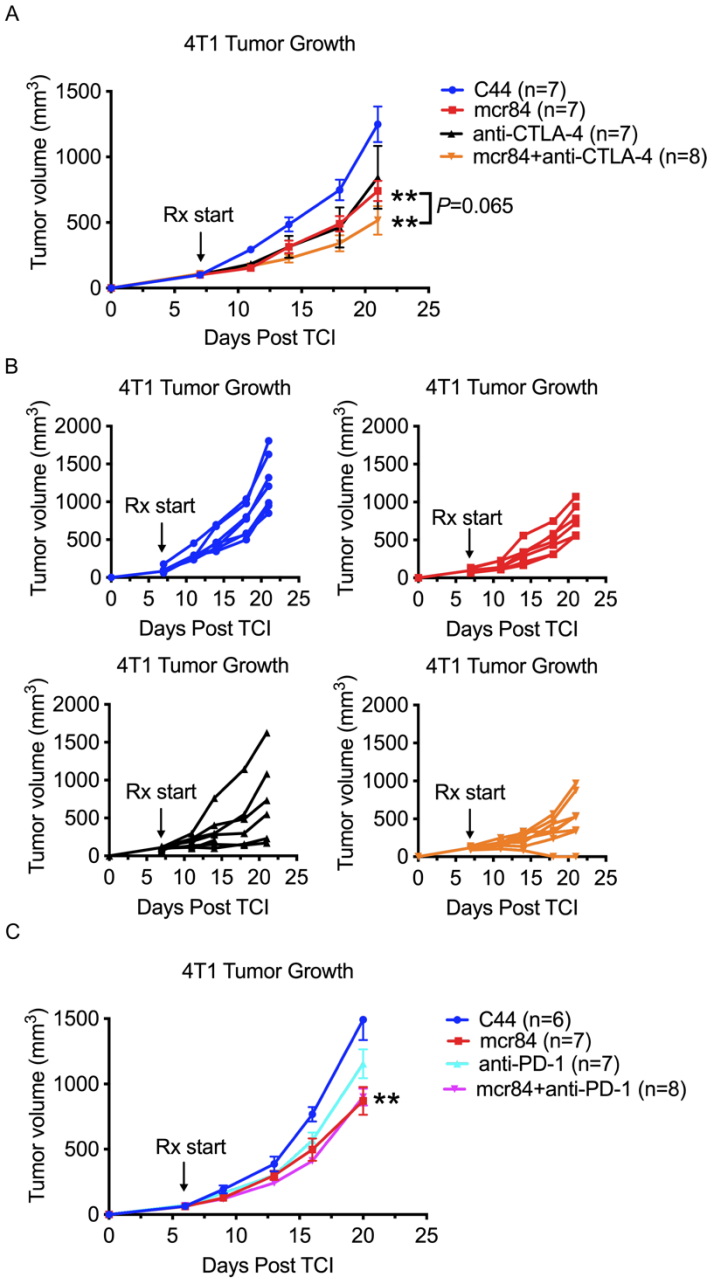

Figure 21. CTLA-4 blockade enhances the antitumor activity of mcr84. (A) 1×10^5 4T1 cells (n=7-8/group) were injected orthotopically into 8-week-old BALB/c mice. Mice with established tumors (50–150 mm^3) were treated with control antibody (C44, 250 µg/dose, twice per week), mcr84 (250 µg/dose, twice per week), anti-CTLA-4 antibody (clone: 9d9, 100 µg/dose, every 3 days) or mcr84 + anti-CTLA-4. Mice were monitored daily and tumor volume was measured twice per week. All mice were sacrificed when tumor volume in the control group reached 2000 mm^3. Tumor growth was analyzed. Data are displayed with mean ± SEM. **, $P < 0.005$ vs. control C44, by Welch's *t* test. **(B)** Growth curves of individual tumors. Arrows indicate start of treatments (Day 7). Colors of labeling corresponds to legends in (A). **(C)** Combination efficacy of VEGF and PD-1 blockade in 4T1 syngeneic model. Experiment was performed similarly as described in (A). Anti-PD-1 antibody (clone: RMP14-1, 100 µg/dose, i.p.) was dosed twice per week. Data are displayed with mean ± SEM. **, $P < 0.005$ vs. control C44, by Welch's *t* test.

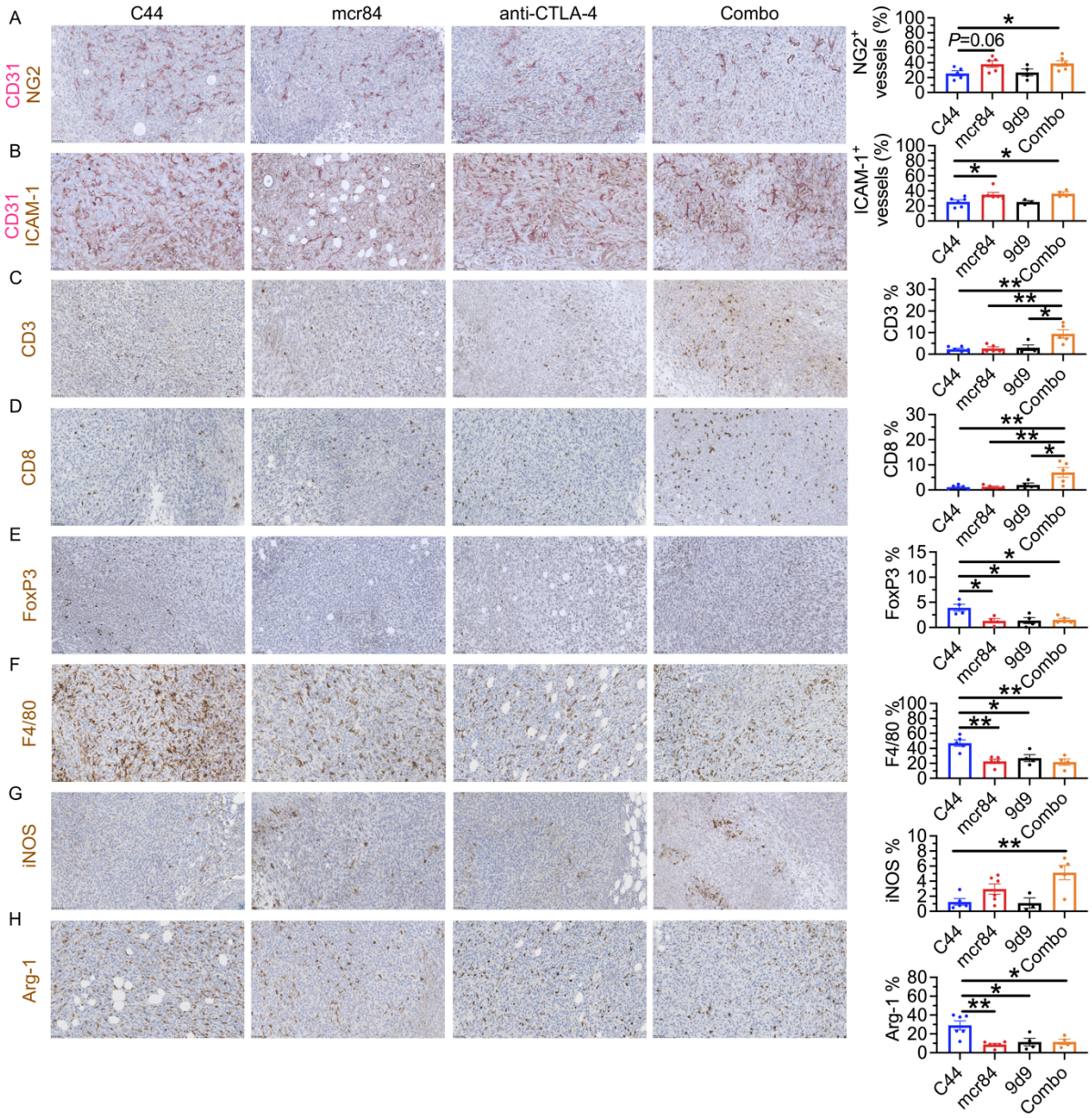

Figure 22. VEGF blockade in combination with anti-CTLA-4 therapy increases T cell infiltration and polarizes macrophages to an immunostimulatory phenotype. FFPE 4T1 tumors were assessed for CD31 and NG2 **(A)**, CD31 and ICAM-1 **(B)**, T cells markers, CD3 **(C)**, CD8 **(D)**, FoxP3 **(E)**, as well as macrophages markers F4/80 **(F)**, iNOS **(G)**, Arg-1 **(H)**. Slides were scanned and images were analyzed using NIS Elements (Nikon) and Fiji software. Representative images are shown with CD31 in red and other markers in brown. Scale bar, 50 µm. Quantification is shown to the right. Data are displayed as mean ± SEM (n=4-6/group). *, $P<0.05$; **, $P<0.005$, by ANOVA with Tukey's MCT.

CHAPTER FOUR

MATERIALS AND METHODS

4.1 Cell lines

Human pancreatic cancer cell lines AsPC-1, HPAF-II were obtained from ATCC. Colo357 was obtained from MD Anderson Cancer Center. AsPC-1 was grown in DMEM, Colo357 and HPAF-II in MEM. Murine breast cancer cell line, 4T1, murine colon adenocarcinoma cell line, MC38 and 293T were obtained from ATCC. E0771, a murine breast cancer cell line, was a gift from Dr. Philip Thorpe (University of Texas Southwestern Medical Center). F246-6, an isogenic breast cancer cell derived from MMTV-PyMT mice (92) was a gift from Dr. Jeff Pollard (University of Edinburgh). J774M, a MDSC-like cell line was a gift from Dr. Kebin Liu (Medical College of Georgia). MC38-OVA cell line was a gift from Dr. Yang-Xin Fu (UT Southwestern). Cells were cultured in DMEM (Invitrogen) or RPMI (Invitrogen) containing 10% FBS and maintained at 37°C in a humidified incubator with 5% CO2 and 95% air and confirmed to be pathogen free before use (e-Myco kit, Boca Scientific). Human cell lines were DNA fingerprinted for provenance using the Power-Plex 1.2 kit (Promega) and confirmed to be the same as the DNA fingerprint library maintained by ATCC.

4.2 Animal studies

All animals were housed in a pathogen-free facility with 24-hour access to food and water. *Kras*$^{LSL\text{-}G12D}$*; Cdkn2a*$^{fl/fl}$*; Ptf1a*$^{Cre/+}$ (*KIC*) mice were generated as previously described in mixed background (229). At 3 weeks of age, mice were randomized to receive saline, mcr84

500 μg/dose i.p. once weekly, Apricoxib 10 mg/kg by oral gavage daily or mcr84 plus Apricoxib. All mice were sacrificed when they were 7 weeks old. Four-to-6-week-old female NOD/SCID mice were obtained from a campus supplier. A total of 1×10^6 Colo357 cells were injected orthotopically and tumor growth was monitored by ultrasound. Mice with established tumors were randomized to receive therapy. Treatment groups were the same as described above. Mice bearing Colo357 tumors received 4 weeks of therapy prior to sacrifice. Tissues from all animal experiments were fixed in 10% formalin or snap-frozen in liquid nitrogen for further studies.

Mouse breast cancer cells, 4T1 (1×10^5) or E0771 (1×10^5) were injected orthotopically into 8-week-old female BALB/c or C57BL/6 mice, respectively. Mouse colorectal carcinoma cells MC38 (1×10^5) cells were injected subcutaneously into 8-week-old C57BL/6 mice. F246-6 cells (5×10^5) were injected orthotopically into *Flk-1*$^{fl/fl}$ and *Csf1r-Cre*$^{+}$ *Flk-1*$^{fl/fl}$ mice on a pure FVB background. MC38-OVA (1×10^5) cells were injected subcutaneously into 6-week-old OT-1 mice. Tumor volumes were measured twice weekly using a digital caliper, and volumes were calculated using the formula: $V = (a \times b^2)/2$, where a is the largest dimension and b is the smallest dimension. Mice were randomized for different treatments and treatments started when tumors were established (50–150 mm^3) and ended when the tumor volume from control group reached 2000 mm^3. Treatment groups consist of C44 (i.p. 12.5 mg/kg (~250 μg), twice per week), mcr84 (i.p. 12.5 mg/kg (~250 μg), twice per week), anti-CTLA-4 (clone: 9d9, i.p. 5 mg/kg (~100 μg), every 3 days), anti-PD-1 (clone: RMP14-1, i.p. 5 mg/kg (~100 μg), twice per week) or anti-CTLA-4, anti-PD-1 in combination with mcr84 at the indicated dose. All

mice were sacrificed at the same time or at similar tumor sizes. Tissues were fixed in 10% formalin or snap frozen in liquid nitrogen for further studies or digested into single cell suspension for flow cytometry.

4.3 Histology and tissue analysis

Formalin-fixed tissues were embedded in paraffin and cut in 5 μm sections. Sections were evaluated by H&E, Masson's Trichrome staining and immunohistochemical analysis following our previously reported protocol (230) using antibodies specific for VEGF (Abcam, ab52917), COX-2 (Abcam, ab23672), E-cadherin (Cell Signaling, 3195), N-cadherin (Cell Signaling, 14215), Slug (Cell Signaling, 9585), Snail (Cell Signaling, 3879), CD3 (Bio-Rad, MCA11477), CD8 (Bioss, bs-0648R), FoxP3 (eBioscience, 14-5773-80), CD31 (dianova, DIA-310-M), CD11b (Abcam, ab133357), endomucin (Santa Cruz, sc-65495), F4/80 (Novus Biologicals, NBP2-12506), CD31 (Cell Signaling, 77699), NG2 (Millipore, ab5320), VCAM-1 (Cell Signaling, 32653S), ICAM-1 (Abcam, ab179707), FasL (Santa Cruz, NOK-1), cleaved caspase-3 (Cell Signaling, 9664), Ki67 (Abcam, ab15580), CD3 (ThermoFisher, PA1-29547), CD8 (Cell Signaling, 98941S), FoxP3 (R&D, MAB8214), F4/80 (Cell Signaling, 70076S), iNOS (ThermoFisher, PA1-21054), Arg-1 (Cell Signaling, 93668S), human CD3 (ThermoFisher, PA1-29547), human CD8 (Abcam, ab93278), human CD206 (Cell Signaling, 91992S) and human PD-L1 (Cell Signaling, 13684S). Negative controls included omission of primary antibody. Fluorescent images were captured with Zeiss Aixoscan Z1 using ZenLite software. Color images were obtained with Hamamatsu Nanozoomer 2.0HT using NDPview2

software. Pictures were analyzed using NIS Elements (Nikon) and Fiji software. Quantification is shown as percentage of area fraction.

4.4 Western blot

To induce EMT, cells were grown on collagen I-coated plates and treated with 50 ng/ml transforming growth factor-β (TGFβ) for 24 hours (231). Cells were lysed using RIPA buffer (Cell Signaling, 9806). Protein concentration was measured using a Pierce BCA Protein Assay Kit (Thermo Fisher Scientific, 23225), and equal amounts of total protein were separated by SDS- PAGE. Proteins were transferred to nitrocellulose membranes (Bio-Rad), followed by a blocking in 5% BSA in TBST. The membranes were incubated overnight at 4°C with primary antibody, E-Cadherin (Cell Signaling, 3195), N-Cadherin (Cell Signaling, 14215), vimentin (Cell Signaling, 5741) and Actin (MilliporeSigma, A2066) followed by corresponding horseradish peroxidase–conjugated secondary antibody (Jackson ImmunoResearch). Specific bands were detected by using WesternSure PREMIUM chemiluminescent substrate (Li-Cor) on a Li-Cor imaging system (Odyssey-Fc).

4.5 Flow cytometry analysis

Tumors were digested with a cocktail containing collagenase I (45 μ/ml; Worthington), collagenase II (15 μ/ml; Worthington), collagenase III (45 μ/ml; Worthington), collagenase IV (45 μ/ml; Worthington), elastase (0.075 μ/ml; Worthington), hyaluronidase (30 μ/ml; MilliporeSigma), and DNase type I (25 μ/ml; MilliporeSigma) for 60 minutes at 37°C and passed through a 70 μm cell strainer (Falcon). Splenocytes were isolated from spleens and

passed through a 70 μm cell strainer (Falcon). Suspensions were washed twice with PBS and stained with Ghost Viability Dye 510 (BD Bioscience) for 15 min. The cell suspensions were then washed and stained with antibodies detecting CD11b (BD Bioscience, 557657), Ly-6C (BD Bioscience, 562728), Ly-6G (BD Bioscience, 740953), F4/80 (Biolegend, 123132), CD274 (PD-L1, BD Bioscience, 563369), CD11c (BD Bioscience, 564079), I-A/I-E (BD Bioscience, 562009), CD3 (BD Bioscience, 553061), CD4 (BD Bioscience, 562891), CD8 (BD Bioscience, 563332), CD279 (PD-1, BD Bioscience, 563059), CD152 (CTLA-4, BD Bioscience, 565778), CD25 (IL-2 receptor α, BD Bioscience, 562694), CD31 (BD Bioscience, 553373), ICAM-1 (CD54, BD Bioscience, 565987), CD45 (BD Bioscience, 553080) and EpCAM (CD326, eBioscience, 17-5791-82) for 1 hour at 4°C. To assess cytokine secretion, tumor single cell suspension was stimulated with PMA (50 ng/ml, Sigma Aldrich)/Ionomycin (1 μg/ml, Sigma Aldrich)/Brefeldin A (10 μg/ml, BD Biosciences) for 4 hours before surface staining. Surface-stained cells were fixed, permeabilized, and stained for intracellular markers Arginase 1 (R&D Systems, IC5868P), iNOS (ThermoFisher, 17-5920-82), FoxP3 (BD Bioscience, 560401), Ki67 (Biolegend, 652404), VEGFR2 (Cell Signaling, 9698S), IFN-γ (BD Bioscience, 564336), Granzyme B (eBioscience, 11-8898-82), TNF-α (eBioscience, 12-7321-82) and EOMES (eBioscience, 25-4875-82). Cells were analyzed using FACS LSRFortessa SORP, and analysis was performed using FlowJo, with the help of the Moody Foundation flow cytometry facility at University of Texas Southwestern Medical Center.

4.6 Co-culture experiment and T cell proliferation assay

The co-culture cytotoxicity assay was performed following the instruction of the basic cytotoxicity assay kit (969, ImmunoChemistry Technologies). In brief, target cancer cells were incubated with Cell Trace CFSE (5 μM) for 20 min at room temperature then washed with cell culture medium with FBS. Splenocytes from mice of different treatments underwent red blood cell lysis and then were stimulated with plate-bound anti-CD3 antibody (1 μg/ml, Biolegend) and soluble anti-CD28 antibody (2.5 μg/ml, Biolegend). Splenocytes and pre-labeled cancer cells were then co-cultured for 72 hours. In the co-culture of splenocytes from OT-1 mice with MC38-OVA or MC38 cells, T cells were not stimulated by anti-CD3/CD28 antibodies and co-culture was 48 hours. Cells were harvested and labeled with 7-AAD. Cell percentages were analyzed by flow cytometry. The cytotoxicity percentage was calculated using the formula (7-AAD-CFSE double positive cells %)/ (CFSE-positive cells %) × 100%.

$CD8^+$ T cells from splenocytes of wild-type C57BL/6 mice were isolated using $CD8a^+$ T Cell Isolation Kit according to manufacturer instructions (Miltenyi Biotec) and labeled with Cell Tracer CFSE (1 μM) (Invitrogen, C34554). Bone marrow derived myeloid cells from different mice at Day 6 or conditioned medium from 48hrs culture of J774M cells were harvested and added to $CD8^+$ T cells at different ratios. Percentage of proliferating $CD8^+$ T cells after 72 hours was analyzed by CFSE signal or intracellular Ki67 staining with flow cytometry. $CD8^+$ T cells stimulated with plate-bound anti-CD3 antibody (1 μg/ml, Biolegend) and soluble anti-CD28 antibody (2 μg/ml, Biolegend) were used as a positive control.

4.7 Enzyme-linked immunosorbent assay (ELISA)

In vitro PGE_2 and VEGF response to apricoxib treatment was evaluated by enzyme-linked immunosorbent assay (ELISA; R&D Systems) of conditioned media over different time points.

For ELISA array, assay was performed with tumor lysates following the instructions of the mIFN-γ DuoSet ELISA kits (R&D Systems). In summary, 96-well plates were incubated with capture antibody overnight at room temperature, washed with wash buffer, blocked with reagent diluent for 1h and washed again. Then, 100 µl of sample was added per well to the plates and incubated for 2h at room temperature. The plates were washed and 100 µl of detection antibody was added per well and incubated for 2h at room temperature. Then, the plates were further washed and 100 µl of substrate solution was added to each well and incubated for 20 min at room temperature. Afterward, 50 µl of stop solution per well was used to stop the reaction and the absorbance at 450 nm was measured.

4.8 Generation of bone marrow derived myeloid cells

Bone marrow cells were obtained from non-tumor bearing C57BL/6 mice, BALB/c mice, *Csf1r-Cre*$^{+}$ *Flk-1*$^{fl/fl}$ mice and 4T1, E0771, MC38, F246-6 tumor-bearing mice using standard techniques (232). 40 ng/ml GM-CSF and 40 ng/ml G-CSF were used to differentiate bone marrow into MDSCs and 20% L929 condition medium was used for macrophages differentiation. Fresh medium with GM-CSF/G-CSF or L929 condition medium was added on Day 3. Bone marrow derived MDSCs (BM-MDSCs) and bone marrow derived macrophages (BM-MQs) were harvested on Day 6 for qPCR or flow cytometry analysis.

4.9 Real-time quantitative PCR

MDSCs sorted from splenocytes, bone marrow derived MDSCs or BM-MQs harvested on Day 6 were subject to RNA extraction using Qiagen RNeasy Mini Kit (74106). Then cDNA was synthesized using a Bio-Rad iScript cDNA synthesis kit. The expression of *Vegfr1* (Forward: 5'-CCAGAGAGGCAGAGTGGTTG-3'; Reverse: 5'-GCTCCTCTCAGACTGCCTTG-3'), *Vegfr2* (Forward: 5'-CGTTAAGCGGGCCAATGAAG-3'; Reverse: 5'-GCTCATCCAAGGGCAATTCATC-3') and *Cd274* (Forward: 5'-GCATTATATTCACAGCCTGC-3'; Reverse: 5'-CCCTTCAAAAGCTGGTCCTT-3') were measured by SYBR-Green dependent q-PCR. Three independent experiments were performed. Duplicates were run in each experiment.

4.10 Isolation of MDSCs from splenocytes and tumors

Splenocytes were isolated from spleens of non-tumor bearing or tumor-bearing animals, passed through a 70-μm cell strainer (Falcon) and underwent red blood cell lysis. Isolation of MDSCs (Gr-1^{+}Ly-6G^{+}) or M-MDSCs (Gr-1^{dim}Ly-6G^{-}) was performed using the myeloid-derived suppressor cell isolation kit (130-094-538, Miltenyi Biotec, Inc.). Tumor infiltrating CD11b^{+}Ly6G^{+} MDSCs from digested tumor single cell suspension were isolated by FACS sorting. Recombinant mouse VEGF-A_{165} (100 ng/ml or 200 ng/ml, Biolegend) was used for stimulation.

4.11 Human VEGFR2 overexpression

pHAGE constructs were prepared from a single colony and used to generate lentivirus for J774M infection as previously described (233). pHAGE-KDR was a gift from Gordon Mills & Kenneth Scott (Addgene plasmid # 116754). pHAGE_puro was a gift from Christopher Vakoc (Addgene plasmid # 118692) and was used as control. 293T cells were plated 18–24 h before transfection at an initial confluence of 70–90%. Lentivirus was generated in 293T cells by transfecting the pHAGE constructs and two packaging plasmids (psPAX2 and pMD2.G) with Lipofectamine 2000 (ThermoFisher) for 24-hour transfection. Virus was harvested every 24 hours for two days and passed through 0.45 μm filter. J774M cells were transduced by centrifugation at 800g, 37°C for 1 hour in the presence of polybrene. After 24 hours, transduction was repeated for a total of three times. 4 μg/ml puromycin was used for selection of the target cells. After selection, J774M-KDR and J774M-Ctrl cells were sorted into single cell in 96 well plates. VEGFR2 expression was evaluated by flow cytometry and clones with high VEGFR2 level (clones A6 and F6) were chosen for further use.

4.12 Statistical analysis

Data were analyzed using GraphPad software. Results are expressed as mean ± SEM or mean ± SD. Data were analyzed by Welch's t-test or by ANOVA with the Tukey's test for multiple comparisons and results are considered significant at $P< 0.05$. All in vitro experiments were performed with two to four biological replicates.

4.13 Study approval

Animal experiments in this study were performed in accordance with an animal protocol (2018-102540) approved by the Institutional Animal Care and Use Committee at UT Southwestern. Liver tissue biopsies from colorectal cancer patients who have received chemotherapy (FOLFOX or FOLFIRINOX) or chemotherapy combined with Avastin followed by surgery for metastatic site resection were obtained under a protocol approved by the UT Southwestern Institutional Review Board (STU 042015-049).

CHAPTER FIVE

Conclusions and Discussion

5.1 Conclusions

Our data support that VEGF production by tumor cells is independent of COX-2, especially following COX-2 inhibition, and the data also strongly support that COX-2 activity on tumor cells is linked closely to the induction and/or maintenance of a less differentiated tumor cell phenotype. Epithelial plasticity is a common pathway exploited by tumors to resist therapeutic interventions, including chemotherapy and targeted therapy. Our data demonstrate that reducing hypoxia-induced epithelial plasticity by blocking COX-2 enhances the therapeutic activity of anti-VEGF in PDA. We have shown previously that anti-VEGF therapy (mcr84) of PDA induces hypoxia, which drives an increase of TGFβ and subsequent increase in collagen deposition. Furthermore we found that collagen and TGFβ in the tumor microenvironment stimulate tumor cell EMT (184). Additionally, we previously reported that COX-2 inhibition (apricoxib) reduces EMT in models of gastrointestinal cancer in vivo and TGFβ-induced EMT in vitro (203,209). Therefore, we further investigated the effect of COX-2 inhibition on the level of active TGFβ in orthotopic Colo357 pancreatic tumors. We found that anti-VEGF (mcr84) increased active TGFβ levels, as anticipated but that this increase was blunted by COX-2 inhibition (data not shown), which suggests that COX-2 inhibition reduces EMT and immune suppression in part by reducing hypoxia-induced TGFβ expression (Figure 8). TGFβ, a multifunctional cytokine, can drive tumor cell EMT and is also a potent immunosuppressive factor produced by tumor cells, fibroblasts and tumor-infiltrating lymphocytes (234). TGFβ

can inhibit innate and adaptive immune responses in the tumor microenvironment. For example, TGFβ can polarize macrophages towards an immunosuppressive phenotype, support regulatory T cell differentiation and directly inhibit effector T cell activity (235). In addition, our results are consistent with reports that celecoxib, another selective COX-2 inhibitor, reduces hepatic expression of TGFβ thereby attenuating EMT of hepatocytes (236). Furthermore, COX-2 has been shown to participate in TGFβ-driven EMT in human hepatocellular carcinoma (237). Thus, there are multiple examples of a connection between COX-2 activity and TGFβ-driven tumor progression.

We also found that COX-2 inhibition might reduce immune suppression in PDA. The immunosuppressive microenvironment is a major limitation for the efficacy of cancer immune therapy (238). Our data are consistent with other studies that have shown that anti-angiogenic agents and COX-2 inhibitors have the potential to reduce the immunosuppressive tumor microenvironment and enhance immunotherapy (239–241). Our results support the findings of Motz et al (35), who found that pharmacologic blockade of VEGF and COX-2 resulted in a significant increase in infiltrating $CD8^+$ T cells and a reduction in $FoxP3^+$ Treg cells by downregulating FasL expression on tumor endothelial cells in multiple murine cancer models. Our data indicate that in *KIC* tumors, VEGF blockade or COX-2 inhibition alone could reduce FasL expression on the tumor endothelium, but combination therapy resulted in higher T effector cell recruitment and lower Treg infiltration than single-agent therapy.

In summary, our data support the rationale of combination of anti-VEGF and COX-2 inhibition in PDA patients and also provide evidence that this combination might prime PDA or other tumors for increased efficacy with immune therapy.

In these studies, I also identified and characterized the function of a population of myeloid cells expressing VEGFR2 specifically in tumor-bearing animals and investigated the mechanism(s) of how VEGF blockade promotes an immunostimulatory tumor microenvironment, including effects on tumor endothelium, tumor associated myeloid cells and TILs. Selective inhibition of VEGF activation of VEGFR2 with mcr84 increases the expression of adhesion molecules while decreasing expression of FasL on tumor endothelial cells, reduces the expression of PD-L1 on myeloid cells, reverses the immunosuppressive phenotype of tumor-infiltrating myeloid cells and reduces the expression of inhibitory immune checkpoint molecules on TILs. These changes result in increased T cell infiltration into tumors and increased TILs anti-tumor activity.

Mechanistically, I found that the decreased PD-L1 expression on tumor-infiltrating myeloid cells is due to direct inhibition of VEGFR2 on myeloid cells in tumor-bearing animals. We have previously demonstrated that a subset of tumor associated macrophages express VEGFR2, which mediates VEGF-induced infiltration into tumors (26). VEGFR2 was also found to be expressed on BM-derived plasmacytoid dendritic cells and responsible for production of type I interferon and cell proliferation (69). A recent study has demonstrated in murine gliomas and glioma patients, elevated VEGFR2 expression on myeloid cells is

associated with malignancy and high disease grade. Deficiency of VEGFR2 in BM-derived cells restrains the differentiation of myeloid lineages and pro-angiogenic function (97). Here, I confirmed that VEGFR2 is selectively upregulated on myeloid cells in tumor-bearing animals and the expression directly contributes to the myeloid cell immunosuppressive phenotype and elevated PD-L1 expression in response to VEGF stimulation. Thus, blocking VEGF binding to VEGFR2 in vivo results in consistent and significant downregulation of PD-L1 expression and less T cell suppressive capacity of myeloid cells, especially MDSCs.

Given the fact that VEGFR2 is expressed by multiple types of immune cells and tumor cells I have used have limited to no VEGFR2 expression, the efficacy of VEGFR2 inhibition I have shown in breast and colon cancer models are due to dual targeting of tumor endothelium and immune cells. To specify the contribution of myeloid cell VEGFR2, I exploited a genetic mouse model that does not express VEGFR2 on myeloid cells (*Csf1r*$^{Cre+}$ *Flk-1*$^{fl/fl}$). My data reveals that specific deletion of *Vegfr2* on myeloid cells leads to reduced response to VEGF blockade in a syngeneic breast cancer model, highlighting the importance of VEGFR2^{+} myeloid cells for the efficacy of anti-VEGF therapy. How VEGFR2^{+} myeloid cells contribute to VEGF-induced angiogenesis is an active area of investigation. However, *Vegfr2* specific single depletion on myeloid cells is not sufficient to restrain tumor progression at least in one MMTV-PyMT-derived syngeneic breast tumor model, since proliferative and cytotoxic capacity of T cells are not significantly improved.

My findings that VEGF inhibition affects T cell infiltration, exhaustion and activation status are consistent with previous studies (33,43). The regulation of inhibitory checkpoint molecule expression on $CD8^+$ T cells by VEGF in tumors was attributed to activation of the VEGFR2-PLCγ-calcineurin-NFAT pathway (43). These observations have been expanded by recent studies that have shown VEGF induced T cell exhaustion-specific transcriptional programs are dependent on TOX in microsatellite stable colorectal cancers (24).

Recently, a global, open-label, phase 3 trial has shown that the VEGF blocking mAb bevacizumab combined with anti-PD-L1 improved overall and progression-free survival outcomes compared to standard-of-care sorafenib in unresectable hepatocellular carcinoma (242,243). Clinical studies are also investigating anti-VEGF strategies in combination with other immune therapies including CTLA-4 blockade or CD40 agonism (30,244,245). My preclinical data reveals that specific inhibition of VEGF binding to VEGFR2 leads to downregulation of PD-L1 on myeloid cells. PD-L1 expressed on myeloid cells was shown previously to directly reduce T cell function, highlighting the contribution of myeloid cells to ICI efficacy (246). Given the importance of PD-L1 expression on host bone marrow derived cells and DCs for the response of PD-L1 blockade (246,247), my data provide a molecular rationale for how anti-VEGF therapy enhances the efficacy of ICIs and highlight that inhibition of VEGFR2 activation might especially improve the efficacy of blocking immune checkpoint molecules besides the PD-1/PD-L1 axis.

5.2 Future perspectives

The mechanism of how and when myeloid cells upregulate VEGFR2 expression in tumor progression as well as the signaling pathway of VEGF regulating PD-L1 expression remain unclear. Further pathway analysis needs to be performed to identify how VEGF signals to PD-L1 specifically on myeloid cells. Our preliminary data has demonstrated that VEGFR2 expression on BM-MQs can be induced by lipopolysaccharide stimulation in vitro. Further experiments to investigate these questions are underway. Mice with a VEGFR2 reporter might be beneficial to identify cell types that express VEGFR2 in tumor progression and study the distribution and infiltration of this $VEGFR2^{+}$ myeloid population. In vivo CRISPR-screening might be a powerful tool to explore genes that can induce VEGFR2 expression on myeloid cells in tumor settings. In addition, macrophage specific RNAseq data from Raphael Nemenoff's group (248) indicate that VEGFR2 expression is strongly correlated with angiopoietin-1 receptor (Tie2) expression in normal and LLC lung cancer macrophages (data not shown), which suggests a relationship between $VEGFR2^{+}$ myeloid cells and Tie2-expressing monocytes (TEMs) as well as myeloid cells expressing other endothelial cells markers (108).

Additionally, I have demonstrated that VEGF inhibition has an effect on bone marrow differentiation where it contributes to macrophages polarization (Figure 16C). My preliminary data also showed downregulated PD-L1 expression on BM-MDSCs from mcr84 treated animals compared to those from isotype control treated mice, which was tumor dependent.

These results suggest an epigenetic program involved in bone marrow differentiation regulating myeloid cells phenotype that could be altered by VEGF inhibition.

Although anti-VEGF therapies have shown the potential to increase lymphocyte infiltration and switch the immunosuppressive microenvironment to more immune stimulatory, elimination of cancer cells by T cell-mediated immune response is a multi-step process (249). So, other obstacles might still exist, limiting the anti-tumor response of immunotherapies. For example, low immunogenicity of tumors could represent a persistent challenge resulting in low levels of tumor antigen-specific T cells. Another challenge is represented by tumors with abundant stroma, such as pancreatic ductal adenocarcinoma. The stroma may represent a barrier to a productive anti-tumor immune response that is not overcome by anti-angiogenic therapy (250). Furthermore, therapy-induced resistance might still develop. The resistance not only includes alternative proangiogenic pathways commonly noticed in anti-angiogenesis therapy, but also can arise from dependence of tumors on other immune checkpoint pathways. For example, in genetically engineered mouse models of lung cancer progressing after anti-PD-1 therapy, TIM-3 is upregulated (251).

Furthermore, optimization of anti-angiogenesis agents in combination with immunotherapy need to be performed. This should include optimization of sequencing of therapy. Although the applications of anti-PD-1/anti-PD-L1 antibody together with bevacizumab or other kinase inhibitors are the majority in clinical trials, my preliminary data has suggested that specific blocking VEGF binding to VEGFR2 leads to downregulation of PD-L1 on myeloid cells.

Considering that PD-L1 expression on host bone marrow derived cells is essential for the response of PD-L1 blockade, my data indicates that anti-VEGF therapy might benefit from blocking other immune checkpoint molecules other than PD-1/PD-L1 (246). Meanwhile, the dosage of agents targeting angiogenesis and the sequence of administrating anti-angiogenesis agents and immune checkpoint inhibitors are also key considerations. The knowledge needs to be obtained to extend the survival benefits of combination therapy.

BIBLIOGRAPHY

1. Leach DR, et al. Enhancement of antitumor immunity by CTLA-4 blockade. *Science (80-)*. 1996;271(5256):1734-1736. doi:10.1126/science.271.5256.1734
2. Khan KA, Kerbel RS. Improving immunotherapy outcomes with anti-angiogenic treatments and vice versa. *Nat Rev Clin Oncol*. 2018;15(5):310-324. doi:10.1038/nrclinonc.2018.9
3. Pardoll DM. The blockade of immune checkpoints in cancer immunotherapy. *Nat Rev Cancer*. 2012;12(4):252-264. doi:10.1038/nrc3239
4. Sznol M, Chen L. Antagonist antibodies to PD-1 and B7-H1 (PD-L1) in the treatment of advanced human cancer. *Clin Cancer Res*. 2013;19(5):1021-1034. doi:10.1158/1078-0432.CCR-12-2063
5. Hodi FS, et al. Improved survival with ipilimumab in patients with metastatic melanoma. *N Engl J Med*. 2010;363(8):711-723. doi:10.1056/NEJMoa1003466
6. Fukumura D, et al. Enhancing cancer immunotherapy using antiangiogenics: opportunities and challenges. *Nat Rev Clin Oncol*. 2018;15(5):325-340. doi:10.1038/nrclinonc.2018.29
7. Li X, et al. Emerging predictors of the response to the blockade of immune checkpoints in cancer therapy. *Cell Mol Immunol*. 2019;16(1):28-39. doi:10.1038/s41423-018-0086-z
8. Ribas A, et al. Association of pembrolizumab with tumor response and survival among patients with advanced melanoma. In: *JAMA - Journal of the American Medical Association*. Vol 315. American Medical Association; 2016:1600-1609.

doi:10.1001/jama.2016.4059

9. Hegde PS, et al. The where, the when, and the how of immune monitoring for cancer immunotherapies in the era of checkpoint inhibition. *Clin Cancer Res*. 2016;22(8):1865-1874. doi:10.1158/1078-0432.CCR-15-1507
10. Munn LL, Jain RK. Vascular regulation of antitumor immunity. *Science (80-)*. 2019;365(6453):544-545. doi:10.1126/science.aaw7875
11. Fukumura D, et al. Enhancing cancer immunotherapy using antiangiogenics: opportunities and challenges. *Nat Rev Clin Oncol*. 2018;15(5):325-340. doi:10.1038/nrclinonc.2018.29
12. Jain RK. Normalization of tumor vasculature: an emerging concept in antiangiogenic therapy. *Science*. 2005;307(5706):58-62. doi:10.1126/science.1104819
13. Motz GT, Coukos G. The parallel lives of angiogenesis and immunosuppression: cancer and other tales. *Nat Rev Immunol*. 2011;11(10):702-711. doi:10.1038/nri3064
14. Horikawa N, et al. Expression of Vascular Endothelial Growth Factor in Ovarian Cancer Inhibits Tumor Immunity through the Accumulation of Myeloid-Derived Suppressor Cells. *Clin Cancer Res*. 2017;23(2):587-599. doi:10.1158/1078-0432.CCR-16-0387
15. Simons M, et al. Mechanisms and regulation of endothelial VEGF receptor signalling. *Nat Rev Mol Cell Biol*. 2016;17(10):611-625. doi:10.1038/nrm.2016.87
16. Veikkola T, et al. *Regulation of Angiogenesis via Vascular Endothelial Growth*

Factor Receptors 1. Vol 60.; 2000.

17. Koch S, et al. Signal transduction by vascular endothelial growth factor receptors. *Biochem J*. 2011;437(2):169-183. doi:10.1042/BJ20110301

18. Shibuya M. JB Review Vascular endothelial growth factor and its receptor system: physiological functions in angiogenesis and pathological roles in various diseases. doi:10.1093/jb/mvs136

19. Kowanetz M, Ferrara N. Vascular Endothelial Growth Factor Signaling Pathways: Therapeutic Perspective. *Clin Cancer Res*. 2006;12(17):5018-5022. doi:10.1158/1078-0432.CCR-06-1520

20. Chen TT, et al. Anchorage of VEGF to the extracellular matrix conveys differential signaling responses to endothelial cells. *J Cell Biol*. 2010;188(4):595-609. doi:10.1083/jcb.200906044

21. Ferrara N, Davis-Smyth T. The biology of vascular endothelial growth factor. *Endocr Rev*. 1997;18(1):4-25. doi:10.1210/edrv.18.1.0287

22. Fong GH, et al. Role of the Flt-1 receptor tyrosine kinase in regulating the assembly of vascular endothelium. *Nature*. 1995;376(6535):66-70. doi:10.1038/376066a0

23. Shalaby F, et al. Failure of blood-island formation and vasculogenesis in Flk-1-deficient mice. *Nature*. 1995;376(6535):62-66. doi:10.1038/376062a0

24. Kim CG, et al. VEGF-A drives TOX-dependent T cell exhaustion in anti-PD-1-resistant microsatellite stable colorectal cancers. *Sci Immunol*. 2019;4(41). doi:10.1126/sciimmunol.aay0555

25. Dikov MM, et al. Differential roles of vascular endothelial growth factor receptors

1 and 2 in dendritic cell differentiation. *J Immunol*. 2005;174(1):215-222. doi:10.4049/JIMMUNOL.174.1.215

26. Dineen SP, et al. Vascular endothelial growth factor receptor 2 mediates macrophage infiltration into orthotopic pancreatic tumors in mice. *Cancer Res*. 2008;68(11):4340-4346. doi:10.1158/0008-5472.CAN-07-6705

27. Piali L, et al. Endothelial vascular cell adhesion molecule 1 expression is suppressed by melanoma and carcinoma. *J Exp Med*. 1995;181(2):811-816. doi:10.1084/jem.181.2.811

28. Riegler J, et al. VCAM-1 Density and Tumor Perfusion Predict T-cell Infiltration and Treatment Response in Preclinical Models. *Neoplasia (United States)*. 2019;21(10):1036-1050. doi:10.1016/j.neo.2019.08.003

29. Kim I, et al. Vascular endothelial growth factor expression of intercellular adhesion molecule 1 (ICAM-1), vascular cell adhesion molecule 1 (VCAM-1), and E-selectin through nuclear factor-kappa B activation in endothelial cells. *J Biol Chem*. 2001;276(10):7614-7620. doi:10.1074/jbc.M009705200

30. Wu X, et al. VEGF neutralization plus CTLA-4 blockade alters soluble and cellular factors associated with enhancing lymphocyte infiltration and humoral recognition in Melanoma. *Cancer Immunol Res*. 2016;4(10):858-868. doi:10.1158/2326-6066.CIR-16-0084

31. Dirkx AEM, et al. Anti-angiogenesis therapy can overcome endothelial cell anergy and promote leukocyte-endothelium interactions and infiltration in tumors. *FASEB J*. 2006;20(6):621-630. doi:10.1096/fj.05-4493com

32. Huang H, et al. VEGF suppresses T-lymphocyte infiltration in the tumor microenvironment through inhibition of NF- κ B-induced endothelial activation. *FASEB J*. 2015;29(1):227-238. doi:10.1096/fj.14-250985

33. Schmittnaegel M, et al. Dual angiopoietin-2 and VEGFA inhibition elicits antitumor immunity that is enhanced by PD-1 checkpoint blockade. *Sci Transl Med*. Published online 2017. doi:10.1126/scitranslmed.aak9670

34. Sidibe A, et al. Angiogenic factor-driven inflammation promotes extravasation of human proangiogenic monocytes to tumours. *Nat Commun*. 2018;9(1). doi:10.1038/s41467-017-02610-0

35. Motz GT, et al. Tumor endothelium FasL establishes a selective immune barrier promoting tolerance in tumors. *Nat Med*. 2014;20(6):607-615. doi:10.1038/nm.3541

36. Lee JJ, et al. Increased angiogenesis and Fas-ligand expression are independent processes in acute myeloid leukemia. *Leuk Res*. 2001;25(12):1067-1073. doi:10.1016/S0145-2126(01)00082-0

37. Zhang Y, et al. Cyclooxygenase-2 inhibition potentiates the efficacy of vascular endothelial growth factor blockade and promotes an immune stimulatory microenvironment in preclinical models of pancreatic cancer. *Mol Cancer Res*. 2019;17(2):348-355. doi:10.1158/1541-7786.MCR-18-0427

38. Huang Y, et al. Vascular normalizing doses of antiangiogenic treatment reprogram the immunosuppressive tumor microenvironment and enhance immunotherapy. *Proc Natl Acad Sci*. 2012;109(43):17561-17566. doi:10.1073/pnas.1215397109

39. Huang Y, et al. Improving immune–vascular crosstalk for cancer immunotherapy. *Nat Rev Immunol*. 2018;18(3):195-203. doi:10.1038/nri.2017.145

40. Ohm JE, et al. VEGF inhibits T-cell development and may contribute to tumor-induced immune suppression. *Blood*. 2003;101(12):4878-4886. doi:10.1182/blood-2002-07-1956

41. Gabrilovich D, et al. Vascular endothelial growth factor inhibits the development of dendritic cells and dramatically affects the differentiation of multiple hematopoietic lineages in vivo. *Blood*. 1998;92(11):4150-4166. doi:10.1182/blood.v92.11.4150.423k45_4150_4166

42. Ziogas AC, et al. VEGF directly suppresses activation of T cells from ovarian cancer patients and healthy individuals via VEGF receptor Type 2. *Int J Cancer*. 2012;130(4):857-864. doi:10.1002/ijc.26094

43. Voron T, et al. VEGF-A modulates expression of inhibitory checkpoints on CD8+ T cells in tumors. *J Exp Med*. 2015;212(2):139-148. doi:10.1084/jem.20140559

44. Mor F, et al. Angiogenesis-inflammation cross-talk: vascular endothelial growth factor is secreted by activated T cells and induces Th1 polarization. *J Immunol*. 2004;172(7):4618-4623. doi:10.4049/JIMMUNOL.172.7.4618

45. Gavalas NG, et al. VEGF directly suppresses activation of T cells from ascites secondary to ovarian cancer via VEGF receptor type 2. *Br J Cancer*. 2012;107(11):1869-1875. doi:10.1038/bjc.2012.468

46. De Almeida PE, et al. Anti-VEGF Treatment Enhances CD8 + T-Cell Antitumor Activity by Amplifying Hypoxia. *Author Manuscr Publ OnlineFirst*. Published

online 2020. doi:10.1158/2326-6066.CIR-19-0360

47. Malo CS, et al. Immunomodulation mediated by anti-angiogenic therapy improves CD8 T cell immunity against experimental glioma. *Front Oncol*. 2018;8(AUG). doi:10.3389/fonc.2018.00320

48. Du Four S, et al. Disease progression in recurrent glioblastoma patients treated with the VEGFR inhibitor axitinib is associated with increased regulatory T cell numbers and T cell exhaustion. *Cancer Immunol Immunother*. 2016;65(6):727-740. doi:10.1007/s00262-016-1836-3

49. Wallin JJ, et al. Atezolizumab in combination with bevacizumab enhances antigen-specific T-cell migration in metastatic renal cell carcinoma. *Nat Commun*. 2016;7:12624. doi:10.1038/ncomms12624

50. Tada Y, et al. Targeting VEGFR2 with Ramucirumab strongly impacts effector/ activated regulatory T cells and CD8+ T cells in the tumor microenvironment. *J Immunother Cancer*. 2018;6(1). doi:10.1186/s40425-018-0403-1

51. Vignali DAA, et al. How regulatory T cells work. *Nat Rev Immunol*. 2008;8(7):523-532. doi:10.1038/nri2343

52. Lapeyre-Prost A, et al. Immunomodulatory Activity of VEGF in Cancer. In: *International Review of Cell and Molecular Biology*. Vol 330. Elsevier Inc.; 2017:295-342. doi:10.1016/bs.ircmb.2016.09.007

53. Terme M, et al. VEGFA-VEGFR pathway blockade inhibits tumor-induced regulatory T-cell proliferation in colorectal cancer. *Cancer Res*. 2013;73(2):539-549. doi:10.1158/0008-5472.CAN-12-2325

54. Zhang Y, et al. Cyclooxygenase-2 Inhibition Potentiates the Efficacy of Vascular Endothelial Growth Factor Blockade and Promotes an Immune Stimulatory Microenvironment in Preclinical Models of Pancreatic Cancer. *Mol Cancer Res*. 2019;17(2):348-355. doi:10.1158/1541-7786.MCR-18-0427

55. Courau T, et al. TGF-β and VEGF cooperatively control the immunotolerant tumor environment and the efficacy of cancer immunotherapies. *JCI insight*. 2016;1(9):e85974. doi:10.1172/jci.insight.85974

56. Wada J, et al. The contribution of vascular endothelial growth factor to the induction of regulatory T- cells in malignant effusions. In: *Anticancer Research*. Vol 29. International Institute of Anticancer Research; 2009:881-888.

57. Thomas AA, et al. Immune modulation associated with vascular endothelial growth factor (VEGF) blockade in patients with glioblastoma. *Cancer Immunol Immunother*. 2017;66(3):379-389. doi:10.1007/s00262-016-1941-3

58. Long Y, et al. Dysregulation of glutamate transport enhances Treg function that promotes VEGF blockade resistance in glioblastoma. *Cancer Res*. 2020;80(3):499-509. doi:10.1158/0008-5472.CAN-19-1577

59. Tan JKH, O'Neill HC. Maturation requirements for dendritic cells in T cell stimulation leading to tolerance versus immunity. *J Leukoc Biol*. 2005;78(2):319-324. doi:10.1189/jlb.1104664

60. Yang J, et al. Targeting VEGF/VEGFR to modulate antitumor immunity. *Front Immunol*. 2018;9(MAY). doi:10.3389/fimmu.2018.00978

61. Gabrilovich DI, et al. Production of vascular endothelial growth factor by human

tumors inhibits the functional maturation of dendritic cells. *Nat Med*. 1996;2(10):1096-1103. doi:10.1038/nm1096-1096

62. Wilson NS, et al. Dendritic cells constitutively present self antigens in their immature state in vivo and regulate antigen presentation by controlling the rates of MHC class II synthesis and endocytosis. *Blood*. 2004;103(6):2187-2195. doi:10.1182/blood-2003-08-2729

63. Almand B, et al. *Clinical Significance of Defective Dendritic Cell Differentiation in Cancer 1*.; 2000.

64. Oyama T, et al. Vascular endothelial growth factor affects dendritic cell maturation through the inhibition of nuclear factor-kappa B activation in hemopoietic progenitor cells. *J Immunol*. 1998;160(3):1224-1232. Accessed October 20, 2019. http://www.ncbi.nlm.nih.gov/pubmed/9570538

65. Boissel N, et al. Defective blood dendritic cells in chronic myeloid leukemia correlate with high plasmatic VEGF and are not normalized by imatinib mesylate. *Leukemia*. 2004;18(10):1656-1661. doi:10.1038/sj.leu.2403474

66. Bai WK, et al. Vascular endothelial growth factor suppresses dendritic cells function of human prostate cancer. *Onco Targets Ther*. 2018;11:1267-1274. doi:10.2147/OTT.S161302

67. Oussa NAE, et al. VEGF Requires the Receptor NRP-1 To Inhibit Lipopolysaccharide-Dependent Dendritic Cell Maturation. *J Immunol*. 2016;197(10):3927-3935. doi:10.4049/jimmunol.1601116

68. Mimura K, et al. Vascular endothelial growth factor inhibits the function of human

mature dendritic cells mediated by VEGF receptor-2. *Cancer Immunol Immunother*. 2007;56(6):761-770. doi:10.1007/s00262-006-0234-7

69. Agudo J, et al. The miR-126-VEGFR2 axis controls the innate response to pathogen-associated nucleic acids. *Nat Immunol*. 2014;15(1):54-62. doi:10.1038/ni.2767

70. Orleans N, Clinic M. Blockade of B7-H1 improves myeloid dendritic cell – mediated antitumor immunity. 2003;9(5). doi:10.1038/nm

71. Hipp MM, et al. Sorafenib, but not sunitinib, affects function of dendritic cells and induction of primary immune responses. *Blood*. 2008;111(12):5610-5620. doi:10.1182/blood-2007-02-075945

72. Alfaro C, et al. Influence of bevacizumab, sunitinib and sorafenib as single agents or in combination on the inhibitory effects of VEGF on human dendritic cell differentiation from monocytes. *Br J Cancer*. 2009;100(7):1111-1119. doi:10.1038/sj.bjc.6604965

73. Van Cruijsen H, et al. Sunitinib-induced myeloid lineage redistribution in renal cell cancer patients: CD1c+ dendritic cell frequency predicts progression-free survival. *Clin Cancer Res*. 2008;14(18):5884-5892. doi:10.1158/1078-0432.CCR-08-0656

74. Heine A, et al. The VEGF-receptor inhibitor axitinib impairs dendritic cell phenotype and function. *PLoS One*. 2015;10(6). doi:10.1371/journal.pone.0128897

75. Osada T, et al. The effect of anti-VEGF therapy on immature myeloid cell and dendritic cells in cancer patients. *Cancer Immunol Immunother*. 2008;57(8):1115-1124. doi:10.1007/s00262-007-0441-x

76. Wang H, et al. Inhibition of vascular endothelial growth factor by small interfering

RNA upregulates differentiation, Maturation and function of dendritic cells. *Exp Ther Med*. 2015;9(1):120-124. doi:10.3892/etm.2014.2059

77. Glass CK, Natoli G. Molecular control of activation and priming in macrophages. *Nat Immunol*. 2016;17(1):26-33. doi:10.1038/ni.3306

78. Albini A, et al. Contribution to tumor angiogenesis from innate immune cells within the tumor microenvironment: Implications for immunotherapy. *Front Immunol*. 2018;9(APR). doi:10.3389/fimmu.2018.00527

79. Martinez FO, Gordon S. The M1 and M2 paradigm of macrophage activation: Time for reassessment. *F1000Prime Rep*. 2014;6. doi:10.12703/P6-13

80. Krzyszczyk P, et al. The role of macrophages in acute and chronic wound healing and interventions to promote pro-wound healing phenotypes. *Front Physiol*. 2018;9(MAY):419. doi:10.3389/fphys.2018.00419

81. Allavena P, Mantovani A. Immunology in the clinic review series; focus on cancer: tumour-associated macrophages: undisputed stars of the inflammatory tumour microenvironment. *Clin Exp Immunol*. 2012;167(2):195-205. doi:10.1111/j.1365-2249.2011.04515.x

82. Mantovani A, et al. Tumour-associated macrophages as treatment targets in oncology. *Nat Rev Clin Oncol*. 2017;14(7):399-416. doi:10.1038/nrclinonc.2016.217

83. Qian BZ, Pollard JW. Macrophage Diversity Enhances Tumor Progression and Metastasis. *Cell*. 2010;141(1):39-51. doi:10.1016/j.cell.2010.03.014

84. Sica A, Bronte V. Altered macrophage differentiation and immune dysfunction in

tumor development. *J Clin Invest*. 2007;117(5):1155-1166. doi:10.1172/JCI31422

85. Hu H, et al. The M2 phenotype of tumor-associated macrophages in the stroma confers a poor prognosis in pancreatic cancer. *Tumor Biol*. 2016;37(7):8657-8664. doi:10.1007/s13277-015-4741-z

86. Xu J, et al. CSF1R signaling blockade stanches tumor-infiltrating myeloid cells and improves the efficacy of radiotherapy in prostate cancer. *Cancer Res*. 2013;73(9):2782-2794. doi:10.1158/0008-5472.CAN-12-3981

87. Steidl C, et al. Tumor-associated macrophages and survival in classic Hodgkin's lymphoma. *N Engl J Med*. 2010;362(10):875-885. doi:10.1056/NEJMoa0905680

88. Biswas SK, Mantovani A. Macrophage plasticity and interaction with lymphocyte subsets: Cancer as a paradigm. *Nat Immunol*. 2010;11(10):889-896. doi:10.1038/ni.1937

89. Murakami M, et al. VEGFR1 tyrosine kinase signaling promotes lymphangiogenesis as well as angiogenesis indirectly via macrophage recruitment. *Arterioscler Thromb Vasc Biol*. 2008;28(4):658-664. doi:10.1161/ATVBAHA.107.150433

90. Casazza A, et al. Impeding Macrophage Entry into Hypoxic Tumor Areas by Sema3A/Nrp1 Signaling Blockade Inhibits Angiogenesis and Restores Antitumor Immunity. *Cancer Cell*. 2013;24(6):695-709. doi:10.1016/j.ccr.2013.11.007

91. Barleon B, et al. Migration of human monocytes in response to vascular endothelial growth factor (VEGF) is mediated via the VEGF receptor flt-1. *Blood*. 1996;87(8):3336-3343. doi:10.1182/blood.v87.8.3336.bloodjournal8783336

92. Qian B-Z, et al. FLT1 signaling in metastasis-associated macrophages activates an inflammatory signature that promotes breast cancer metastasis. *J Exp Med*. 2015;212(9):1433-1448. doi:10.1084/jem.20141555

93. Valls AF, et al. VEGFR1+ metastasis-associated macrophages contribute to metastatic angiogenesis and influence colorectal cancer patient outcome. *Clin Cancer Res*. 2019;25(18):5674-5685. doi:10.1158/1078-0432.CCR-18-2123

94. Zou Y, et al. VEGFR1 Signaling Regulates IL-4-Mediated Arginase 1 Expression in Macrophages. *Curr Mol Med*. 2017;17(4). doi:10.2174/1566524017666171106114537

95. Roland CL, et al. Inhibition of vascular endothelial growth factor reduces angiogenesis and modulates immune cell infiltration of orthotopic breast cancer xenografts. *Mol Cancer Ther*. Published online 2009. doi:10.1158/1535-7163.MCT-09-0280

96. Vroling L, et al. VEGFR2 expressing circulating (progenitor) cell populations in volunteers and cancer patients. *Thromb Haemost*. 2007;98(2):440-450. doi:10.1160/TH07-03-0225

97. Huang Y, et al. A proangiogenic signaling axis in myeloid cells promotes malignant progression of glioma. *J Clin Invest*. 2017;127(5):1826-1838. doi:10.1172/JCI86443

98. Riabov V, et al. Role of tumor associated macrophages in tumor angiogenesis and lymphangiogenesis. *Front Physiol*. 2014;5 MAR. doi:10.3389/fphys.2014.00075

99. Lin EY, et al. Vascular endothelial growth factor restores delayed tumor progression

in tumors depleted of macrophages. *Mol Oncol*. 2007;1(3):288-302. doi:10.1016/j.molonc.2007.10.003

100. Stockmann C, et al. Deletion of vascular endothelial growth factor in myeloid cells accelerates tumorigenesis. *Nature*. 2008;456(7223):814-819. doi:10.1038/nature07445

101. Roland CL, et al. Cytokine levels correlate with immune cell infiltration after anti-VEGF therapy in preclinical mouse models of breast cancer. *PLoS One*. Published online 2009. doi:10.1371/journal.pone.0007669

102. Zhao S, et al. Low-dose apatinib optimizes tumor microenvironment and potentiates antitumor effect of PD-1/PD-L1 blockade in lung cancer. *Cancer Immunol Res*. 2019;7(4):630-643. doi:10.1158/2326-6066.CIR-17-0640

103. De Palma M, Lewis CE. Macrophage regulation of tumor responses to anticancer therapies. *Cancer Cell*. 2013;23(3):277-286. doi:10.1016/j.ccr.2013.02.013

104. Wroblewski M, et al. Mast cells decrease efficacy of anti-angiogenic therapy by secreting matrix-degrading granzyme B. *Nat Commun*. 2017;8(1). doi:10.1038/s41467-017-00327-8

105. Dalton HJ, et al. Macrophages facilitate resistance to anti-VEGF therapy by altered VEGFR expression. *Clin Cancer Res*. 2017;23(22):7034-7046. doi:10.1158/1078-0432.CCR-17-0647

106. Castro BA, et al. Macrophage migration inhibitory factor downregulation: A novel mechanism of resistance to anti-angiogenic therapy. *Oncogene*. 2017;36(26):3749-3759. doi:10.1038/onc.2017.1

107. Gabrusiewicz K, et al. Anti-vascular endothelial growth factor therapy-induced glioma invasion is associated with accumulation of Tie2-expressing monocytes. *Oncotarget*. 2014;5(8):2208-2220. doi:10.18632/oncotarget.1893

108. De Palma M, et al. Tie2 identifies a hematopoietic lineage of proangiogenic monocytes required for tumor vessel formation and a mesenchymal population of pericyte progenitors. *Cancer Cell*. 2005;8(3):211-226. doi:10.1016/j.ccr.2005.08.002

109. Coffelt SB, et al. Angiopoietin-2 regulates gene expression in TIE2-expressing monocytes and augments their inherent proangiogenic functions. *Cancer Res*. 2010;70(13):5270-5280. doi:10.1158/0008-5472.CAN-10-0012

110. Peterson TE, et al. Dual inhibition of Ang-2 and VEGF receptors normalizes tumor vasculature and prolongs survival in glioblastoma by altering macrophages. *Proc Natl Acad Sci U S A*. 2016;113(16):4470-4475. doi:10.1073/pnas.1525349113

111. Kloepper J, et al. Ang-2/VEGF bispecific antibody reprograms macrophages and resident microglia to anti-tumor phenotype and prolongs glioblastoma survival. *Proc Natl Acad Sci U S A*. 2016;113(16):4476-4481. doi:10.1073/pnas.1525360113

112. Gabrilovich DI, et al. Coordinated regulation of myeloid cells by tumours. *Nat Rev Immunol*. 2012;12(4):253-268. doi:10.1038/nri3175

113. Youn J-I, et al. Subsets of Myeloid-Derived Suppressor Cells in Tumor-Bearing Mice. *J Immunol*. 2008;181(8):5791-5802. doi:10.4049/jimmunol.181.8.5791

114. Movahedi K, et al. Identification of discrete tumor-induced myeloid-derived suppressor cell subpopulations with distinct T cell suppressive activity. *Blood*.

2008;111(8):4233-4244. doi:10.1182/blood-2007-07-099226

115. Srivastava MK, et al. Myeloid-derived suppressor cells inhibit T-cell activation by depleting cystine and cysteine. *Cancer Res*. 2010;70(1):68-77. doi:10.1158/0008-5472.CAN-09-2587

116. Pan PY, et al. Immune stimulatory receptor CD40 is required for T-cell suppression and T regulatory cell activation mediated by myeloid-derived suppressor cells in cancer. *Cancer Res*. 2010;70(1):99-108. doi:10.1158/0008-5472.CAN-09-1882

117. Marigo I, et al. Tumor-induced tolerance and immune suppression depend on the C/EBPβ transcription factor. *Immunity*. 2010;32(6):790-802. doi:10.1016/j.immuni.2010.05.010

118. Gallina G, et al. Tumors induce a subset of inflammatory monocytes with immunosuppressive activity on CD8+ T cells. *J Clin Invest*. 2006;116(10):2777-2790. doi:10.1172/JCI28828

119. Arihara F, et al. Increase in CD14+HLA-DR-/low myeloid-derived suppressor cells in hepatocellular carcinoma patients and its impact on prognosis. *Cancer Immunol Immunother*. 2013;62(8):1421-1430. doi:10.1007/s00262-013-1447-1

120. Shen P, et al. Increased circulating Lin-/lowCD33+HLA-DR- myeloid-derived suppressor cells in hepatocellular carcinoma patients. *Hepatol Res*. 2014;44(6):639-650. doi:10.1111/hepr.12167

121. Koinis F, et al. Effect of first-line treatment on myeloid-derived suppressor cells' subpopulations in the peripheral blood of patients with non-small cell lung cancer. *J Thorac Oncol*. 2016;11(8):1263-1272. doi:10.1016/j.jtho.2016.04.026

122. Karakhanova S, et al. Characterization of myeloid leukocytes and soluble mediators in pancreatic cancer: Importance of myeloid-derived suppressor cells. *Oncoimmunology*. 2015;4(4). doi:10.1080/2162402X.2014.998519

123. Huang Y, et al. Distinct roles of VEGFR-1 and VEGFR-2 in the aberrant hematopoiesis associated with elevated levels of VEGF. *Blood*. 2007;110(2):624-631. doi:10.1182/blood-2007-01-065714

124. Nefedova Y, et al. Hyperactivation of STAT3 Is Involved in Abnormal Differentiation of Dendritic Cells in Cancer. *J Immunol*. 2004;172(1):464-474. doi:10.4049/jimmunol.172.1.464

125. Horikawa N, et al. Expression of Vascular Endothelial Growth Factor in Ovarian Cancer Inhibits Tumor Immunity through the Accumulation of Myeloid-Derived Suppressor Cells. *Clin Cancer Res*. 2017;23(2):587-599. doi:10.1158/1078-0432.CCR-16-0387

126. Ozao-Choy J, et al. The novel role of tyrosine kinase inhibitor in the reversal of immune suppression and modulation of tumor microenvironment for immune-based cancer therapies. *Cancer Res*. 2009;69(6):2514-2522. doi:10.1158/0008-5472.CAN-08-4709

127. Xin H, et al. Sunitinib inhibition of Stat3 induces renal cell carcinoma tumor cell apoptosis and reduces immunosuppressive cells. *Cancer Res*. 2009;69(6):2506-2513. doi:10.1158/0008-5472.CAN-08-4323

128. Draghiciu O, et al. Sunitinib depletes myeloid-derived suppressor cells and synergizes with a cancer vaccine to enhance antigen-specific immune responses and

tumor eradication. *Oncoimmunology*. 2015;4(3):1-11. doi:10.4161/2162402X.2014.989764

129. Secondini C, et al. Arginase inhibition suppresses lung metastasis in the 4T1 breast cancer model independently of the immunomodulatory and anti-metastatic effects of VEGFR-2 blockade. *Oncoimmunology*. 2017;6(6). doi:10.1080/2162402X.2017.1316437

130. Du Four S, et al. Axitinib increases the infiltration of immune cells and reduces the suppressive capacity of monocytic MDSCs in an intracranial mouse melanoma model. *Oncoimmunology*. 2015;4(4):e998107. doi:10.1080/2162402X.2014.998107

131. Ko JS, et al. Sunitinib mediates reversal of myeloid-derived suppressor cell accumulation in renal cell carcinoma patients. *Clin Cancer Res*. 2009;15(6):2148-2157. doi:10.1158/1078-0432.CCR-08-1332

132. Shojaei F, Ferrara N. Refractoriness to antivascular endothelial growth factor treatment: Role of myeloid cells. *Cancer Res*. 2008;68(14):5501-5504. doi:10.1158/0008-5472.CAN-08-0925

133. Yang L, et al. Expansion of myeloid immune suppressor Gr+CD11b+ cells in tumor-bearing host directly promotes tumor angiogenesis. *Cancer Cell*. 2004;6(4):409-421. doi:10.1016/j.ccr.2004.08.031

134. Kujawski M, et al. Stat3 mediates myeloid cell-dependent tumor angiogenesis in mice. *J Clin Invest*. 2008;118(10):3367-3377. doi:10.1172/JCI35213

135. Horikawa N, et al. Anti-VEGF therapy resistance in ovarian cancer is caused by

GM-CSF-induced myeloid-derived suppressor cell recruitment. *Br J Cancer*. 2020;122(6):778-788. doi:10.1038/s41416-019-0725-x

136. Iwai T, et al. Capecitabine reverses tumor escape from anti-VEGF through the eliminating CD11bhigh/Gr1high myeloid cells. *Oncotarget*. 2018;9(25):17620-17630. doi:10.18632/oncotarget.24811

137. Bauer R, et al. Blockade of myeloid-derived suppressor cell expansion with all-trans retinoic acid increases the efficacy of antiangiogenic therapy. *Cancer Res*. 2018;78(12):3220-3232. doi:10.1158/0008-5472.CAN-17-3415

138. Chang CJ, et al. Targeting tumor-infiltrating Ly6G+ myeloid cells improves sorafenib efficacy in mouse orthotopic hepatocellular carcinoma. *Int J Cancer*. 2018;142(9):1878-1889. doi:10.1002/ijc.31216

139. Allen E, et al. Combined antiangiogenic and anti-PD-L1 therapy stimulates tumor immunity through HEV formation. *Sci Transl Med*. 2017;9(385):eaak9679. doi:10.1126/scitranslmed.aak9679

140. Di Tacchio M, et al. Tumor vessel normalization, immunostimulatory reprogramming, and improved survival in glioblastoma with combined inhibition of PD-1, angiopoietin-2, and VEGF. *Cancer Immunol Res*. 2019;7(12):1910-1927. doi:10.1158/2326-6066.CIR-18-0865

141. Läubli H, et al. The multi-receptor inhibitor axitinib reverses tumor-induced immunosuppression and potentiates treatment with immune-modulatory antibodies in preclinical murine models. *Cancer Immunol Immunother*. 2018;67(5):815-824. doi:10.1007/s00262-018-2136-x

142. Zhang X, et al. Blocking CD47 efficiently potentiated therapeutic effects of anti-angiogenic therapy in non-small cell lung cancer. *J Immunother Cancer*. 2019;7(1). doi:10.1186/s40425-019-0812-9

143. Yuan J, et al. Pretreatment serum VEGF is associated with clinical response and overall survival in advanced melanoma patients treated with ipilimumab. *Cancer Immunol Res*. 2014;2(2):127-132. doi:10.1158/2326-6066.CIR-13-0163

144. Shibaki R, et al. Predictive value of serum VEGF levels for elderly patients or for patients with poor performance status receiving anti-PD-1 antibody therapy for advanced non-small-cell lung cancer. *Cancer Immunol Immunother*. Published online 2020. doi:10.1007/s00262-020-02539-2

145. Atkins MB, et al. Axitinib in combination with pembrolizumab in patients with advanced renal cell cancer: a non-randomised, open-label, dose-finding, and dose-expansion phase 1b trial. *Lancet Oncol*. 2018;19(3):405-415. doi:10.1016/S1470-2045(18)30081-0

146. McDermott DF, et al. Clinical activity and molecular correlates of response to atezolizumab alone or in combination with bevacizumab versus sunitinib in renal cell carcinoma. *Nat Med*. 2018;24(6):749-757. doi:10.1038/s41591-018-0053-3

147. Shah AY, et al. Outcomes of patients with metastatic clear-cell renal cell carcinoma treated with second-line VEGFR-TKI after first-line immune checkpoint inhibitors. *Eur J Cancer*. 2019;114:67-75. doi:10.1016/j.ejca.2019.04.003

148. Wilky BA, et al. Axitinib plus pembrolizumab in patients with advanced sarcomas including alveolar soft-part sarcoma: a single-centre, single-arm, phase 2 trial.

Lancet Oncol. 2019;20(6):837-848. doi:10.1016/S1470-2045(19)30153-6

149. Liu JF, et al. Assessment of Combined Nivolumab and Bevacizumab in Relapsed Ovarian Cancer: A Phase 2 Clinical Trial. *JAMA Oncol*. 2019;5(12):1731-1738. doi:10.1001/jamaoncol.2019.3343

150. Wentink MQ, et al. Vaccination approach to anti-angiogenic treatment of cancer. *Biochim Biophys Acta - Rev Cancer*. 2015;1855(2):155-171. doi:10.1016/j.bbcan.2015.01.005

151. Vansteenkiste JF, et al. Magrit, a Double-Blind, Randomized, Placebo-Controlled Phase III Study to Assess the Efficacy of the Recmage-A3 + As15 Cancer Immunotherapeutic As Adjuvant Therapy in Patients with Resected Mage-A3-Positive Non-Small Cell Lung Cancer (Nsclc). *Ann Oncol*. 2014;25:iv409. doi:10.1093/annonc/mdu347.1

152. Butts C, et al. Tecemotide (L-BLP25) versus placebo after chemoradiotherapy for stage III non-small-cell lung cancer (START): A randomised, double-blind, phase 3 trial. *Lancet Oncol*. 2014;15(1):59-68. doi:10.1016/S1470-2045(13)70510-2

153. Facciponte JG, et al. Tumor endothelial marker 1-specific DNA vaccination targets tumor vasculature. *J Clin Invest*. 2014;124(4):1497-1511. doi:10.1172/JCI67382

154. Bose A, et al. Sunitinib facilitates the activation and recruitment of therapeutic anti-tumor immunity in concert with specific vaccination. *Int J Cancer*. 2011;129(9):2158. doi:10.1002/IJC.25863

155. Manning EA, et al. A vascular endothelial growth factor receptor-2 inhibitor enhances antitumor immunity through an immune-based mechanism. *Clin Cancer*

Res. 2007;13(13):3951-3959. doi:10.1158/1078-0432.CCR-07-0374

156. Bota DA, et al. Use of ERC-1671 Vaccine in a Patient with Recurrent Glioblastoma Multiforme after Progression during Bevacizumab Therapy: First Published Report. *Perm J*. 2015;19(2):41. doi:10.7812/TPP/14-042

157. Schijns VEJC, et al. First clinical results of a personalized immunotherapeutic vaccine against recurrent, incompletely resected, treatment-resistant glioblastoma multiforme (GBM) tumors, based on combined allo- and auto-immune tumor reactivity. *Vaccine*. 2015;33(23):2690-2696. doi:10.1016/j.vaccine.2015.03.095

158. Bota DA, et al. Phase II study of ERC1671 plus bevacizumab versus bevacizumab plus placebo in recurrent glioblastoma: interim results and correlations with CD4+ T-lymphocyte counts. *CNS Oncol*. 2018;7(3):CNS22. doi:10.2217/cns-2018-0009

159. Tanyi JL, et al. Personalized cancer vaccine effectively mobilizes antitumor T cell immunity in ovarian cancer. *Sci Transl Med*. 2018;10(436). doi:10.1126/scitranslmed.aao5931

160. Rini BI, et al. IMA901, a multipeptide cancer vaccine, plus sunitinib versus sunitinib alone, as first-line therapy for advanced or metastatic renal cell carcinoma (IMPRINT): a multicentre, open-label, randomised, controlled, phase 3 trial. *Lancet Oncol*. 2016;17(11):1599-1611. doi:10.1016/S1470-2045(16)30408-9

161. Niederman TMJ, et al. Antitumor activity of cytotoxic T lymphocytes engineered to target vascular endothelial growth factor receptors. *Proc Natl Acad Sci U S A*. 2002;99(10):7009-7014. doi:10.1073/pnas.092562399

162. Chinnasamy D, et al. Gene therapy using genetically modified lymphocytes

targeting VEGFR-2 inhibits the growth of vascularized syngenic tumors in mice. *J Clin Invest*. 2010;120(11):3953-3968. doi:10.1172/JCI43490

163. Chinnasamy D, et al. Local delivery of interleukin-12 using T cells targeting VEGF receptor-2 eradicates multiple vascularized tumors in mice. *Clin Cancer Res*. 2012;18(6):1672-1683. doi:10.1158/1078-0432.CCR-11-3050

164. Chinnasamy D, et al. Simultaneous targeting of tumor antigens and the tumor vasculature using t lymphocyte transfer synergize to induce regression of established tumors in mice. *Cancer Res*. 2013;73(11):3371-3380. doi:10.1158/0008-5472.CAN-12-3913

165. Shrimali RK, et al. Antiangiogenic agents can increase lymphocyte infiltration into tumor and enhance the effectiveness of adoptive immunotherapy of cancer. *Cancer Res*. 2010;70(15):6171-6180. doi:10.1158/0008-5472.CAN-10-0153

166. Tao L, et al. Bevacizumab improves the antitumor efficacy of adoptive cytokine-induced killer cells therapy in non-small cell lung cancer models. *Med Oncol*. 2014;31(1). doi:10.1007/s12032-013-0777-3

167. Kandalaft LE, et al. Autologous lysate-pulsed dendritic cell vaccination followed by adoptive transfer of vaccine-primed ex vivo co-stimulated t cells in recurrent ovarian cancer. *Oncoimmunology*. 2013;2(1). doi:10.4161/onci.22664

168. Parker BS, et al. Antitumour actions of interferons: Implications for cancer therapy. *Nat Rev Cancer*. 2016;16(3):131-144. doi:10.1038/nrc.2016.14

169. Minn AJ. Interferons and the Immunogenic Effects of Cancer Therapy. *Trends Immunol*. 2015;36(11):725-737. doi:10.1016/j.it.2015.09.007

170. Stein BL, Tiu R V. Biological Rationale and Clinical Use of Interferon in the Classical BCR-ABL-Negative Myeloproliferative Neoplasms. *J Interf Cytokine Res*. 2013;33(4):145-153. doi:10.1089/jir.2012.0120

171. Mocellin S, et al. Interferon alpha adjuvant therapy in patients with high-risk melanoma: A systematic review and meta-analysis. *J Natl Cancer Inst*. 2010;102(7):493-501. doi:10.1093/jnci/djq009

172. Rini BI, et al. Phase III trial of bevacizumab plus interferon alfa versus interferon alfa monotherapy in patients with metastatic renal cell carcinoma: Final results of CALGB 90206. *J Clin Oncol*. 2010;28(13):2137-2143. doi:10.1200/JCO.2009.26.5561

173. Escudier B, et al. Phase III trial of bevacizumab plus interferon alfa-2a in patients with metastatic renal cell carcinoma (AVOREN): Final analysis of overall survival. *J Clin Oncol*. 2010;28(13):2144-2150. doi:10.1200/JCO.2009.26.7849

174. Woo SR, et al. STING-dependent cytosolic DNA sensing mediates innate immune recognition of immunogenic tumors. *Immunity*. 2014;41(5):830-842. doi:10.1016/j.immuni.2014.10.017

175. Yang H, et al. STING activation reprograms tumor vasculatures and synergizes with VEGFR2 blockade. *J Clin Invest*. 2019;129(10):4350-4364. doi:10.1172/JCI125413

176. Sullivan LA, et al. r84, a novel therapeutic antibody against mouse and human VEGF with potent anti-tumor activity and limited toxicity induction. Gartel AL, ed. *PLoS One*. 2010;5(8):e12031. doi:10.1371/journal.pone.0012031

177. Carmeliet P, Jain RK. Molecular mechanisms and clinical applications of angiogenesis. *Nature*. 2011;473(7347):298-307. doi:10.1038/nature10144

178. Nagy JA, et al. VEGF-A and the Induction of Pathological Angiogenesis. *Annu Rev Pathol Mech Dis*. 2007;2(1):251-275. doi:10.1146/annurev.pathol.2.010506.134925

179. Kerbel RS. Tumor Angiogenesis. *N Engl J Med*. 2008;358(19):2039-2049. doi:10.1056/NEJMra0706596

180. Goel HL, Mercurio AM. VEGF targets the tumour cell. *Nat Rev Cancer*. 2013;13(12):871-882. doi:10.1038/nrc3627

181. Welti J, et al. Recent molecular discoveries in angiogenesis and antiangiogenic therapies in cancer. *J Clin Invest*. 2013;123(8):3190-3200. doi:10.1172/JCI70212

182. Lambrechts D, et al. Markers of Response for the Antiangiogenic Agent Bevacizumab. *J Clin Oncol*. 2013;31(9):1219-1230. doi:10.1200/JCO.2012.46.2762

183. Pàez-Ribes M, et al. Antiangiogenic Therapy Elicits Malignant Progression of Tumors to Increased Local Invasion and Distant Metastasis. *Cancer Cell*. 2009;15(3):220-231. doi:10.1016/j.ccr.2009.01.027

184. Aguilera KY, et al. Collagen signaling enhances tumor progression after anti-VEGF therapy in a murine model of pancreatic ductal adenocarcinoma. *Cancer Res*. 2014;74(4):1032-1044. doi:10.1158/0008-5472.CAN-13-2800

185. Siegel RL, et al. Cancer statistics, 2017. *CA Cancer J Clin*. 2017;67(1):7-30. doi:10.3322/caac.21387

186. Steeg PS. Targeting metastasis. *Nat Publ Gr*. 2016;16. doi:10.1038/nrc.2016.25

187. Feng M, et al. PD-1/PD-L1 and immunotherapy for pancreatic cancer. *Cancer Lett*. Published online August 2017. doi:10.1016/j.canlet.2017.08.006

188. Foley K, et al. Current progress in immunotherapy for pancreatic cancer. *Cancer Lett*. 2016;381(1):244-251. doi:10.1016/j.canlet.2015.12.020

189. Van Cutsem E, et al. Phase III Trial of Bevacizumab in Combination With Gemcitabine and Erlotinib in Patients With Metastatic Pancreatic Cancer. *J Clin Oncol*. 2009;27(13):2231-2237. doi:10.1200/JCO.2008.20.0238

190. Kindler HL, et al. Gemcitabine plus bevacizumab compared with gemcitabine plus placebo in patients with advanced pancreatic cancer: phase III trial of the Cancer and Leukemia Group B (CALGB 80303). *J Clin Oncol*. 2010;28(22):3617-3622. doi:10.1200/JCO.2010.28.1386

191. Wolfgang CL, et al. Recent progress in pancreatic cancer. *CA Cancer J Clin*. 2013;63(5):318-348. doi:10.3322/caac.21190

192. Sullivan LA, et al. r84, a novel therapeutic antibody against mouse and human VEGF with potent anti-tumor activity and limited toxicity induction. Gartel AL, ed. *PLoS One*. 2010;5(8):e12031. doi:10.1371/journal.pone.0012031

193. Hanahan D, Weinberg RA. Hallmarks of cancer: the next generation. *Cell*. 2011;144(5):646-674. doi:10.1016/j.cell.2011.02.013

194. Sobolewski C, et al. The role of cyclooxygenase-2 in cell proliferation and cell death in human malignancies. *Int J Cell Biol*. 2010;2010:215158. doi:10.1155/2010/215158

195. Wang D, Dubois RN. Eicosanoids and cancer. *Nat Rev Cancer*. 2010;10(3):181-193. doi:10.1038/nrc2809

196. Eberhart CE, et al. Up-regulation of cyclooxygenase 2 gene expression in human colorectal adenomas and adenocarcinomas. *Gastroenterology*. 1994;107(4):1183-1188. Accessed April 20, 2017. http://www.ncbi.nlm.nih.gov/pubmed/7926468

197. Lunardi S, et al. The stromal compartments in pancreatic cancer: are there any therapeutic targets? *Cancer Lett*. 2014;343(2):147-155. doi:10.1016/j.canlet.2013.09.039

198. de Groot DJA, et al. Non-steroidal anti-inflammatory drugs to potentiate chemotherapy effects: from lab to clinic. *Crit Rev Oncol Hematol*. 2007;61(1):52-69. doi:10.1016/j.critrevonc.2006.07.001

199. Ghosh N, et al. COX-2 as a target for cancer chemotherapy. *Pharmacol Rep*. 62(2):233-244. Accessed April 20, 2017. http://www.ncbi.nlm.nih.gov/pubmed/20508278

200. Xu L, et al. COX-2 inhibition potentiates antiangiogenic cancer therapy and prevents metastasis in preclinical models. *Sci Transl Med*. 2014;6(242):242ra84. doi:10.1126/scitranslmed.3008455

201. Khan Z, et al. Biology of Cox-2: an application in cancer therapeutics. *Curr Drug Targets*. 2011;12(7):1082-1093. Accessed April 21, 2017. http://www.ncbi.nlm.nih.gov/pubmed/21443470

202. Ben-Batalla I, et al. Cyclooxygenase-2 blockade can improve efficacy of VEGF-targeting drugs. *Oncotarget*. 2015;6(8):6341-6358. doi:10.18632/oncotarget.3437

203. Kirane A, et al. Epithelial-mesenchymal transition increases tumor sensitivity to COX-2 inhibition by apricoxib. *Carcinogenesis*. 2012;33(9):1639-1646. doi:10.1093/carcin/bgs195

204. Kirane A, et al. Apricoxib, a novel inhibitor of COX-2, markedly improves standard therapy response in molecularly defined models of pancreatic cancer. *Clin Cancer Res*. 2012;18(18):5031-5042. doi:10.1158/1078-0432.CCR-12-0453

205. Dongre A, et al. Epithelial-to-Mesenchymal Transition Contributes to Immunosuppression in Breast Carcinomas. *Cancer Res*. 2017;77(15):3982-3989. doi:10.1158/0008-5472.CAN-16-3292

206. Kudo-Saito C, et al. Cancer Metastasis Is Accelerated through Immunosuppression during Snail-Induced EMT of Cancer Cells. *Cancer Cell*. 2009;15(3):195-206. doi:10.1016/j.ccr.2009.01.023

207. Sangaletti S, et al. Mesenchymal Transition of High-Grade Breast Carcinomas Depends on Extracellular Matrix Control of Myeloid Suppressor Cell Activity. *Cell Rep*. 2016;17(1):233-248. doi:10.1016/j.celrep.2016.08.075

208. Thiery JP, et al. Epithelial-mesenchymal transitions in development and disease. *Cell*. 2009;139(5):871-890. doi:10.1016/j.cell.2009.11.007

209. Kirane A, et al. Apricoxib, a novel inhibitor of COX-2, markedly improves standard therapy response in molecularly defined models of pancreatic cancer. *Clin Cancer Res*. 2012;18(18):5031-5042. doi:10.1158/1078-0432.CCR-12-0453

210. Gately S. The contributions of cyclooxygenase-2 to tumor angiogenesis. *Cancer Metastasis Rev*. 2000;19(1-2):19-27. Accessed August 14, 2017.

http://www.ncbi.nlm.nih.gov/pubmed/11191059

211. Gately S, Li WW. Multiple roles of COX-2 in tumor angiogenesis: a target for antiangiogenic therapy. *Semin Oncol*. 2004;31(2 Suppl 7):2-11. Accessed August 14, 2017. http://www.ncbi.nlm.nih.gov/pubmed/15179620

212. Cheng T, et al. Prostaglandin E2 induces vascular endothelial growth factor and basic fibroblast growth factor mRNA expression in cultured rat Müller cells. *Invest Ophthalmol Vis Sci*. 1998;39(3):581-591. Accessed July 21, 2018. http://www.ncbi.nlm.nih.gov/pubmed/9501870

213. Jones MK, et al. Inhibition of angiogenesis by nonsteroidal anti-inflammatory drugs: insight into mechanisms and implications for cancer growth and ulcer healing. *Nat Med*. 1999;5(12):1418-1423. doi:10.1038/70995

214. Williams CS, et al. Host cyclooxygenase-2 modulates carcinoma growth. *J Clin Invest*. 2000;105(11):1589-1594. doi:10.1172/JCI9621

215. Ye X, et al. Distinct EMT programs control normal mammary stem cells and tumour-initiating cells. *Nature*. 2015;525(7568):256-260. doi:10.1038/nature14897

216. Wang D, Dubois RN. Eicosanoids and cancer. *Nat Rev Cancer*. 2010;10(3):181-193. doi:10.1038/nrc2809

217. Sullivan LA, et al. r84, a novel therapeutic antibody against mouse and human vegf with potent anti-tumor activity and limited toxicity induction. *PLoS One*. Published online 2010. doi:10.1371/journal.pone.0012031

218. Pàez-Ribes M, et al. Antiangiogenic Therapy Elicits Malignant Progression of Tumors to Increased Local Invasion and Distant Metastasis. *Cancer Cell*.

2009;15(3):220-231. doi:10.1016/j.ccr.2009.01.027

219. Lasaro MO, et al. Active immunotherapy combined with blockade of a coinhibitory pathway achieves regression of large tumor masses in cancer-prone mice. *Mol Ther*. 2011;19(9):1727-1736. doi:10.1038/mt.2011.88

220. Motz GT, Coukos G. The parallel lives of angiogenesis and immunosuppression: cancer and other tales. *Nat Rev Immunol*. 2011;11(10):702-711. doi:10.1038/nri3064

221. Oyama T, et al. Vascular endothelial growth factor affects dendritic cell maturation through the inhibition of nuclear factor-kappa B activation in hemopoietic progenitor cells. *J Immunol*. 1998;160(3):1224-1232. Accessed September 20, 2019. http://www.ncbi.nlm.nih.gov/pubmed/9570538

222. Kusmartsev S, Gabrilovich DI. Immature myeloid cells and cancer-associated immune suppression. *Cancer Immunol Immunother 2002 516*. 2002;51(6):293-298. doi:10.1007/S00262-002-0280-8

223. Brekken RA, et al. Vascular endothelial growth factor as a marker of tumor endothelium. *Cancer Res*. 1998;58(9):1952-1959. doi:10.1158/0008-5472.can-07-6705

224. Barone A, et al. Combined VEGF and CXCR4 antagonism targets the GBM stem cell population and synergistically improves survival in an intracranial mouse model of glioblastoma. *Oncotarget*. 2014;5(20):9811-9822. doi:10.18632/oncotarget.2443

225. Tong RT, et al. Vascular normalization by vascular endothelial growth factor receptor 2 blockade induces a pressure gradient across the vasculature and improves

drug penetration in tumors. *Cancer Res*. 2004;64(11):3731-3736. doi:10.1158/0008-5472.CAN-04-0074

226. Motz GT, et al. Tumor endothelium FasL establishes a selective immune barrier promoting tolerance in tumors. *Nat Med*. 2014;20(6):607-615. doi:10.1038/nm.3541

227. Xiao W, et al. IFNAR1 Controls Autocrine Type I IFN Regulation of PD-L1 Expression in Myeloid-Derived Suppressor Cells. *J Immunol*. 2018;201(1):264-277. doi:10.4049/jimmunol.1800129

228. Sichien D, et al. Development of conventional dendritic cells: From common bone marrow progenitors to multiple subsets in peripheral tissues. *Mucosal Immunol*. 2017;10(4):831-844. doi:10.1038/mi.2017.8

229. Aguirre AJ, et al. Activated Kras and Ink4a/Arf deficiency cooperate to produce metastatic pancreatic ductal adenocarcinoma. *Genes Dev*. 2003;17(24):3112-3126. doi:10.1101/gad.1158703

230. Sorrelle N, et al. Improved Multiplex Immunohistochemistry for Immune Microenvironment Evaluation of Mouse Formalin-Fixed, Paraffin-Embedded Tissues. *J Immunol*. 2019;202(1):292-299. doi:10.4049/jimmunol.1800878

231. Aguilera KY, et al. Collagen signaling enhances tumor progression after anti-VEGF therapy in a murine model of pancreatic ductal adenocarcinoma. *Cancer Res*. 2014;74(4):1032-1044. doi:10.1158/0008-5472.CAN-13-2800

232. Manzanero S. Generation of mouse bone marrow-derived macrophages. *Methods Mol Biol*. 2012;844:177-181. doi:10.1007/978-1-61779-527-5_12

233. Ng PKS, et al. Systematic Functional Annotation of Somatic Mutations in Cancer. *Cancer Cell*. 2018;33(3):450-462.e10. doi:10.1016/j.ccell.2018.01.021

234. Flavell RA, et al. The polarization of immune cells in the tumour environment by TGFbeta. *Nat Rev Immunol*. 2010;10(8):554-567. doi:10.1038/nri2808

235. Li MO, et al. TRANSFORMING GROWTH FACTOR-β REGULATION OF IMMUNE RESPONSES. *Annu Rev Immunol*. 2006;24(1):99-146. doi:10.1146/annurev.immunol.24.021605.090737

236. Wen SL, et al. Celecoxib attenuates hepatic cirrhosis through inhibition of epithelial-to-mesenchymal transition of hepatocytes. *J Gastroenterol Hepatol*. 2014;29(11):1932-1942. doi:10.1111/jgh.12641

237. Sambasivarao S V. Cox-2 and Akt mediate multiple growth factor-induced epithelial-mesenchhymal transition in human hepatocellular carcinoma. *J Gastroenterol Hepatol*. 2013;18(9):1199-1216. doi:10.1111/j.1440-1746.2011.06980.x.COX-2

238. Kerkar SP, Restifo NP. Cellular constituents of immune escape within the tumor microenvironment. *Cancer Res*. 2012;72(13):3125-3130. doi:10.1158/0008-5472.CAN-11-4094

239. Huang Y, et al. Vascular normalizing doses of antiangiogenic treatment reprogram the immunosuppressive tumor microenvironment and enhance immunotherapy. *Proc Natl Acad Sci U S A*. 2012;109(43):17561-17566. doi:10.1073/pnas.1215397109

240. Sharma S, et al. Tumor Cyclooxygenase 2-dependent Suppression of Dendritic Cell

Function. *Clin Cancer Res*. 2003;9(3). Accessed August 27, 2017. http://clincancerres.aacrjournals.org/content/9/3/961.long

241. Chen JH, et al. Prostaglandin E2 and programmed cell death 1 signaling coordinately impair CTL function and survival during chronic viral infection. *Nat Med*. 2015;21(4):327-334. http://dx.doi.org/10.1038/nm.3831

242. Yang† X, et al. Atezolizumab plus bevacizumab for unresectable hepatocellular carcinoma. *Lancet Oncol*. 2020;21(9):e412. doi:10.1016/S1470-2045(20)30430-7

243. Finn RS, et al. Atezolizumab plus Bevacizumab in Unresectable Hepatocellular Carcinoma. *https://doi.org/101056/NEJMoa1915745*. Published online May 13, 2020. doi:10.1056/NEJMOA1915745

244. Hodi FS, et al. Bevacizumab plus Ipilimumab in Patients with Metastatic Melanoma. *Cancer Immunol Res*. 2014;2(7):632-642. doi:10.1158/2326-6066.CIR-14-0053

245. Kashyap AS, et al. Optimized antiangiogenic reprogramming of the tumor microenvironment potentiates CD40 immunotherapy. *Proc Natl Acad Sci U S A*. 2020;117(1):541-551. doi:10.1073/pnas.1902145116

246. Tang H, et al. PD-L1 on host cells is essential for PD-L1 blockade–mediated tumor regression. *J Clin Invest*. 2018;128(2):580-588. doi:10.1172/JCI96061

247. Peng Q, et al. PD-L1 on dendritic cells attenuates T cell activation and regulates response to immune checkpoint blockade. *Nat Commun*. 2020;11(1). doi:10.1038/s41467-020-18570-x

248. Poczobutt JM, et al. Expression Profiling of Macrophages Reveals Multiple Populations with Distinct Biological Roles in an Immunocompetent Orthotopic

Model of Lung Cancer. *J Immunol*. 2016;196(6):2847-2859. doi:10.4049/jimmunol.1502364

249. Chen DS, Mellman I. Oncology meets immunology: The cancer-immunity cycle. *Immunity*. 2013;39(1):1-10. doi:10.1016/j.immuni.2013.07.012

250. Feig C, et al. The pancreas cancer microenvironment. *Clin Cancer Res*. 2012;18(16):4266-4276. doi:10.1158/1078-0432.CCR-11-3114

251. Koyama S, et al. Adaptive resistance to therapeutic PD-1 blockade is associated with upregulation of alternative immune checkpoints. *Nat Commun*. 2016;7. doi:10.1038/ncomms10501